Master's thesis

NTNU
Norwegian University of Science and Technology
Faculty of Engineering
Department of Energy and Process Engineering

Jesús Tajes Vázquez

Flow streaming mediated particle separation inside a droplet induced by surface acoustic waves

Master's thesis in Industrial Engineering
Supervisor: Carlos Alberto Dorao
June 2022

Particle ring formation 20MHz

NTNU
Norwegian University of
Science and Technology

Jesús Tajes Vázquez

Flow streaming mediated particle separation inside a droplet induced by surface acoustic waves

Master's thesis in Industrial Engineering
Supervisor: Carlos Alberto Dorao
June 2022

Norwegian University of Science and Technology
Faculty of Engineering
Department of Energy and Process Engineering

NTNU
Norwegian University of
Science and Technology

Preface

This project thesis, titled" Flow streaming mediated particle separation inside a droplet induced by surface acoustic waves," concludes the project work assigned during the spring of 2022. The project work, worth 30 ECTS, has been conducted as part of the Master in Industrial Engineering" at the Norwegian University of Science and Technology.

Primarily, I would like to thank to my supervisor Carlos Alberto Dorao of the Department of Energy and Process Engineering at Norwegian University of Science and Technology NTNU. Prof. Dorao gave me the opportunity to acquire knowledge in the world of nanotechnology creating in my enthusiasm and desire to learn. He was leading me, and he always was encouraging me to go further. Thank you for all the knowledge you transmitted me, the guidance, and for the wonderful time I spent during my days in Trondheim working with the team colleagues.

Secondly, my practical coach Diego Sánchez Saldaña is appreciated for accompanying me from the beginning. Without your knowledge and dedication this project would have been not possible.

Third, I would like to recognize the work of the nanolab staff for the care of the facilities as well as the engineers for the time you have spent training me and the advice received.

Last but not the least, The Research Council of Norway is acknowledged for the support to the Norwegian Micro-and Nano-Fabrication Facility, NorFab, project number 71642510.

Narvik, September 28,2022

Jesus Maria Tajes Vázquez

Abstract

In recent times, the manipulation of nanoparticles at nanoscale has become a topic of great interest among the scientific community. The advantages of using SAW represent a great advance in fields such as biomedicine or biosensors. The develop of these techniques is actually related with the advances achieved in the microfluidics science. For this reason, the knowledge of the physics that prevails in the handling of tiny size particles becomes something essential.

This project wants to advance in the understanding of physics behind and discuss the effects produced by the forces involved in the interaction with nanoparticles at nanoscale. For that purpose, the experiments carried out compare the obtained results with those which were made by other groups of researchers and pretends to shed light on the gaps identified in the related literature. In this regard, an attempt is made to find an answer to how a change in, for example, surface tension, the contact angle of the drop with the substrate, the viscosity and the density of the fluid affects the movement of the particles.

The use of SAW implies the development of a specific device that can channel the wave to the surface in question, this device is called interdigital transducer IDT. A SAW is the acoustic wave produced by the IDT when an electric current is applied to its electrodes. Thanks to the piezoelectric effect of the substrate where the IDT is located, the electrical signal becomes into an acoustic wave that interacts with the surface of the droplet causing an acoustic field to be created within it.

With the intention of proving the predicted events that take place inside the water droplet when it is subdue to the SAW, diverse types of IDTs able to operate at different frequencies are produced. Other parameters like the input power, frequency or the particles diameter are considered also to evaluate the involved forces when handling nanoparticles inside the sessile water droplet. The combination of these different parameters directly affects the movement of the particles inside the droplet and raises the following questions.

For instance, the interaction of the SAW with the droplet when it propagates along the substrate generates three known distinct types of forces inside the droplet. The acoustic streaming force ASF emerged from the propagation of the acoustic wave, the acoustic radiation force ARF and the centrifugal force F_c arisen as a consequence of the leakage of the propagated SAW over the substrate. In this sense, these forces are perceived by the particles arising a movement around the droplet in which they are immersed and forming different patterns of movement which are studied in this project. On the other hand, as it has been described in the literature, these forces are closely related with the particle diameter, the frequency and the input power applied to the IDT. In this vein, different particles sizes 7 μm and 1 μm of polystyrene nanoparticles immersed in a 2 μL droplet water volume were tested and four different IDTs with varying nominal frequencies 20,40,80 and 160 MHz are produced.

Sammendrag

I nyere tid har manipulering av nanopartikler på nanoskala blitt et tema av stor interesse blant det vitenskapelige miljøet. Fordelene ved å bruke SAW representerer et stort fremskritt innen felt som biomedisin eller biosensorer. Utviklingen av disse teknikkene er faktisk relatert til fremskrittene som er oppnådd innen mikrofluidikkvitenskapen. Av denne grunn blir kunnskapen om fysikken som råder i håndteringen av små partikler noe vesentlig.

Dette prosjektet ønsker å komme videre i forståelsen av fysikk bak og diskutere effektene produsert av kreftene involvert i samspillet med nanopartikler på nanoskala. For det formål sammenligner eksperimentene som er utført de oppnådde resultatene med de som ble gjort av andre grupper av forskere og later til å kaste lys over hullene som er identifisert i den relaterte litteraturen. I denne forbindelse forsøkes det å finne svar på hvordan en endring i for eksempel overflatespenning, kontaktvinkelen til dråpen med underlaget, viskositeten og væskens tetthet påvirker partiklenes bevegelse.

Bruken av SAW innebærer utvikling av en spesifikk enhet som kan kanalisere bølgen til den aktuelle overflaten, denne enheten kalles interdigital transducer IDT. En SAW er den akustiske bølgen som produseres av IDT når en elektrisk strøm påføres elektrodene. Takket være den piezoelektriske effekten av substratet der IDT er plassert, blir det elektriske signalet til en akustisk bølge som samhandler med overflaten til dråpen og forårsaker at det dannes et akustisk felt i den.

Med den hensikt å bevise de forutsagte hendelsene som finner sted inne i vanndråpen når den er underlagt SAW, produseres forskjellige typer IDT-er som kan operere ved forskjellige frekvenser. Andre parametere som inngangseffekt, frekvens eller partikkeldiameter vurderes også for å evaluere de involverte kreftene ved håndtering av nanopartikler inne i den fastsittende vanndråpen. Kombinasjonen av disse forskjellige parameterne påvirker direkte bevegelsen av partiklene inne i dråpen og reiser følgende spørsmål.

For eksempel genererer samspillet mellom SAW og dråpen når den forplanter seg langs substratet tre kjente forskjellige typer krefter inne i dråpen. Den akustiske strømningskraften ASF oppsto fra forplantningen av den akustiske bølgen, den akustiske strålingskraften ARF og sentrifugalkraften Fc oppsto som en konsekvens av lekkasjen av den forplantede SAW over underlaget. Slik sett blir disse kreftene oppfattet av partiklene som oppstår en bevegelse rundt dråpen de er nedsenket i og danner forskjellige bevegelsesmønstre som studeres i dette prosjektet. På den annen side, slik det er beskrevet i litteraturen, er disse kreftene nært knyttet til partikkeldiameteren, frekvensen og inngangseffekten som påføres IDT. I denne venen ble forskjellige partikkelstørrelser 7 µm og 1 µm av polystyrennanopartikler nedsenket i et 2 µL dråpevannvolum testet og fire forskjellige IDT-er med varierende nominelle frekvenser 20,40,80 og 160 MHz ble produsert.

Table of Contents

List of Figures

List of Graphics

List of Units

Unit	Description
Kg m^{-3}	Kilograms per cubic metre
m s^{-1}	Metre per second
Pa^{-1}	Pascal
mPa s	Millipascal
mJ	Megajoule
cm^2	Square centimetres
N_2	Nitrogen
g	Gram
ml	Millilitre
nm	Nanometres
µL	Microliters
µm	Micrometres
mW	Milliwatts
mg/mL	Milligram per millilitre
Kg m^{-1} s^{-1}	Kilograms per metre and second
°C	Celsius degrees

List of Abbreviations (or Symbols)

Symbol	**Description**
DPI	Dots per inches
NTNU	The Norwegian University of Science and Technology
PDF	Portable Document Format
Prof	Professor
SAWs	Surfing Acoustic Waves
ASF	Acoustic Streaming Flow
ARF	Acoustic Radiation Force
IDT	Interdigital Transducer
R1	Regimen 1
$LiNbO_3$	Lithium niobate
F_D	Drag force
F_R	Radiation force
ISO	International Organization for Standardization
DEP	Dielectrophoresis
kDa	KiloDalton
bct	Body centred tetragonal
R	Particle radius
PS	Polystyrene
TSAW	Travelling Surface Acoustic Wave
λ_s	Sound wavelength on the substrate
λ_f	Sound wavelength on the fluid
C_s	Speed of the sound in the substrate
C_f	Speed of the sound in fluid
ρ_s	Density of the substrate
ρ_f	Density of the fluid
X_s	Attenuation of the acoustic wave on the surface
X_f	Attenuation of the acoustic wave on the fluid
f	Frequency
d	Spacing and fingers width
TSAW	Travelling acoustic wave
SSAW	Standing surface acoustic wave
Φ	Contrast factor
ρ_p	Density of the particle
β_p	Compressibility of the particles
β_f	Compressibility of the fluid
P_0	Acoustic pressure
V_p	Volume of the particle
λ	Wavelength
k	Wave vector
x	Distance from a pressure node

η	Viscosity of the fluid
v	Dynamic ASF velocity
CN	Catalogue number
MD	Mean diameter
PC	Particle concentration
U	Relative streaming velocity
μ	Dynamic viscosity of the fluid
PDMS	Polydimethylsiloxane
N_p	Number of fingers
Q	Quality factor
Δf	Frequency deviation
d	Finger width and spacing
W	Aperture
λ	IDT period
$\hat{A}$	Acoustic displacement
U_{as}	Acoustic streaming velocity
U_{sm}	Convective particle velocity

1 Introduction

1.1 Motivation and background

From its approach until recent years, many research groups have tried to explain the flows that take place inside a droplet when it is subjected to surface acoustic waves. To the date three main forces have been identified to explain the particle movement inside the droplet. The centrifugal force (F_c), the acoustic streaming flow (ASF) and the acoustic radiation flow (ARF). The discussion raised by some groups of researchers like Destgeer et al [1], Yuka et al [2], Rogers et al [3], Raghavan et al [4] or Li et al [5] about how these forces interact with the nanoparticles is not only whether these three forces alone are entirely responsible for the movement of the particles, but also to quantify these forces. A suitable method to analyse this process consists of placing a droplet over a piezoelectric surface where an embedded IDT generates an ultrasound field.

In this regard, the study of the ultrasound imposed on a fluid containing a suspension of particles is a suitable method for the observation of how the above commented forces interacts with particles. The latter will be affected by the so-called acoustic radiation force arising from the scattering of the acoustic waves on the particle. The particle motion resulting from the acoustic radiation force is denoted acoustophoresis [6]. Therefore, depending on the strength of the ultrasound field created, different movement patterns of the particles suspended on a fluid can be observed. In addition, this method has been found useful in applications such as biology and medicine for concentration [7], [8] mixing [9], [10],delivery [11], and cell/particle separation [12] [8], [9], [10]. Surface acoustic wave devices have become popular as well as a practical and effective tool for fluid jetting and atomization in various acoustofluidics and biomedical applications in recent years [15].

However, the use of the surface acoustic waves remains an emerging field of research. The acting forces behind particle movements demands to advance the understanding of the interactions of the acoustic forces with the particles. In particular, the radius and densities of the particles, the density and viscosity of the fluid, the frequency, wavelength, and attenuation coefficient of the acoustic wave [9], play a significant role in the movement of the particles.

In this work, an approximation to the understanding of how these parameters are related to each other to generate different particle movements using acoustofluidic devices will be studied. Gaps in the literature are identified and from the observation in the experimentation a discussion of them is elaborated. As well the obtained results will be analysed with a particle tracking software and will be compared with the results exposed by other researcher groups in the literature. The approach will consist in the analyse of the relationship between acoustic forces and a set of polystyrene particles suspended inside of a water sessile droplet when an ultrasound flied is imposed.

1.2 Objectives

The main goal of the project is to understand the physics of the acoustofluidics induced forced in the motion of micro nano size particles. For that purpose, a video was recorded during the experiments for its posterior analyse. In this regard, a discussion of the results is also included with the aim to shed light on parameters that have been not mentioned in the selected literature. These parameters are the surface tension, the viscosity, the density, and the contact angle of the droplet.

The main objective of this project is to study the motion of particles inside a sessile droplet under flow streaming induced by surface acoustic waves. In terms of the parameters like frequency, input power and the particles diameter, the study is intended to reproduce the conditions that leads to different patterns of movement inside of the sessile droplet. Thus, a concentration of particles as well as the ring formation around the perimeter of the droplet as a consequence of the forces arising from the imposed ultrasound field.

To accomplish this objective the following sub-tasks were carried out:

1- To design and produce a variety of devices capable of generating acoustic waves, thus an interdigital transducer (IDT).

2- To prepare samples and set up a specific stage to carry out the relevant experiments to observe the movement of the particles.

3- Evaluate the experiments by using a fluorescent microscope and the corresponding software to analyse the collected data.

4- Discuss and compare the obtained results with previous studies.

1.3 Scope of the work

This project consists in an experimental study in which a water droplet is submitted to a surface acoustic wave (SAW) produced by an interdigital transducer (IDT). Particles of 1μm and 7 μm of diameter will be used. Four different IDTs were produced with 20, 40, 80, 160 MHz as nominal operation frequency, respectively. The volume of the droplet will be a fixed parameter for all the experiments in 2 μL. The type of the designed acoustofluidic device is a straight IDT and the droplet will be placed in its offset.

The material of the used particles is polystyrene with a density of 1050 Kg m^{-3}.

The substrate of the device is made of Lithium niobate (YX 128º $LiNbO_3$) with a density of 4630 kg m^{-3}.

The density of the water droplet at the temperature of the room (20°C) is 998 kg m^{-3}.

1.4 Structure

With the intention of organize all the information acquired during the process, the document is divided in different chapters as follows below.

Chapter 2, in this section, the physics phenomena beyond SAWs is detailed.

Chapter 3, in this chapter, studies related to the forces involved in the particles movements inside of sessile droplets are presented.

Chapter 4, the IDT parameters, and the fabrication process of the IDT is described. The result of the manufacturing is presented as well as a description of the stage for the experiments.

Chapter 5, the followed method to process the collected data is reported in detail in these lines.

Chapter 6, this episode is dedicated to compare the obtained results with the previous observations made in other studies.

Chapter 7, conclusions of the obtained results related to this project are commented in this chapter.

Chapter 8, in this last section new lines for the researching are proposed.

2 Theory background and IDTs

2.1 Surface acoustic waves SAWs

An acoustic wave is a type of mechanical wave that propagates along a longitudinal wave driven by an acoustic source, generated by the mechanical stress from a piezoelectric transducer. An acoustic wave that propagates in one direction and radiate away from the acoustic sources are defined as the surface acoustic wave (SAW).

A typical SAW device uses at least one interdigital transducers (IDTs) fabricated on the surface of a piezoelectric substrate. An IDT consists of a set of connected metallic fingers interspaced with an opposite set of connected metallic fingers.

To generate a SAW, an alternating current electrical signal is applied across the two sets of connected fingers of the IDT. Given the piezoelectric property of the substrate this electrical signal turns into acoustic waves that propagate along the surface.

The following picture illustrate an acoustofluidic device. The IDT produces SAWs that interact with the sessile droplet placed at a position offset from the centre of the IDT.

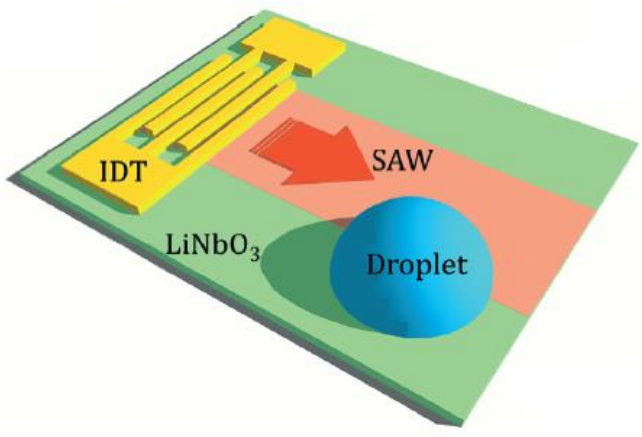

Figure 1. Schematic diagram of the acoustofluidic device

For a water droplet placed upon the piezoelectric substrate of a SAW device, the incident SAW radiation is strongly absorbed. As a SAW (Rayleigh wave) interacts with the liquid droplet, it attenuates at a length scale of X_s on the surface whereas the leaky SAW (a compressional wave) attenuates inside the fluid at X_f. The SAW propagating on the surface (with lower frequency) is reflected back from the boundary of the liquid droplet and produces strong standing surface acoustic waves (SSAW) [16].

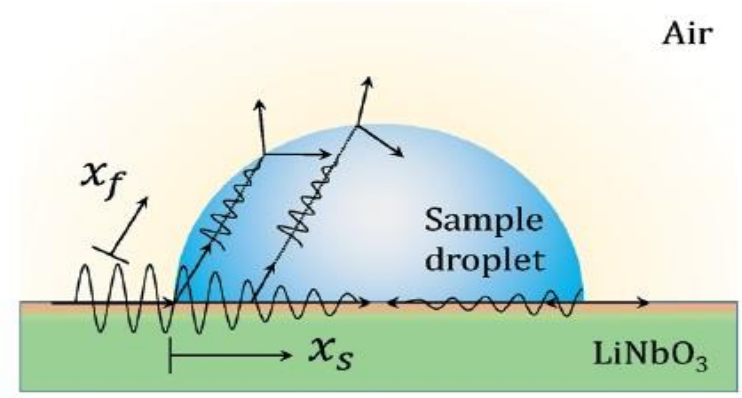

Figure 2. Schematic representation of the rayleigh wave

The leakage acoustic wave into the droplet occurs at the Rayleigh angle at:

$$\theta_R = Sin^{-1}.\left(\frac{C_f}{C_s}\right)$$

Where C_f and C_s are the acoustic velocities of liquid and substrate material, respectively. This will generate a longitudinal sound wave, which induces acoustic streaming within the droplet.

Generally, acoustic streaming is the time-averaged steady flow that is forced by the effect of Reynolds stresses, where the momentum that forces fluid to flow is related to the dissipation of acoustic energy [17].

The particles suspended inside the sessile droplet are not only influenced by the acoustic streaming flow (ASF), but also by the acoustic radiation force (ARF). Fig. 3 illustrates the schematics of the representation of micro-object manipulation and microfluidic actuation via SSAWs.

Firstly, for constant-frequency SSAW and particles with smaller diameters, the particles are trapped in the ASF vortices (see Fig.3 (A)). The particles subjected to the ASF experience the drag force F_D, and the ASF-based Stokes drag force is defined by [18], [19].

$$F_D = 3\pi\eta d_p v$$

Where η and v are the dynamic viscosity of the fluid, respectively, and d_p is the diameter of the particles

Secondly, a pair of acoustic waves propagating in opposite directions forms a standing acoustic wave field with regions of pressure nodes and anti-nodes, respectively, as shown schematically in (Fig. 3 (B)). The sound pressure fluctuations of the standing acoustic wave bring the ARF acting on the particles, which is based on the scattering of sound pressure

by the particles, as shown schematically in (Fig. 3 (C)). Particles flowing into the SSAW field experience the acoustic radiation force, F_R, which can be expressed as [21], [27].

$$F_R = -\left[\frac{\pi P_0^2 V_p B_f}{2\lambda}\right].\Phi(\beta,\rho).Sin(2kx)$$

Where P_0, V_p, λ, k, x, *are* acoustic pressure, volume of the particle, wavelength, wave vector and distance from a pressure node, respectively.

$$\Phi(\beta,\rho) = \frac{5\rho_p - 2\rho_f}{5\rho_p + 2\rho_f} - \frac{\beta_p}{\beta_p}$$

This term equation describes the acoustic contrast factor Φ, which determines whether the particle moves to pressure nodes or pressure antinodes in the SSAW field: the particle will move towards pressure nodes when $\Phi > 0$ and pressure anti-nodes when $\Phi < 0$. Where ρ_p, ρ_f, β_p and β_f density of the particle, density of the fluid, compressibility of the particle, compressibility of the fluid respectively

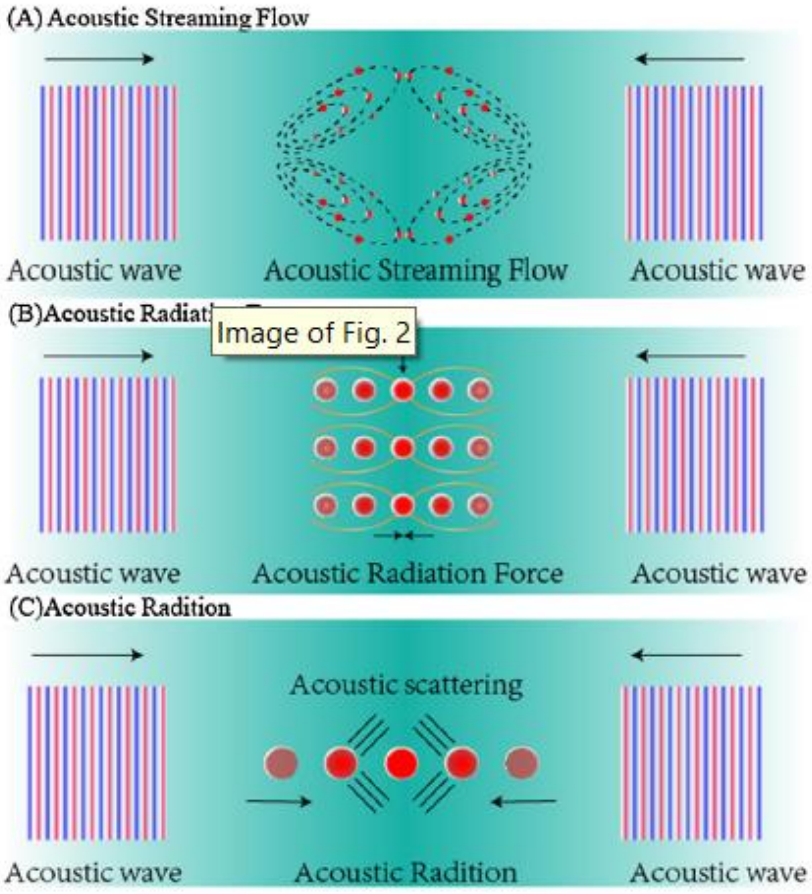

Figure 3. Manipulation of micro-object and microfluidic actuation via SSAWs. [25]

2.2 SAW generation

As previously mentioned, an IDT device able to generate a SAW is required. Basically, an IDT consists in a determinate number of periodic metallic bars called fingers (N). These strips which are aligned and connected to the busbars periodically are deposited on the surface of a piezoelectric substrate, such as Z_NO or $LiNbO_3$, and conducts the generated surfing acoustic waves (SAW) through the surface [26]. To achieve this, first, is necessary to convert the electrical signal received from a signal generator into surfing acoustic waves (SAW). This conversion occurs thanks to a piezoelectric effect that takes place in the substrate in which after a painstaking fabrication process IDT is embedded. In the following picture an example of two-faced IDTs is observed.

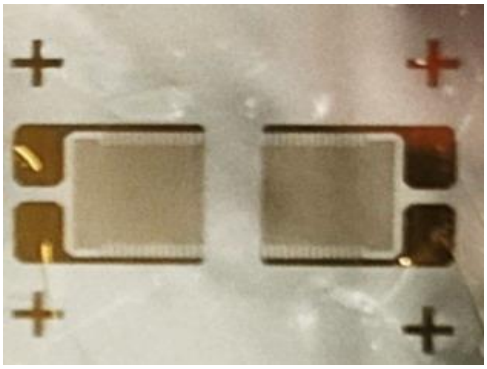

Figure 4. Structure of a two-faced straight IDTs fabricated in NTNU nano-lab

2.3 Design of the IDTs

The formation of the SAW depends mainly on the nominal frequency at which the IDT operates. Find an optimal frequency depends on many parameters that should be considered, such as, the droplet location (offset), the particles diameter d_p, the k factor, the attenuation of the acoustic wave in the positive X-axis direction denoted in this work by X_s. Parameters related to the architecture of the IDT like the number of fingers and the reflectors have an important impact in the efficiency SAW production. The thermal effects are also an important parameter of design. For instance, in the experiments in which the time is a crucial factor. The higher hot dissipation of the substrate related to operational parameters in the experiment leads to a faster droplet evaporation causing a distortion at the time to acquire relative data.

2.3.1 Droplet Offset

The ASF field depends greatly on the SAW actuation frequency, droplet volume and droplet exposure to SAW.

It has been observed that the SAW attenuation length (X_s) on the surface of a piezoelectric substrate as it interacts with a droplet (with radius r_d) plays an important role in driving the ASF, and that it is difficult to create ASF symmetrical vortices at low frequencies (~10 MHz) when ($X_s > r_d$) and the exposure to the acoustic field is uniform [16]. For that reason, to produce an ASF at low frequencies (with $X_s > r_d$), the droplet is either placed at the edge of an interdigitated transducer (IDT) for asymmetric exposure to the sound waves. This explain why the droplet is placed in the offset of the IDT. The following pictures illustrate this idea which was followed in this project.

In the first picture can be observed how the SAW reach the limit boundary of the droplet and it is reflected back facing the incoming pressure wave creating standing surface acoustic waves SSAW which leads to a unstable vortex. For that reason, if the aim is to create a single vortex is preferably an asymmetric set up [2].

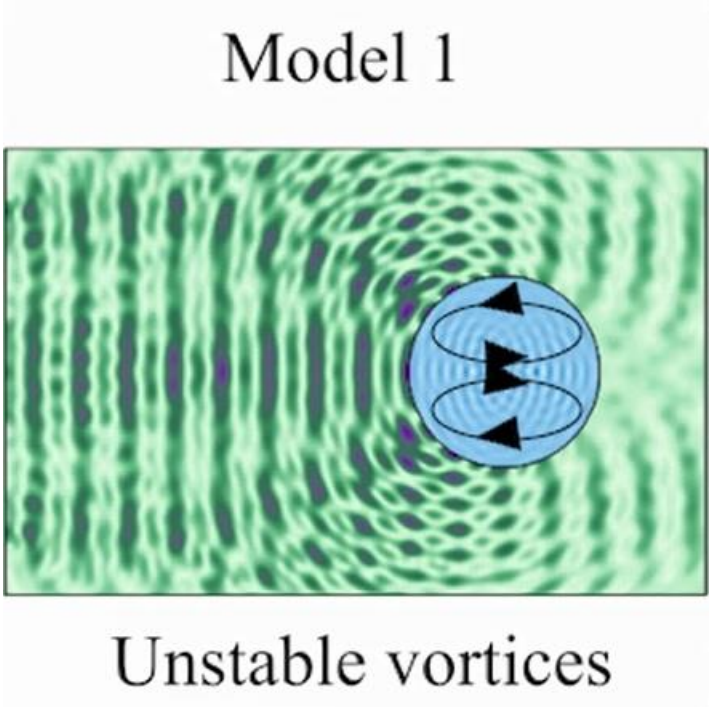

Figure 5. Symmetrical SAW device [2]

In this picture an asymmetric exposure to the SAW is depicted. The SAW encounters the droplet and the reflected SAW from the boundary of the droplet constructively couples with the incident wave originating a single vortex inside of the sessile droplet as can be seen in the picture.

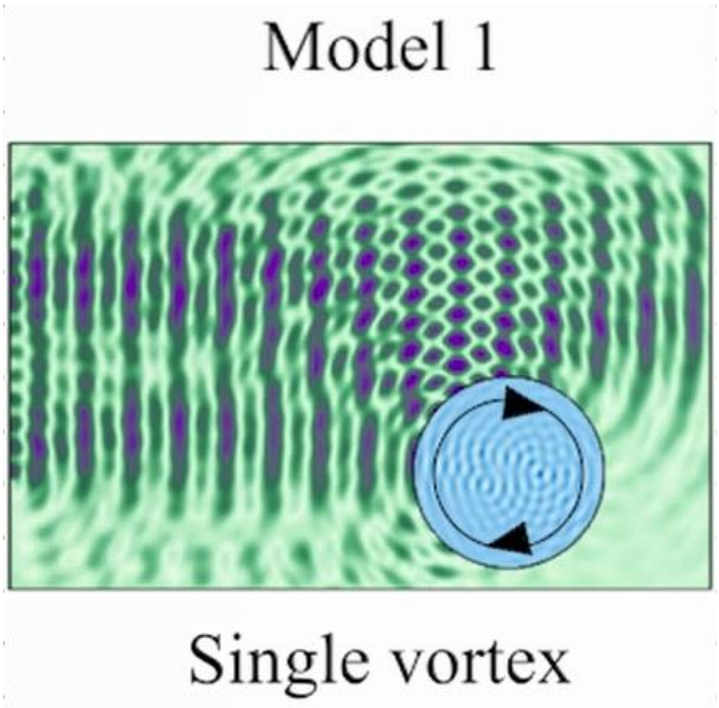

Figure 6. Asymmetrical SAW device [2]

2.3.2 Particles diameter

As will be commented in the next sections, the size of the particles plays a key role in terms of the dominant force causing the movement of the particles. Considering the sound pressure fluctuations of the standing acoustic wave bring the ARF acting on the particles [25]. The operating frequency and the input power for the experiments will be obtained as a function of the size of the particles of 1 μm and 7 μm forming a ring shape around the droplet periphery or a particle concentration.

2.3.3 k factor

The size of the particle with respect to the wavelength of the acoustic wave plays a vital role in the microparticle manipulation and can be determined using the k factor.

$$k = \pi \frac{d_p}{\lambda_f}$$

Where λ_f is the wavelength of the acoustic wave in fluid and d_p is the diameter of the particle [16].

It has been reported that the ARF acting on a PS (Polystyrene) particle due to a TSAW dictates the motion of the particle if $k > 1$. However, the ARF due to standing surface acoustic waves (SSAWs) is usually dominant over that due to the TSAWs for $k < 1$ [16].

Attending to the relationship between wavelength and frequency $\lambda_f = C_f/f$.Where C_f is the speed of the sound in the fluid and f is the frequency applied to the IDT. For a SSAW formation and a strong ARF, a lower frequency of acoustic waves is used, which results in a smaller value of k.

2.3.4 Attenuation X_s

The calculation of X_s is crucial to characterising the different acoustic field formations inside the fluid domain. For example, at low frequencies (when $X_s > r_d$), the formation of standing acoustic waves concentrates the particles at the centre of the droplet [16].

To calculate the attenuation of SAW at a length scale of X_s on the surface the following equation is employed.

$$X_s = \frac{\rho_s C_s \lambda_s}{\rho_f C_f}$$

Where ρ_s = 4630 kg m^{-3} and ρ_f = 998 kg m^{-3} are the densities of the piezoelectric (LiNbO3, lithium niobate) substrate and the fluid (water), respectively; $C_s \cong$ 3950 m s^{-1} and $C_f \cong$ 1480 m s^{-1} are the speeds of sound in the substrate and fluid respectively; and $\lambda_s = C_s/f$ is the sound wavelength on the substrate [16].

On the other hand, the attenuation of sound wave in fluid X_f is given by the following expression where μ represents the dynamic viscosity of the fluid (water at 20°C ~.0,001003 Kg/m s).

$$X_f = \left(\frac{3}{16}\right) \times \left(\frac{C_f^3 \rho_f}{\mu \pi^2 f^2}\right) \qquad [4]$$

However, the compressional wave inside the fluid attenuates at a much longer distance; therefore, we can neglect the attenuation of sound wave in the fluid (X_f) and focus on the rapidly attenuating SAW (X_s) [16].

2.3.5 Number of fingers N_p

The efficiency of a SAW device is commonly linked to its quality factor Q [27]

$$Q = \frac{f_r}{\Delta f}$$

where Δf is the width of the resonant peak in frequency space measured at one-half the peak's highest amplitude and f_r is the centre frequency.

The quality factor is influenced by dielectric losses of the piezoelectric materials, loading effects, ohmic losses, and acoustic leakage to the substrate.

A high Q value means higher SAW efficiency. The number of finger pairs N_p of an IDT is an important parameter partially due to its effect on the quality factor [27]. Since a Δf supposes an optimal manufacturing result. By this equation, an appropriate number of fingers for a determinate frequency of operation can be estimated. In this project an optimistic value of $\Delta f \sim 4\ MHz$ of desviation is accepted.

$$\frac{\Delta f}{f_r} = \frac{1}{N_p}$$

The other aspect that drives the choice of the number of finger pairs in a SAW IDT is the effective piezoelectric coupling coefficient of the substrate, which can be defined in terms of the change of SAW velocity from an open-circuit configuration to a short-circuit configuration, divided by one-half of the average of that velocity, $2\Delta v/v$ [27].

The greater the coupling, the greater the amount of energy that can be transduced in the IDT to mechanical output as a SAW [27].

A priori one might think that a high number of fingers or electrodes would notably increase efficiency, however, this is not true. An excessive N_p implies a greater insertion loss cause of the reflection of the waves and consequently a lack of effectiveness of the SAW.

2.3.6 Reflectors

Reflection waves are related to the generation of the saw and arise by a simple physical process. A surface wave incident on the transducer causes a voltage to appear across the bus bars. This voltage causes excitation of secondary surface waves (in both directions), just as it would if there were no incident surface wave. One of these waves is of course in the direction opposite to the incident wave, and this is the reflected wave.

This effect is of great relevance in «single-electrode» IDTs. Each electrode reflects only weakly, but the reflections become significant if they are added in phase, such is the case of the single-electrode IDT that was designed in this project.

To reduce the insertion loss of the IDT, a SAW reflector can be used to reflect one of these waves in the opposite direction. A SAW reflector, also called reflection gratings, are composed of periodically spaced discontinuities on the piezoelectric SAW propagating surface. To construct these reflection gratings, short-circuited electrode fingers, identical to the ones of the SAW generating IDT, are deposited on the piezoelectric surface. These electrodes are not connected to an electrical potential, nor ground. When a series of reflector electrodes are located at a distance λ/4 from the closest electrode finger on the IDT, the reflected SAW will have an additive effect to the SAW propagating in the direction away from the reflectors [28] [29].

2.3.7 Thermal effects

Other important aspect in the design of IDTs is the thermal effects that occurs over the surfaces when SAW propagates.

This phenomenon has already been described in the literature. In this case, the researchers used a rectangular piece of PDMS to observe the thermal effects that took place as a consequence of the propagation of SAW. As leaky SAWs propagate in the PDMS, they are attenuated to have a limited depth of penetration due to the viscosity-associated thermal dissipation of energy [30].

In addition to this, exist a relationship between the penetration depth of the leaky SAW with the medium in which it is attenuated and the frequency at SAW was generated. The following equation show this relation.

$$\delta \sim f^{-\gamma}$$

Where δ is the penetration depth, f is the acoustic wave frequency, and γ is a real non-negative material parameter fitted to be approximately 0,7 for PDMS. In the same vein this effect occurs in other surfaces like a droplet. The following images show how at low frequencies the penetration of the wave is greater and the thermal effects related to the energy dissipation increase, producing greater heating on the surface as can be observed in the figure 7 and 8.

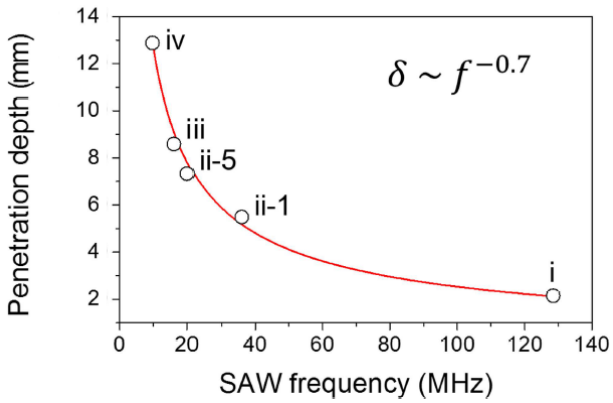

Figure 7. Penetration depth vs SAW frequency [30]

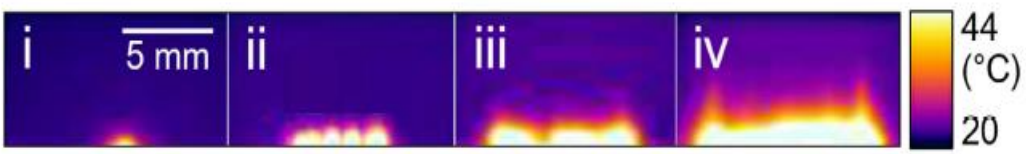

Figure 8. Heating of the surface in function of the penetration and SAW frequency [30]

3 Relevant studies conducted on SAW in droplets

This section summarizes chronologically some of the most important works carried out in the last decades. The purpose of these works is to explain the movement of particles inside a sessile droplet when is submitted to a SAW over a piezoelectric substrate. Based on the acting forces over the particles commented on the previous section these studies conduct to a better understanding of how by controlling theses forces different patterns of movements are observed.

3.1 Li et al (2007) "Surface acoustic wave concentration of particle and bioparticle suspensions"

The group of Li et al. conducted their experiments with the motivation of using SAW to concentrate particles inside a droplet. The purpose is to establish a method to overcome the disadvantages of using piezoelectric biosensors or conventional methods, such as centrifugation [5]. The scope of the experiment was that one which was able to keep fixed the droplet over the substrate. If the intensity of the acoustic radiation component into the fluid is sufficiently high and the liquid consists of a free droplet whose contact line is not pinned, the SAW can induce the droplet to translate in the direction of the SAW. This study considers the case where the acoustic intensity is lower than the threshold required to translate the drop [5].The scope of the work is a droplet is subdued to a SAW in an asymmetrically configuration respect the SAW propagation direction. The frequency used in this experiment was 8,611 MHz and the studied objects consisted in fluorescent particles suspended into a 5 μL sessile droplet (1 μm). polystyrene microspheres (3, 6, 20, 45 μm). Living yeast cells (10–20 μm). To evaluate the forces involved the following schema was created.

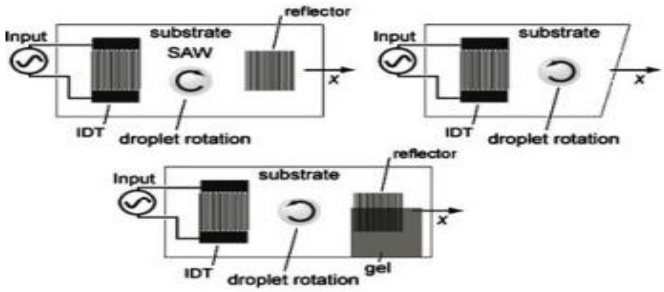

Figure 9. Schemes for symmetry breaking of SAW propagation. [5]

When the SAW intensity is such that the droplet is not vibrating or transporting a recirculation fluid bulk is observed and it creates an azimuthal streaming.

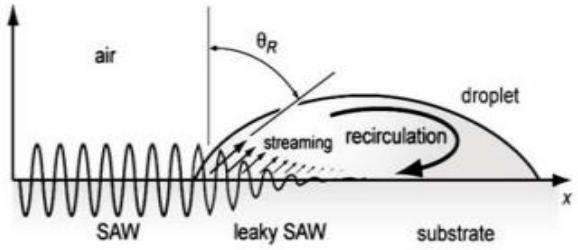

Figure 10. Sketch of the acoustic streaming acting on a small droplet on the SAW surface. [5]

In the next picture, images at 60 frames/s showing the visualisation of azimuthal bulk recirculation generated by asymmetric SAW propagation through dye streamlines induced by the flow [5].

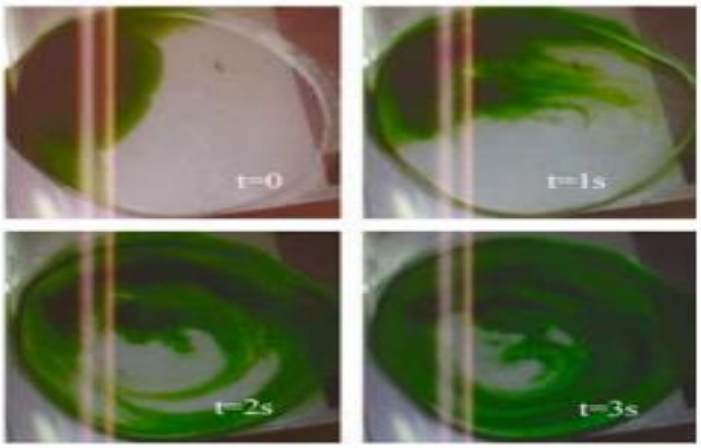

Figure 11. Visualisation of azimuthal bulk recirculation generated by asymmetric SAW [5]

The observations after the experiments were that the shear induced migration arise due to azimuthal velocity gradients which result in the transportation of particles across azimuthal streamlines into the interior of the vortex. (Inward direction).

Azimuthal acoustic streaming arises of the recirculation flow inside the droplet. (Outward direction) [5].

Regarding to the input power was found that for the given frequency an optimal value of 300 mW has the best performance in particle concentration. For the values below the critical convection velocity is not enough for particle concentration, however, higher values the large acoustic streaming velocity cause a redispersion [5].

The dominance between shear induce migration and bulk internal convection is described as follows.

$$\chi \equiv \frac{U_{as}}{U_{sm}}$$

Where U_{as} is the acoustic streaming velocity while U_{sm} refers to the convective particle velocity. The next expression was obtained to describe the relationship between some parameters affecting the dominance in this experiment.

$$\mu_{as} = \frac{PR^2}{7.11\mathrm{c}\mu Al}$$

Where *P* is the acoustic streaming power. *R* is the particle radius. *A* is the area across the power is applied and l is referred to the acoustic absorption length and finally μ is related to the fluid viscosity [5].

From this expression is easy to see how the above-mentioned parameters play an important role in the particles motion when a droplet is subdued to a SAW. To establish how these forces act the following experimental relationship was obtained.

Depending on the input power applied one effect dominated over the other.

$\chi \approx 2$ Shear induced migration dominates and particle concentration is achieved [5].

$\chi \neq 2$ Bulk internal convection dominates; the large acoustic streaming velocity cause a redispersion [5].

3.2 Raghavan et al (2009) "Particle concentration via acoustically driven microcentrifugation"

Following with this idea Raghavan et al. was the first in introduce a 3D model to study the three-dimensional flow field structure of the azimuthal fluid recirculation in a sessile drop induced by asymmetric surface acoustic wave radiation. In the study a frequency of 19,37 MHz generating the SAW over 5 µL volume droplet in which particles of 30 µm (melamine) were immersed. Similar as Li et al (2007) the following schema was proposed to break the SAW symmetry propagation.

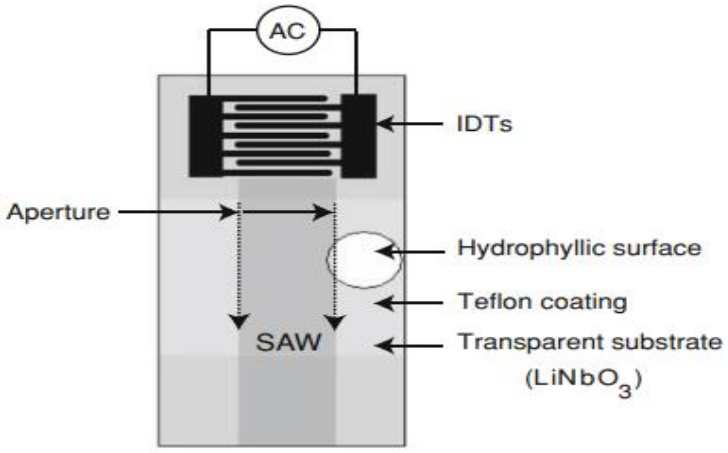

Figure 12. The SAW device used in the particle concentration experiments [4]

The observations made in during the experiments were as follows. Fluid recirculates downward in a spiral-like manner around the periphery of the drop. Particles suspended in the flow field therefore follow the fluid trajectory and are convected in a spiral-like manner akin to an inverted cone structure to the bottom region of the drop. Azimuthal velocities generated in the fluid increase both with height in the drop and radial distance from the centre [4].

In the left-hand plane of the droplet velocities seems to be higher because it is closer to the SAW radiation path. In the following picture this idea is depicted.

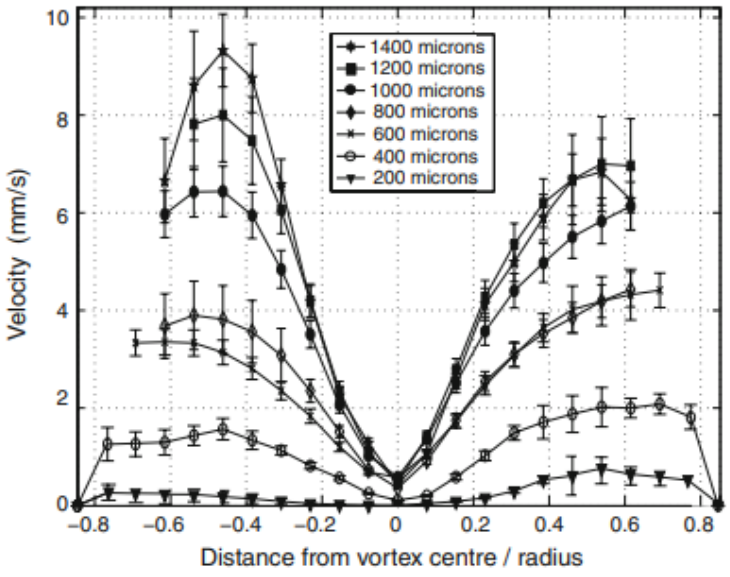

Figure 13. In-plane velocities across the height of the drop obtained from experiments [4]

Fluid recirculates downward in a spiral-like manner around the periphery of the drop. Particles suspended in the flow field therefore follow the fluid trajectory and are convected

in a spiral-like manner akin to an inverted cone structure to the bottom region of the drop. In the vicinity footprint the fluid flows diagonally and following the Rayleigh angle and decays on the SAW propagation direction. Is observed how the bigger size particle reach higher velocities which is consistent with the observed relation between the AFR and the particles diameter [4].

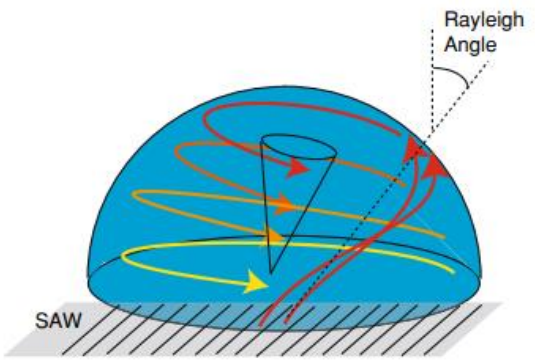

Figure 14. Schematic illustrating the fluid-SAW interaction leading to the azimuthal velocities observed [4]

Close to the friction surface at the fluid-substrate interface, this layer is also known as the noun of Eckman layer, the particles together with the fluid are then forced inwards radially once they enter this boundary layer region [4].

The fluid recirculates back up a central column in the middle of the drop due to flow conservation, but the particles are trapped and stack into a heap at a central stagnation point at the bottom [4].

If, however, the convection is sufficiently strong, for example, by increasing the applied power beyond a threshold value, these particles escape from the agglomerate and are redispersed in the bulk, consistent with previous two-dimensional observation. This is illustrated in the following picture.

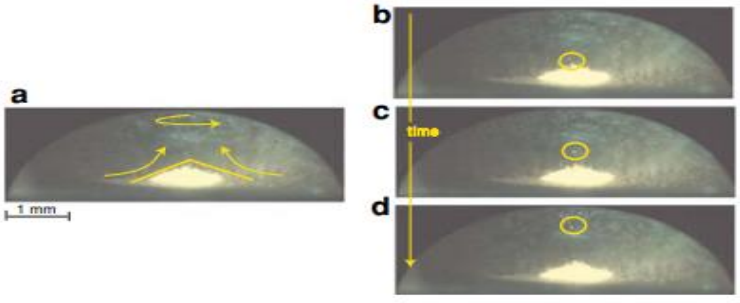

Figure 15. Illustration of the effect of the Ekman layer in establishing the meridional flow which leads to the conical heap of particles in the centre [4]

3.3 Rogers et al (2010) "Exploitation of surface acoustic waves to drive size-dependent microparticle concentration within a droplet"

The motivation of this work was to elucidate the physics between fluid drag and acoustic forcing on the particles within a droplet. The novelty of this study was to consider the particles as rigid bodies. The scope of the experiment was based on an asymmetric SAW distribution creating a bulk acoustic streaming due to the closed volume of the droplet. Different droplets with volumes in the range of 1,5-3 μL with immersed polystyrene particles sizes between 2–31 μm were used. The frequencies employed were 10,20,30 MHz.

The main observation of the experiment was as follows. Acoustic streaming is the time-averaged steady flow that is forced by the action of Reynolds stresses, where the gradient in momentum flux that forces fluid to flow is associated with the dissipation of acoustic energy flux. A suspended particle subjected to these streaming experiences a steady drag force and is given by the following expression [3].

$$F_D = 6\pi\mu UR$$

Where R is the particles radius while U and μ is the relative streaming velocity and the dynamic viscosity of the fluid, respectively.

By managing the parameters involved in the next expression. Acoustic radiation force arising from the radiation pressure over the particle surface can also be exploited for particle manipulation [3].

$$F_{AR,L} = 2\pi\rho\left(\frac{2\pi f}{cf}\right)^4 R^6|\xi^2|\frac{1+\frac{2}{9}\left(1-\frac{\rho}{\rho_P}\right)^2}{\left(2+\frac{\rho}{\rho_P}\right)^2}$$

The schema for the experiments is shown in the next picture, the arrow represents the horizontal–plane projection of the acoustic streaming. Once again, the asymmetric SAW is employed to generate a vortex inside the droplet.

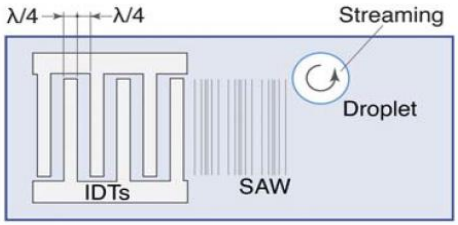

Figure 16. Illustration of the experiment set up [3].

Other important observation was made by the researcher group. For particle manipulation exist a critical size range in which the acoustic radiation force dominates over the drag force. Depending on the frequency applied there is a critical particle size which defines the domination of the F_D or F_{AR}. This critical size is given by $F_{AR}=F_D$ [3]

The critical particle size is given as follows. When a frequency of 20 MHz is applied the particle size is between 20-25 μm. On the other hand, 30 MHz is necessary when the suspended particles have a size in the range of 15-20 μm [3].

This shows that is possible to manipulate particles based on both frequency and particle size.

The researcher group observed also that the previous experiment could be applied for particle partitioning where two different sizes particles are partitioned based on the force which affects each one related to the size of the particles. In this case particles of 6 μm concentrate due to the drag force, secondly, 31 μm are driven to the periphery due to radiation force. This is depicted in the next picture.

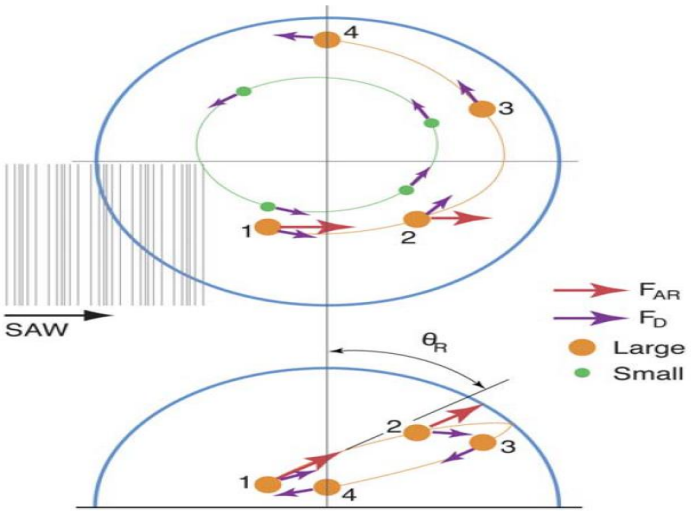

Figure 17. Schematic representation of the involved forces [3].

3.4 Destgeer et al (2016) " Acoustofluidic particle manipulation inside a sessile droplet: four distinct regimes of particle concentration"

In this work is presented the influence of ASF and ARF in the particle concentration inside of a droplet. Given the existence of the ARF between particles is possible through a controlled frequency establish a correlation between the involved forces to create different patterns of particles movement. Through these experiments asymmetrical flow is deepened and new point of view to explain the interactions between particles is introduced. In this project elastic particles are considered, and this leads to different behaviours of the particles under SAWs. The frequencies used range from 10 to 133 MHz with input power from 150 mW to 600 mW. Particles with 1μm, 3μm, 5μm 10 μm are utilized for the different experiments. The volume droplet is fixed for all experiments in 5μL.

The principal observations are based on considering the elasticity of the particles which leads to different behaviors of the particles under SAWs. 4 different movement regimes are observed.

In this study the difference between travelling and standing surface waves S_{SAW} is introduced. In this manner, to make the difference between these proposed differences a factor *k* was presented under the effect of travelling surface acoustic waves T_{SAW}. On the other hand, the expression of X_s quantify the attenuation of the SAW in the substrate.

The k factor relates the diameter of the particles with the wavelength of the frequency applied for any case.

$$k = \pi \frac{d_p}{\lambda_f}$$

The attenuation of the SAW in the surface is given by the following expression.

$$X_s = \frac{\rho_s C_s \lambda_s}{\rho_f C_f}$$

Also, an expression for the attenuation of SAW in the fluid was proposed.

$$X_f = \left(\frac{3}{16}\right) \times \left(\frac{C_f^3 \rho_f}{\mu \pi^2 f^2}\right)$$

The correlation between theses formulations is gathered in the next illustration. Can be observed how for the different operating parameters different movements regimes were recorded and four different regimes identified as R1, R2, R3 and R4 were achieved during

the experiments. By describing the process, (a) Interdigitated transducer (IDT) producing surface acoustic waves (SAWs) that interact with the sessile droplet placed at a position offset from the centre of the IDT. (b) As a SAW (Rayleigh wave) interacts with the liquid droplet, it attenuates at a length scale of X_s on the surface whereas the leaky SAW (a compressional wave) attenuates inside the fluid at X_f. The SAW propagating on the surface (with lower frequency) is reflected back from the boundary of the liquid droplet and produces strong standing waves. (c) The SAW interacts with the droplet at the top-left boundary (top view) and creates an ASF with a single vortex. Four different regimes (R1–R4) of particle concentration are identified based on values of k and X_s, and are colour-coded as green, orange, gold and blue, respectively. Solid lines indicate the location of the particles being concentrated in a particular case. (d) Experimental representation of the four regimes, where particle diameters and actuation frequencies are also listed. Snapshots of the sessile drops, before and after the SAW actuation, are shown [16].

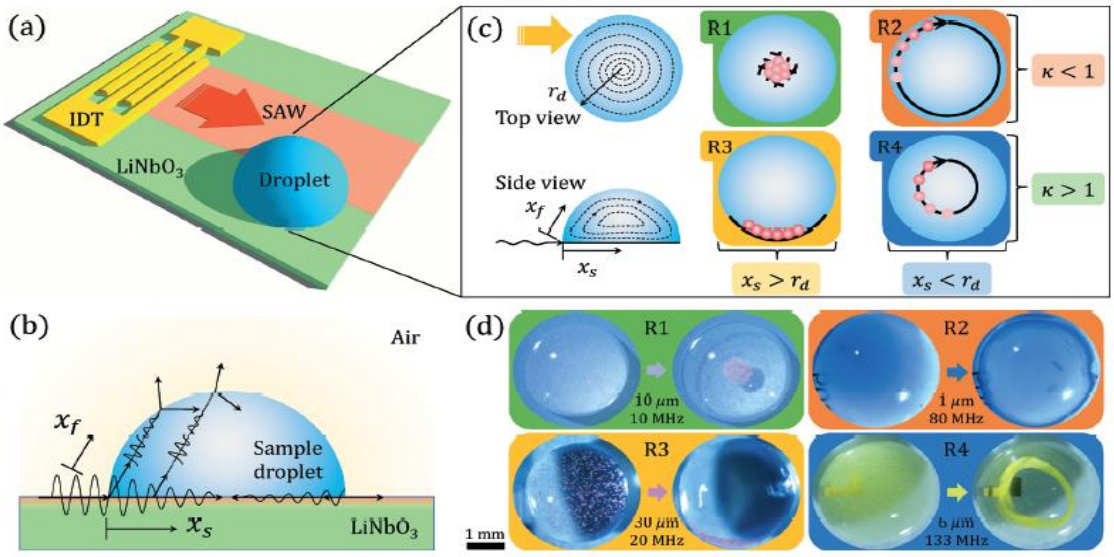

Figure 18. Four different regimes of particle movement are obtained [16].

Therefore, in the light of these assumptions the following results were presented. When K>1 ARF due to T_{SAW} dominates, conversely, when K<1 ARF due to S_{SAWs} dominate over that ARF due to T_{SAW}. In this situation the smaller particles are not captured by S_{SAWs} and are dominated by ASF. Moreover, four different regimes for particles movements were achieved. R1 k<1 Xs>rd ARF due to S_{SAW} capture and concentrate longer particles. in the centre. Smaller particles are not captured and are pushed to the periphery forming a ring-like structure. R2 k<1 Xs<rd The S_{SAW} forms close to the wave liquid interface and the SSAW forms to the periphery of the droplet creating a form like ring. R3 k>1 Xs>rd large particles are pushed to the periphery under the influence of ARF, ASF drags them towards the region of least acoustic field pressure. R4 k>1 Xs<rd ARF due to TSAW dominates and no S_{SAW} in the middle of the droplet [16]. These results can be visualized in the next picture.

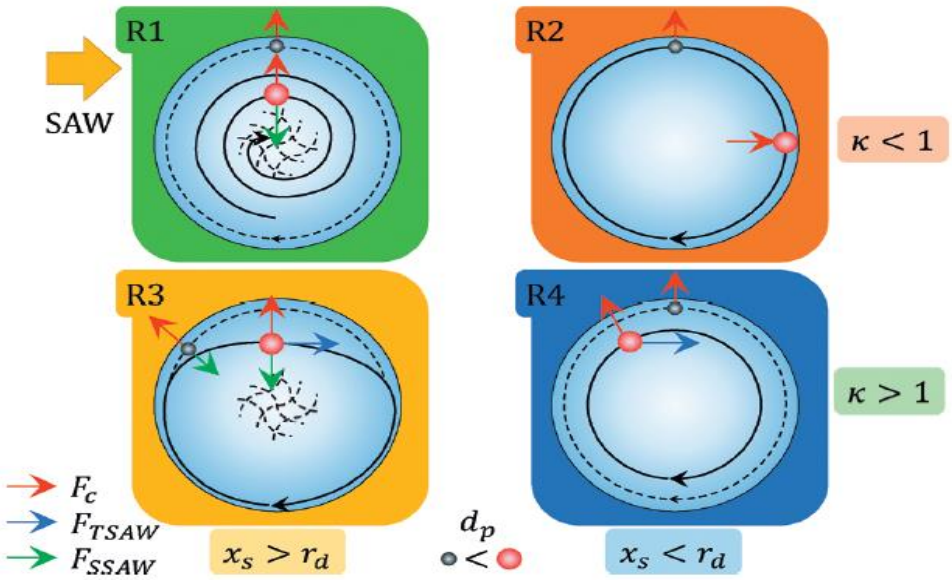

Figure 19. Summary of the four regimes obtained [16]

Simulation results showing the flow streamlines inside the droplets subjected to SAWs with frequencies of 10, 20, 80, and 133 MHz. A single vortex structure with its centre located at the droplet centre was observed in all cases. (b) Schematic of different regimes (R1–R4) of particle aggregation realized under the varying influence of ARF because of travelling (FT_{SAW}) or standing (FS_{SAW}) acoustic waves and the centrifugal force (F_c). The solid lines indicate the trajectories of the particles. R1: For κ < 1 and xs > rd, the larger particles are driven towards the centre of the droplet as FS_{SAW} > Fc, and FT_{SAW} is not affective. R2: For κ < 1 and Xs < rd, Fc drives the particle towards the periphery of the droplet in the absence of FT_{SAW} or FS_{SAW}. R3: For κ > 1 and Xs > rd, the particles experience FT_{SAW} as well as FS_{SAW} in addition to F_c. A tug of war brings the particles to the side of the droplet. The smaller particles (κ < 1) would move along the periphery. R4: For κ > 1 and Xs < rd, a smaller ring of particles (κ < 1) is formed as FT_{SAW} balances with F_c while FS_{SAW} is absent [16].

3.5 Yukai Liu (2022) "Enhanced Detection in Droplet Microfluidics by acoustic Vortex Modulation of Particle Rings and Particle Clusters via asymmetric Propagation of Surface AcousticWaves"

In many ways this study is a continuation of the experiment conducted by Destgeer et al (2016). The novelty is based on the introduction a new relationship by which the input power is related to the acoustic displacement. This new relation is the main reason by which the particles concentrate in the centre of the droplet or form a ring in the periphery of the droplet. The scope of the project is based on a fixed droplet volume of 8 µL with polystyrene particles suspended the microspheres of various sizes (5, 20, 40 µm) are used.

The principal goal of this project was to present a novel approach of free transition between the particle ring and cluster via modulating the acoustic amplitude of TSAW.

The difference with the study realized by Destgeer et al was that although Destgeer et al successfully discovered and verified the existence of particle rings, the influence of signal intensity on acoustic streaming flow was ignored. The signal intensity determines the leakage of acoustic amplitude and energy in the liquid, which affects the vortex velocity and the centrifugal force of suspended particles [22]. Therefore, in this paper a novel method for realizing free transformation between clusters and rings of particles by modulating the acoustic amplitude of travelling SAW is proposed.

To achieve the results, a configuration like the shown in the picture was utilized. (a) Can be observed that the SAW forms an asymmetrically displacement at any position, without influence by the initial position of the droplet. This allows the particles to follow the vortex in a certain direction and speed, which plays a significant role in particle agglomeration. The inset depicts the particle ring shape was exhibited under acoustic vortex capture with 5 μm particles. (b) Design diagram of the device. Acoustic vortex induced by asymmetric propagation of Travelling SAW excited by the interdigitated transducer (IDT) in a sample droplet. (c) Numerical simulation of the propagation and radiation of TSAWs in water.

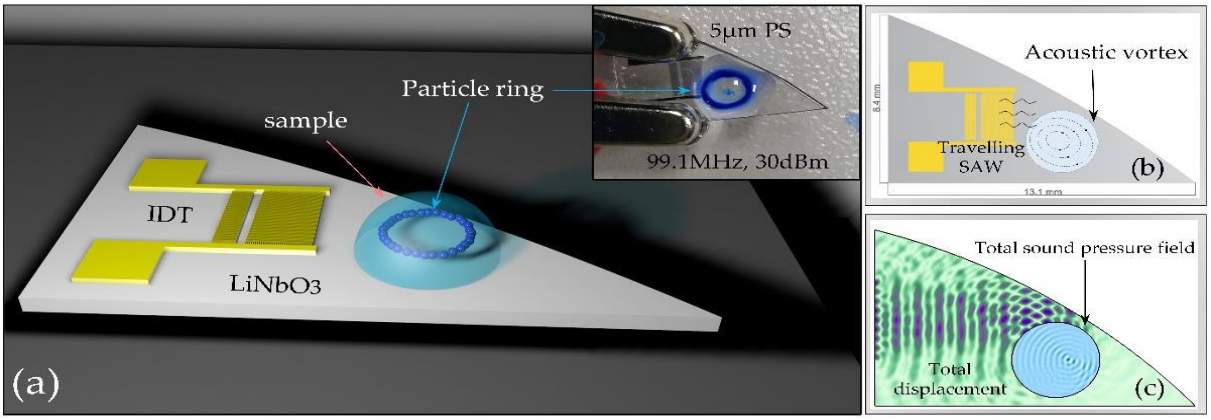

Figure 20. Schematic diagram of the acoustofluidic device [31]

As commented above, the displacement amplitude Â is the main parameter of this study. It is only influenced by the energy of SAW in the investigated power range. The estimation of Â with the supplied electrical power P_{el} is based on the following relationship.

$$\hat{A} = \sqrt{\frac{\kappa_n P_{el} \lambda_{SAW}}{APF_N}}$$

Where AP =2,3 mm is the aperture of the IDTs and F_N = 2.47×1015 W/m^2 is a material dependent factor. $\kappa_n \in [0, 1]$ is an additionally implemented parameter, which represents the loss due to the reflection of the voltage signal and the propagation attenuation during the excitation of the acoustic surface wave. According with experiment, TSAW propagates without any obstruction before entering the droplet, so the propagation attenuation can be

ignored. Here was assumed that there is not the reflection of the voltage signal and take κ_n=1 [31]. The correlation between acoustic amplitude $\hat{A}$ and the supplied electrical power P_{el} can be obtained in as it is depicted in the next picture.

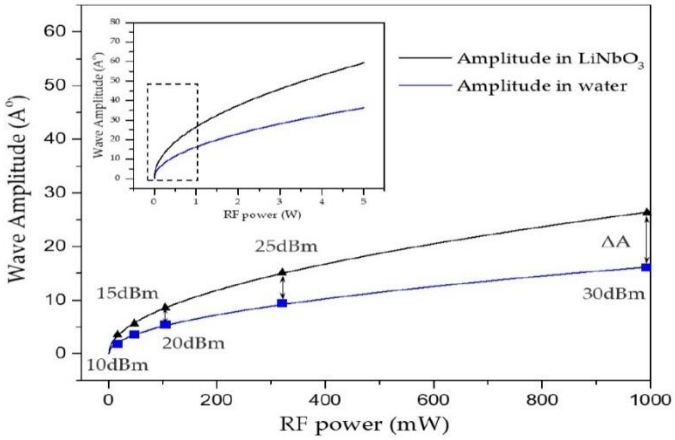

Figure 21. Acoustic displacement amplitudes Â at different electrical power levels [31].

Regarding the forces considered in this work, the centrifugal force is also a non-negligible force which affects the movement of particles in vortex. The vortex velocity is related to the change in the amplitude of the acoustic wave as it enters the droplet, which determines the magnitude of the centrifugal force. It is well known that centrifugal force F_C is proportional to the square of angular velocity of centrifugal motion ω ($F_C \propto \omega^2$). The centrifugal force increases when particles spin along the vortex at high speed. It begins to dominate the motion of the particles when the centrifugal force is large enough to exceed the acoustic vortex drag force. In other words, due to the different dominant force in the droplet, the particles will be captured by TSAW-induced acoustic vortex and show different trapped forms [31].

Based on the previous observations made by Destgeer et al, the experiment suggests the following hypothesis as a plausible explanation for the process by which the particles are captured by the streaming or form a particle cluster as well as a particle ring and the transition between one shape to another.

Given the particle diameter is small compared to the wavelength $\lambda_w = {}^{c_f}/_{f}$ of the SAW in the fluid, ARF cannot change the particle motion, and the effect is almost negligible [32]. When $dp \ll \lambda_w$ (30.3 μm, 5 μm particles in this experiment), the scattering effect of SAW can be equivalent to spherical isotropy with almost no backscattering. This SAW-based ARF caused by leakage has minimal effect on the particles and cannot effectively control the movement of 5μm particles (see Figure 22a). In addition, due to the small velocity of the vortex with 10 dBm power applied, the centrifugal force of the particles is weak. The drag force caused by ASF plays a dominant role (top and side views in Figure 22b) and drags 5 μm particles along the acoustic vortex streamlines eventually (see Figure 22c), which is called particle streaming [31].

The particle diameter d_P (=20 μm) cannot be neglected compared to the wavelength λ_w (30.3 μm $\approx {}^{c_f}/_{f}$) in the fluid when k > 1 for the 20 μm particles in this experiment, and the scattering is no longer isotropic, and backscattering dominates [32]. At this point, the

ARF caused by Leaky-SAW would change the trajectory of the particles (see Figure 22d). In addition, the applied power (10 dBm) is small, and the centrifugal force is difficult to handle, the leaky SAW-based ARF will play a dominant role ($F_C < F_{ASF} < F_{ARF}$) to control the particles ultimately. Thus, the leaky SAW-based ARF changes the trajectory of the particles when the 20 μm particles are flowing through the Leaky-SAW region and pushes them from the outer vortex line to inner line (see Figure 22e). Eventually, the particles are pushed to the centre of the vortex, where they gather into a particle cluster (see Figure 22f) [31].

In case of the particle ring formation, the R_F was changed from 10dBm to 30dbm. The particle ring of the 5 μm particles was difficult to observe due to the parameter limitation of $k << 1$. As mentioned previously, the 20 μm particles will passing through the outer side of the acoustic flow vortex to the inner streamline, and gradually approach the centre when $k > 1$, which is driven by the ARF. The acoustic amplitude attenuates rapidly within the fluid and more loss of energy happens as the signal intensity increases to 30 dBm. The wasted energy is converted into mechanical energy of the fluid, which is driving a faster vortex motion. Therefore, the centrifugal force (F_C) exerted on the particles in the fluid gradually increases and becomes dominant (see Figure 22g, h). Then the enhanced centrifugal force pushed the 20 μm particles away from the vortex centre when rotation speed of the vortex reached its maximum, as the *ARF* is unable to confine them. The 20 μm particles moved from inner line to outer line of vortex to form a stable particle ring when $F_C \approx ARF$ and reached an equilibrium state (see Figure 22i). The ARF pushes the particles towards the centre of acoustic vortex, while the enhanced centrifugal force pushes the particles away from the centre, which is opposite to the ARF. Therefore, the F_C and the *ARF* jointly dominate the ring motion of particles around the streamlines of a specific acoustic vortex, which is named as the particle ring [31].

According with Destgeer et al. this study assumes that these phenomena are explained by the different dominant effects of three forces: drag force caused by *ASF*, *ARF* caused by Leaky-SAW and centrifugal force F_c. It is concluded that the suspended particles can be captured by the acoustic field-induced fluid vortex (acoustic vortex), whose shape is particle cluster or particle ring [31].

To sum up in the following picture the next assumptions are gathered. (a–c) Demonstrate that when ASF > ARF ($k < 1$, 10 dBm), the drag force caused by ASF dominates the vortex motion of the particles (5_m) along the acoustic vortex streamlines. Particle Streaming. (d–f) Demonstrate that when ASF < ARF ($k > 1$, 10 dBm), the ARF caused by Leaky-SAW dominates the motion of the particles (20 _m) towards the centre of the acoustic vortex. Particle Cluster. (g–i) Demonstrate that when ASF < ARF ($k > 1$, 30 dBm), the ARF caused by Leaky-SAW pushes the particles (20 _m) towards the acoustic vortex centre, but the enhanced centrifugal force drives the particles out of the centre again and against the ARF. The FC and ARF co-dominate the ring motion of the particles around a specific acoustic vortex streamline [31].

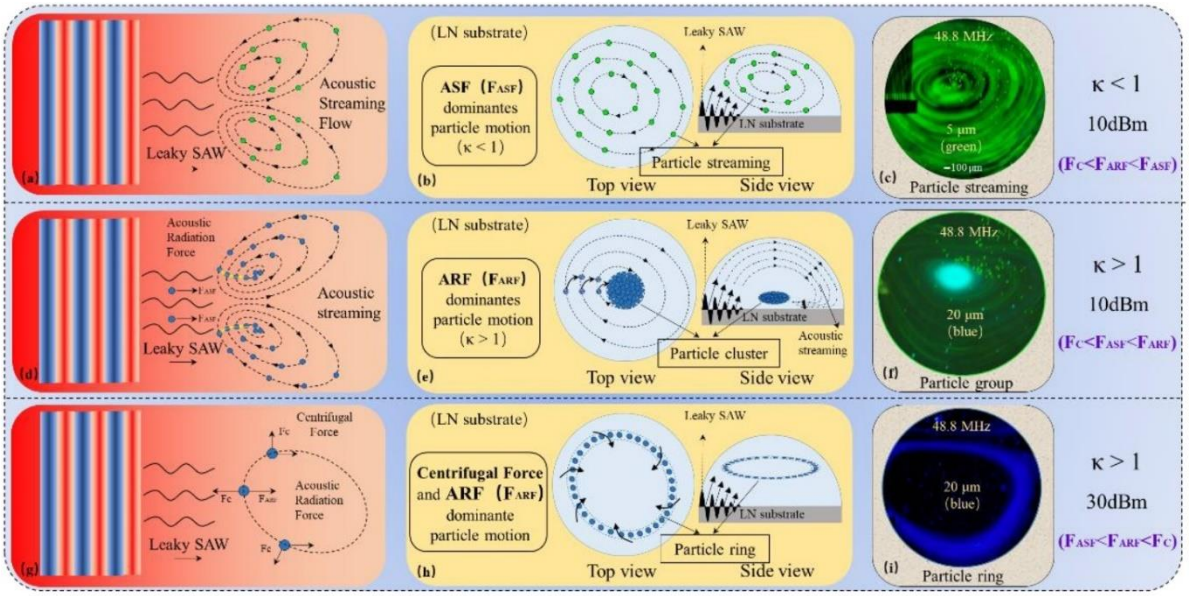

Figure 22. Summary of observed cases [31]

The free transition of particle ring and particle cluster can be explained by the increment of the TSAW acoustic amplitude, particle clusters gradually form particle rings. In order to prove this phenomenon works the other way as well (particle ring also shrinks into particle cluster when the applied TSAW acoustic amplitude decreases), an experiment shown in Figure 23a–f had been carried out for this purpose. It can be seen that the acoustic amplitude gradually decreases as the acoustic power decreases, which leads to a decrease in the vortex velocity. Then, the diameter of the particle ring gradually decreases until it shrinks into a particle cluster.

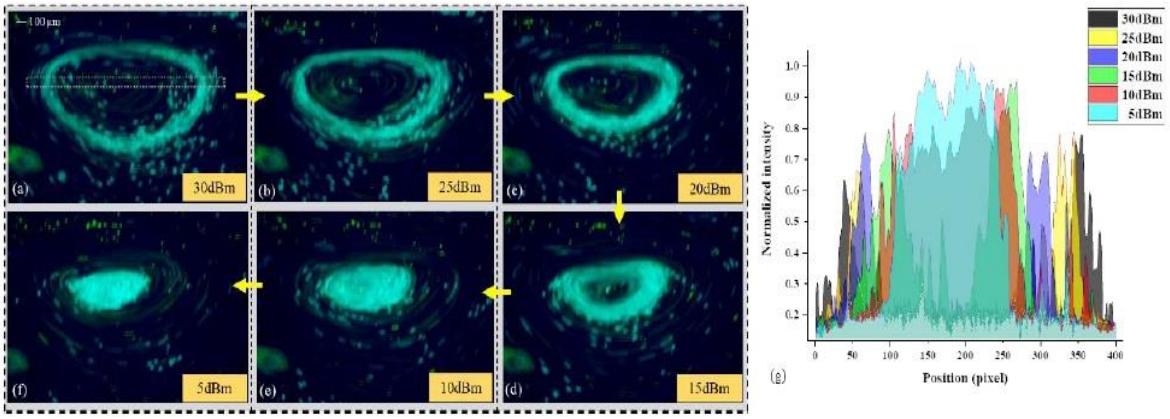

Figure 23. Transition of particle ring and particle cluster [31]

The diagram of the particle outer/inner ring with the signal intensity configurates the shrinking process more visually (Figure 24). The decrease of the outer and inner diameter of the particle ring is consistent with the decreasing power intensity.

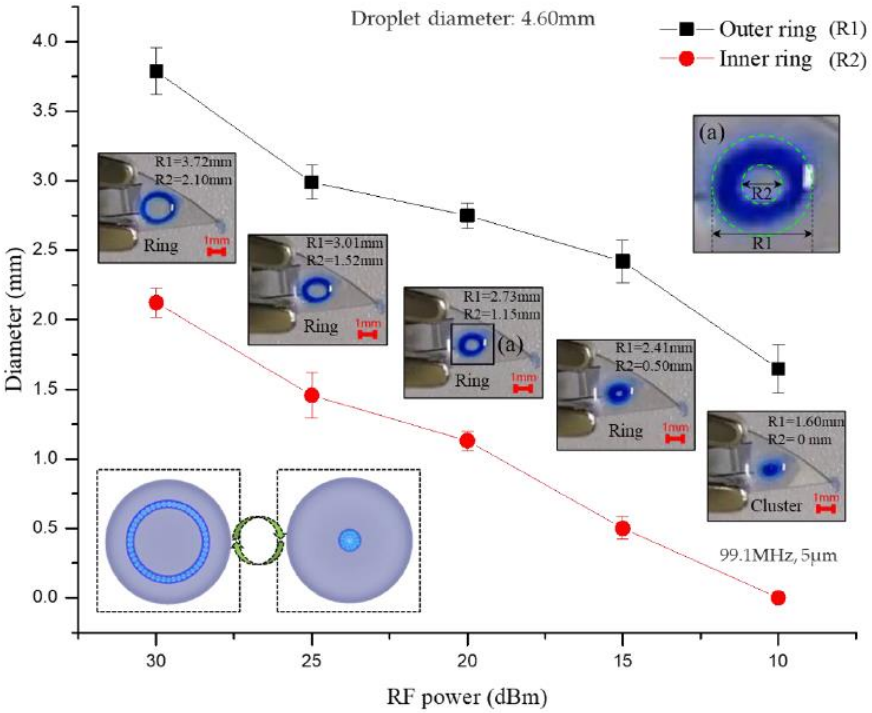

Figure 24. Graph of the variation of the outer/inner ring [33].

It is observed that the amplitude of the acoustic displacement in the substrate and the droplet is different and increases with the increase of the electrical power. The correlation between the inner and outer diameters of the particle ring and the square of the acoustic amplitude is shown in the next picture.

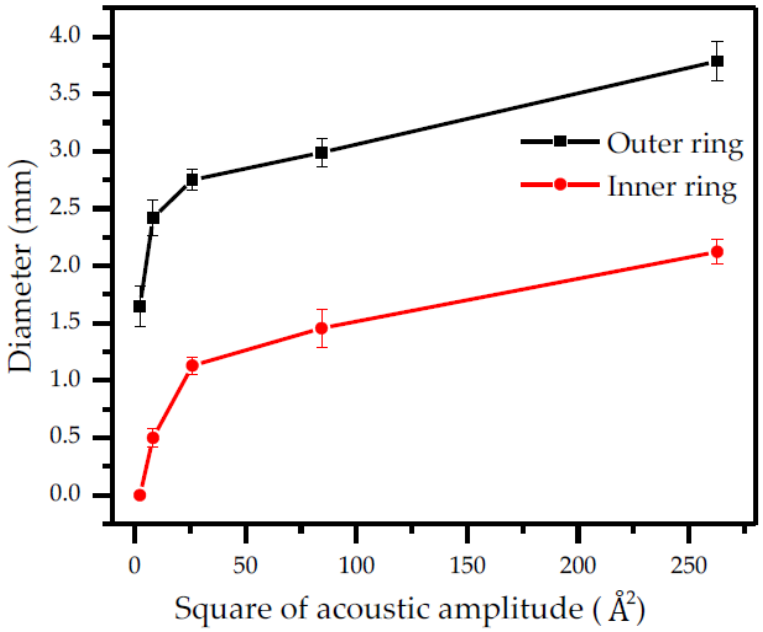

Figure 25. The correlation between the inner and outer diameters of the particle ring and the square of the acoustic amplitude [33].

The energy magnitude of the acoustic leakage determines the size of the particle ring morphology in the droplet. It can be seen that in the first half of the increase of the acoustic amplitude (0–5 Å), the inner and outer diameter of the ring changes more significantly. As the acoustic amplitude continues to increase (5–15 Å), the ring increases more slowly and gradually stabilizes, indicating that a more stable control of the ring morphology can be achieved at larger acoustic amplitudes. Therefore, a conclusion can be generalized that the conversion between particle clusters and particle rings can be realized freely by adjusting TSAW acoustic amplitude [31].

3.6 Literature gaps

This section refers to the knowledge gaps that have been identified after reviewing the existing literature and are considered of relevant importance. For instance, those which are related to the thermodynamics and the hydrophobicity grade of the substrate.

In one hand, when the waves produced in the IDT travel over the substrate, the energy lost cause of the attenuation is transformed into mechanical motion in the fluid [22], and heat which is absorbed by convection for the environment and the droplet that is resting on the substrate [26]. As a consequence of this, the device experiences a rise in temperature and several effects are produced that could be of special interest.

By considering negligible the exchange of energy with the environment and considering the droplet as the main affected element. When the duration time of the experiment is long the greater is the temperature reached in the device and the greater is the heating of the droplet. This provokes some affections that are not considered in the literature.

For example, based on existing evidence when there is an increment in the temperature, the following phenomena are observed. The surface tension of the fluid decreases, as well as the angle of contact of the droplet with the substrate due to rapid evaporation. Also, a change in the viscosity and density of the fluid is appreciated, in both cases decreases with the rise in temperature [34] [35] [36] [37] [38].

Bearing in mind that the aforementioned parameters can also be affected by the degree of hydrophobicity of the substrate, it is necessary to point out that no mention is made of this factor in the literature as well as neither the existent relation between each other.

In any case, the degree of hydrophobicity plays a relevant role in the friction that occurs between the drop and the substrate when it begins to rotate. The higher hydrophobicity of the substrate the less surface is in contact, and the less friction should be expected. However, for a given hydrophobicity when under certain values of frequency and input power an ultrasound is imposed to the droplet a rotational vortex occurs. By increasing the input power is possible to increase the rotational speed of the created vortex as has been described in the literature. As a consequence of this speed increment some affections in the nearest layer of fluid in contact with substrate can be succeed.

Although some researchers such as Raghavan et al [4] did mention the Eckman layer as a layer where friction between the fluid and the substrate occurs, this force has not been quantified by any of the studies presented in this work.

Given the difficulty involved in quantifying these forces, this work offers a discussion based on the phenomena observed during the experiments carried out and humbly intends to shed some light on these phenomena that have not been treated in the literature.

4 IDTs design, fabrication process and stage description

4.1 IDTs parameters

In this project, the concentration and the dispersion of the particles are studied. Based on the features of the experiments that will be carried out a properly set of IDTs were designed. For example, the effect of the frequency and the input power play a crucial role in the characterization of the regime state of the particles. In order to observe clearer the effect over the particles when changing the frequency or the input power, is necessary to develop different IDT with different nominal frequency. According to the previously studied in the specialization project, the production of the IDTs was designed regarding to the operational frequency for the consecution of the experiments.

As the scope of the experiments is different for any case different IDTs are needed. For instance, for the study of the effect on the particle concentration and ring formation two pair of IDTs of 20 and 40 MHz were designed. However, for observing the effect of the particles diameter when a particle ring is achieved an IDT with 80 MHz as nominal frequency was tested. Additionally, to reach the formation of a middle ring inside the droplet a more powerful IDT 160 MHz was designed.

In this regard, the frequency f is determined by the following design parameters of the IDT. The sum of the space between fingers and the finger width, d, and the substrate acoustic velocity C_s=3950 m s^{-1}. The relation among these parameters is given as follows.

$$f = \frac{C_s}{4d}$$

The parameters involved in the design of the IDTs for this studied is shown in the following picture.

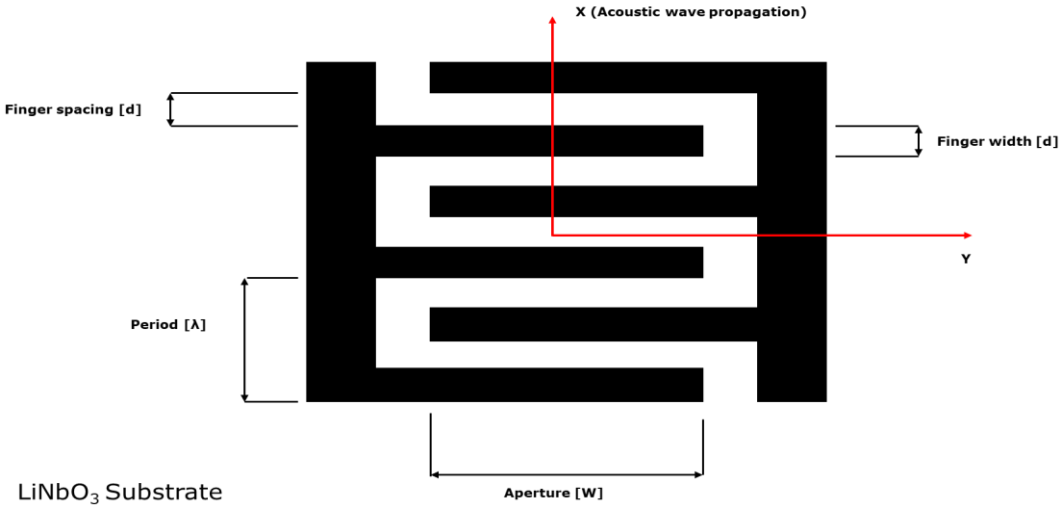

Figure 26. Schematic representation of IDT parameters

4.2 Fabrication process

The IDT is considered as a fundamental tool to achieve the movement described above. This device is in fact a nanodevice and often is made through a gold deposition over the substrate surface as it will be commented further. Because of the nature of the device is a mandatory to use nanotechnology and specific machinery to produce this device.

Consequently, in order to achieve a satisfactory IDT a specific recipe in which all steps are detailed was followed. The recipe can be found in the appendix section of this document.

Lithium Niobate ($LiNbO_3$) is the material elected for the substrate. Is an anisotropic crystal that possess piezoelectric properties. For many applications, $LiNbO_3$ has been the piezoelectric material of choice, is the most commonly used piezoelectric material in SAW acoustophoresis due to its excellent electromechanical coupling, biocompatibility, and optical transparency [39]. The fabrication is made in different stages which are explained below.

4.2.1 Cleaning

The first task in this process is the cleaning. The purpose of this is to ensure an accurate result, otherwise, tiny dusty particles could contaminate the sample and it could negatively affect in the next steps resulting in a faulty device. To avoid this, the sample is cleaned by splashing acetone until the whole surface is covered.

Immediately after the acetone was splashed, it is showered with isopropanol (IPA), this will avoid stains and debris of acetone in the surface of the sample. Then, $LiNbO_3$ sample is completely dried with N_2.

Figure 27. Cleaning bench

4.2.2 Plasma cleaning

This facility Plasma cleaner (Femto, Diener Electronic) is used with the objective of achieving a more hydrophilic surface. It will create a higher rate of adhesion; this is relevant for the next step in which the photoresist will be deposed. To get this all the organic contaminants are removed from the surface thanks to a chemical reaction with O2.

Figure 28. Plasma cleaner, Diener Electronics

4.2.3 Photoresist Spin coating

Following with the recipe a positive photoresist (SPR700) will be deposed in the sample. This chemical will create a thin layer which will cover the entire surface. As a pattern will be created after exposure, a positive photoresist was elected. Positive photoresists consist of 3 components: a photoactive compound, a base resin, and an organic solvent. The exposed regions become more soluble and can be removed during the development process. The pattern formed is the same as the one on the mask. (Note: prior to exposure, it is insoluble in the developer solution. To get an accurate width of photoresist in the sample surface, a spin coater is used. First, the sample is set centred on the chunk of the spinner and fixed through a vacuum pump. Then a pipette is utilized to apply photoresist at the centre of the sample. After this, depending on the required width of the layer, the setup of the machine can be completed. In this setup parameters like acceleration and revolutions are chosen.

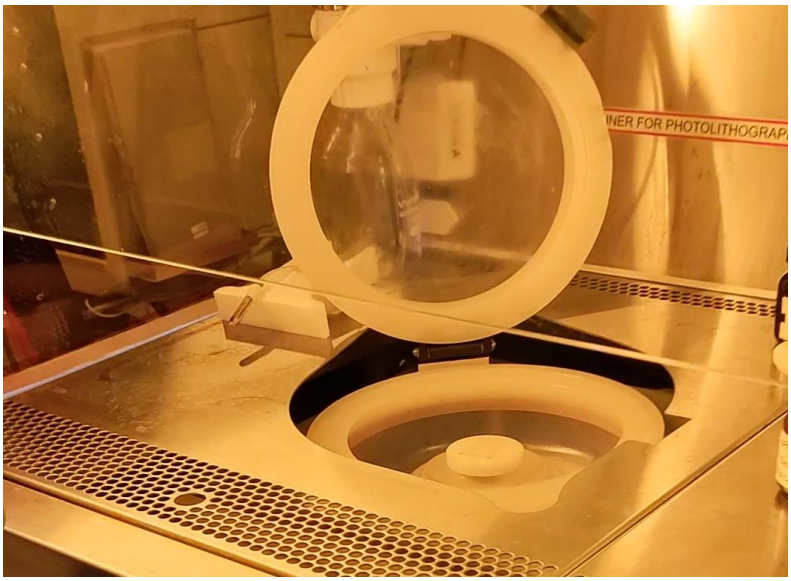

Figure 29. Spin coating detail

4.2.4 Evaluating the thickenss

To ensure that the thickness is optimal for the process a reflectometer was used. A reflectometer uses a technique called spectral reflectance in which light reflected from a surface is analyzed giving film thickness and optical constants (n and k) of semiconductor and dielectric thin films. This technique is amazingly fast and simple. In case that the thickness of the deposed photoresist was higher than permitted, the process should be repeated from the beginning as an excess of the photoresist could difficult the creation of the pattern in the exposure step.

Figure 30. Reflectometer of the nano-lab in NTNU

4.2.5 Soft baking for $LiNbO_3$

To create a consistent photoresist layer in the surface a soft baking is required. Then the solvents are evaporated, and the molecular structure of the photoresist is compacted. Finally, to obtain an optimal condition for the exposure the sample is cooled down in a cool plate.

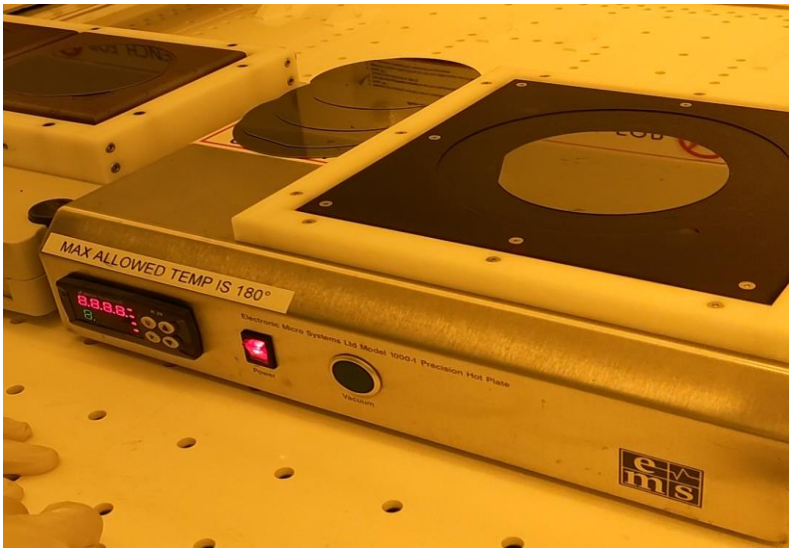

Figure 31. Hot plates station

4.2.6 Exposure MLA 150 405 nm wavelength laser

In this step we want to create a pattern in the photoresist which cover the surface of the sample. The MLA150 Maskless aligner is a direct laser write tool. Two laser sources 405nm

and 375nm, according to the recipe 405 nm wavelength was selected. Some features of the system are the topside alignment accuracy of 500nm and the backside of 1µm. Minimum line width is 1µm. Before this, a design was created using AutoCAD, the model created is loaded in the machine software and desired parameters for the design are elected. Theses parameters are primarily the wavelength of the laser bean or dose per mJ/cm^2 which is the time the beam spends in a dot and determines the final writing time and quality of the exposure. The desired pattern is designed considering that the part exposed is going to disappear after applying the developer in the next step after the post exposure bake.

Figure 32. Plate of MLA-150

4.2.7 Post exposure bake

A second baking is carried out to consolidate the properties of the photoresist after the exposure, this second baking is expected to improve the developer action in the next step. This step is placed also in the hot plat station shown in the figure 10.

4.2.8 Development

To reveal the originated pattern in the exposure a chemical is employed to remove the parts of the non-exposed photoresist over the surface. This process takes place inside of a fumehood of the lithography area designed for this purpose. Thereby, one beaker with enough developer and other one with water are necessary, first, the sample is immersed in the developer beaker for a determinate time and after that was softly rinsed with water. In this moment, the pattern can be visible with the naked eye.

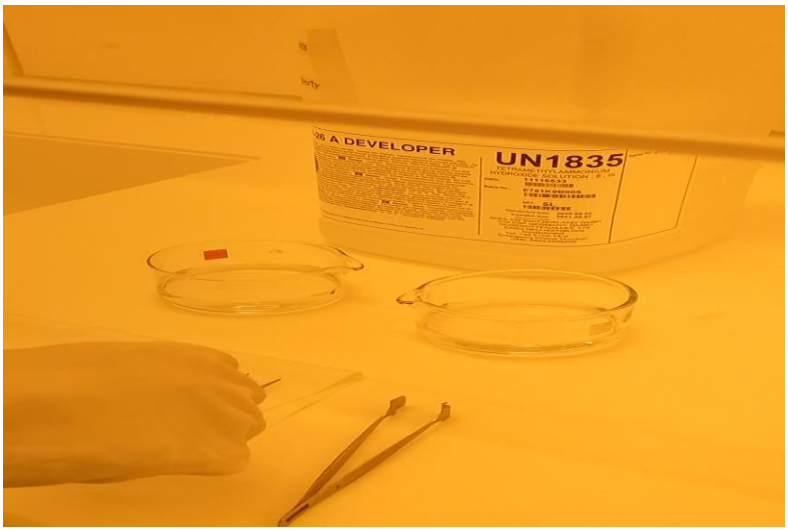

Figure 33. Devolpment bench

4.2.9 AJA evaporation

Approaching to final of the process, now is necessary to embed some metals in the holes that the exposure created in the surface covered with the photoresist and the posterior development revealed. An e-beam evaporator is used to deposit single or multilayer thin films of metals, oxides, magnetic materials, and dielectrics. An electron beam is sweeped over the target surface transforming target atoms into gaseous phase which precipitates into solid form coating the chamber. This takes place under high vacuum (~10E-7 Torr) enabling the atoms to evaporate freely in the chamber. A quartz crystal monitor controls the deposition thickness. Minimum controlled deposition is ~1 nm and maximum are up to 2 um (NOT Au or Pt). The deposition rate can be varied from 1Å/s to 10Å/s. Available targets for e-beam evaporation: Au, Ti, Pt, Ge, Pd, Si/open for requests. Since we need to embed two metals, this process is carried out in two evaporations. Then, it was proceeded in two stages. In our case, in order of embedment, the metals were embedded were titanium and gold. The underlying reason for embedding two different metals, such as, Ti and Au, is because it improves the conductivity of the device.

Figure 34. E-Beam AJA

4.2.10 Lift-off

As the embedment of the metals is not directed to a determined area all the surface of the sample is covered by the deposed metals. lift off is necessary to remove the excess of the deposed metals. To remove all the gold which was deposited in the sample PG Remover is employed. To perform an ultrasonic bath one beaker of acetone is needed to submerge the sample on it for later put into the machine of ultrasonic bath.

Figure 35. Lift off station

4.2.11 Result inspection

The following pictures were obtained with a microscope in which the quality of the fabrication process is observed.

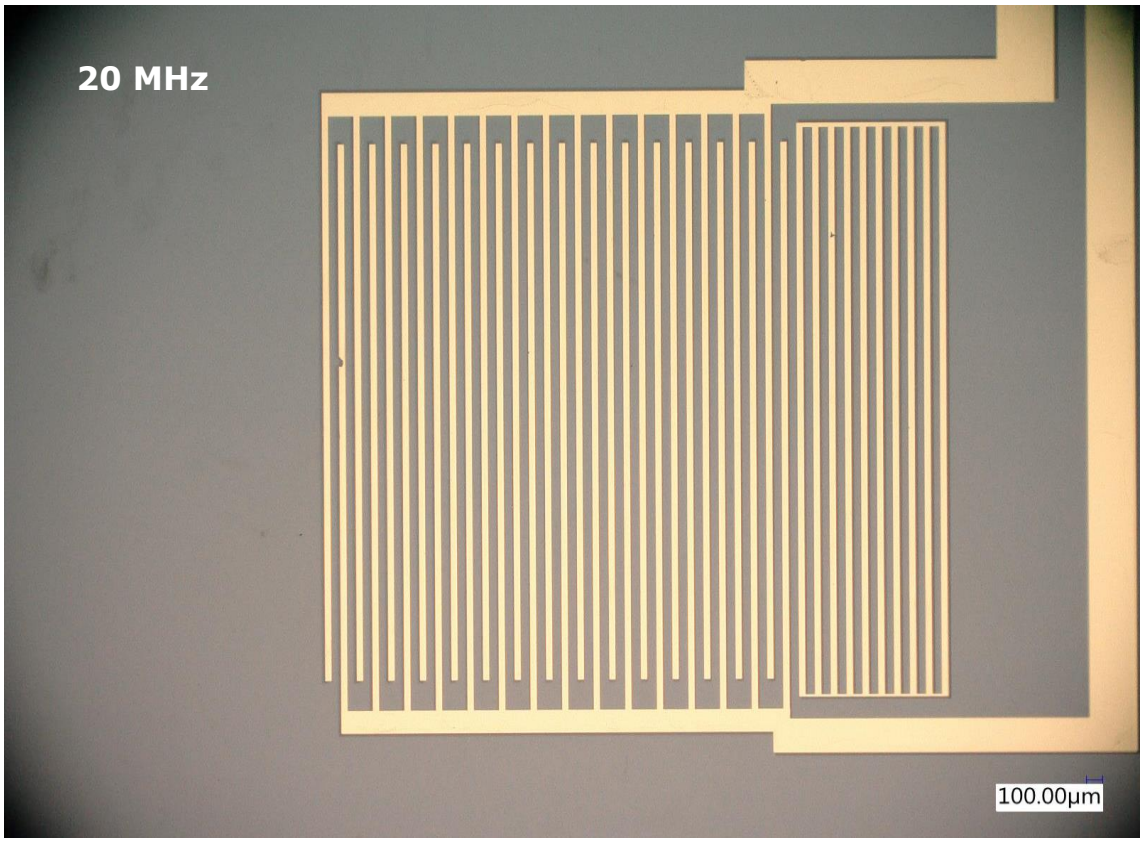

Figure 36. Detail of straight IDT 20MHz

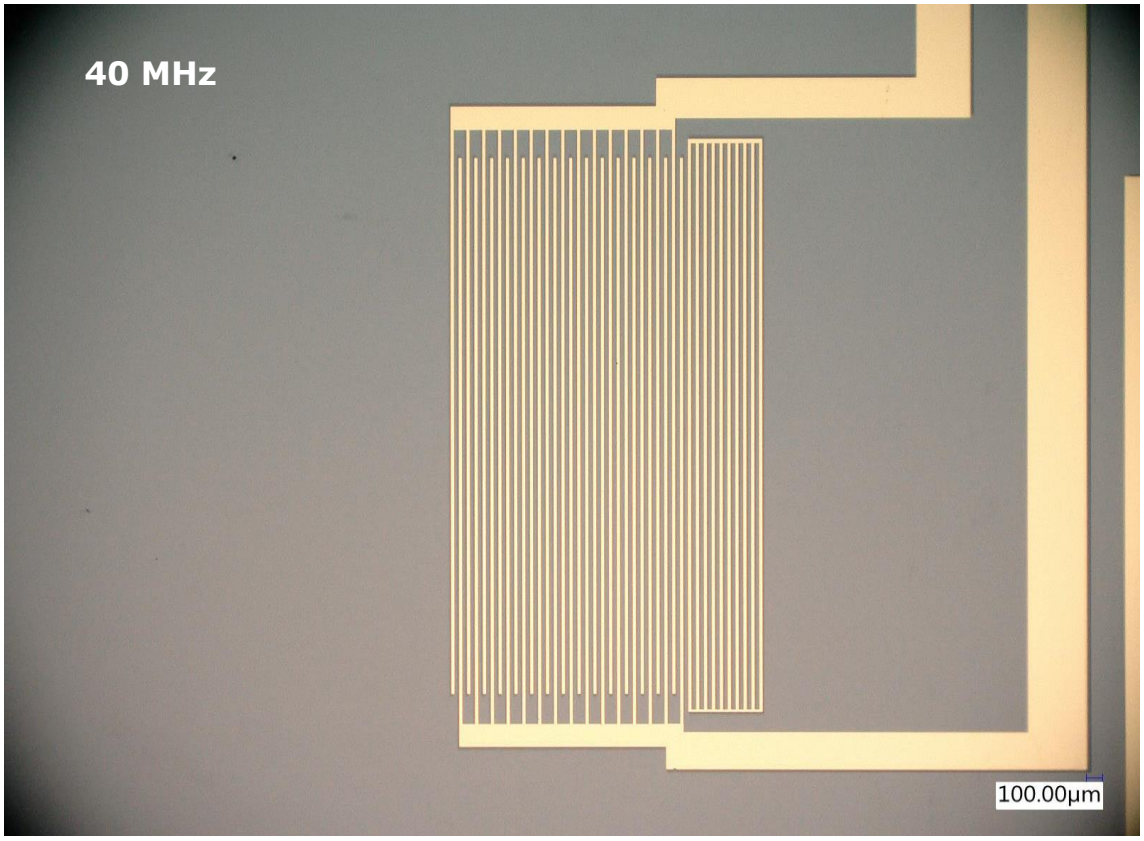

Figure 37. Detail of straight IDT 40 MHz

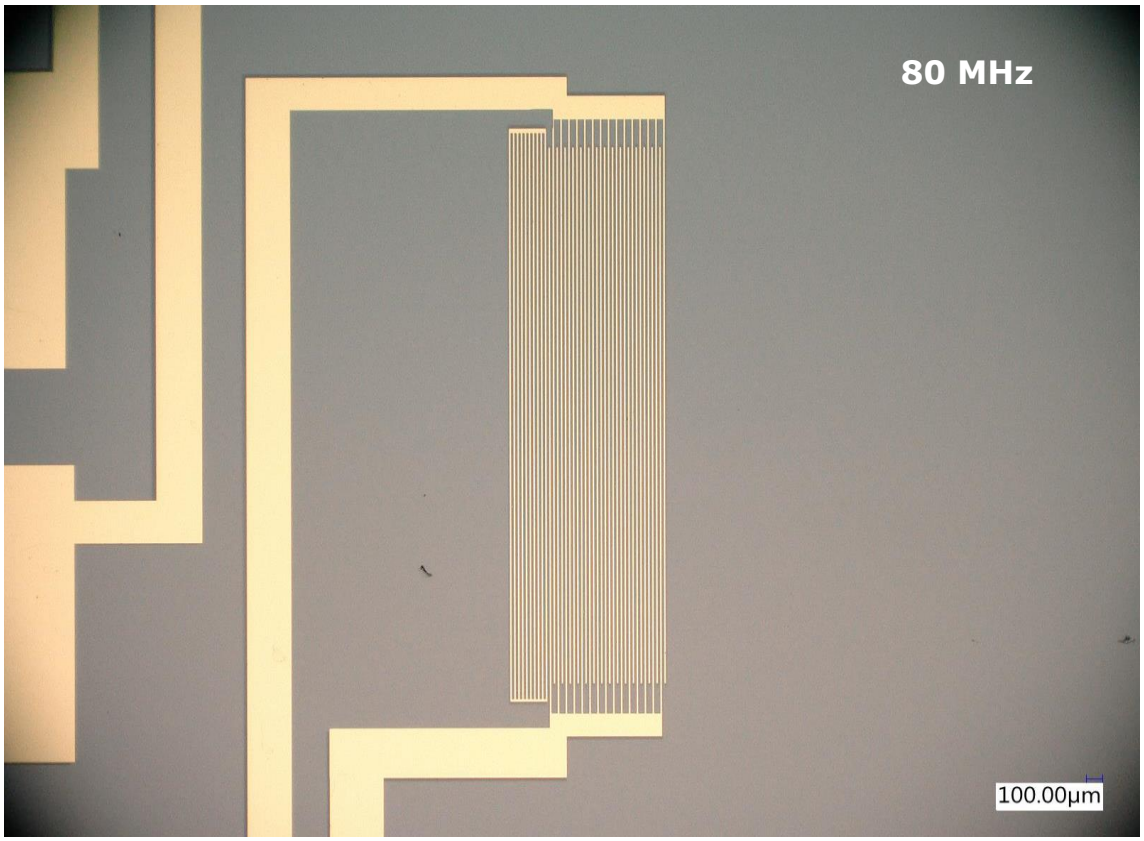

Figure 38 Detail of straight IDT 80 MHz

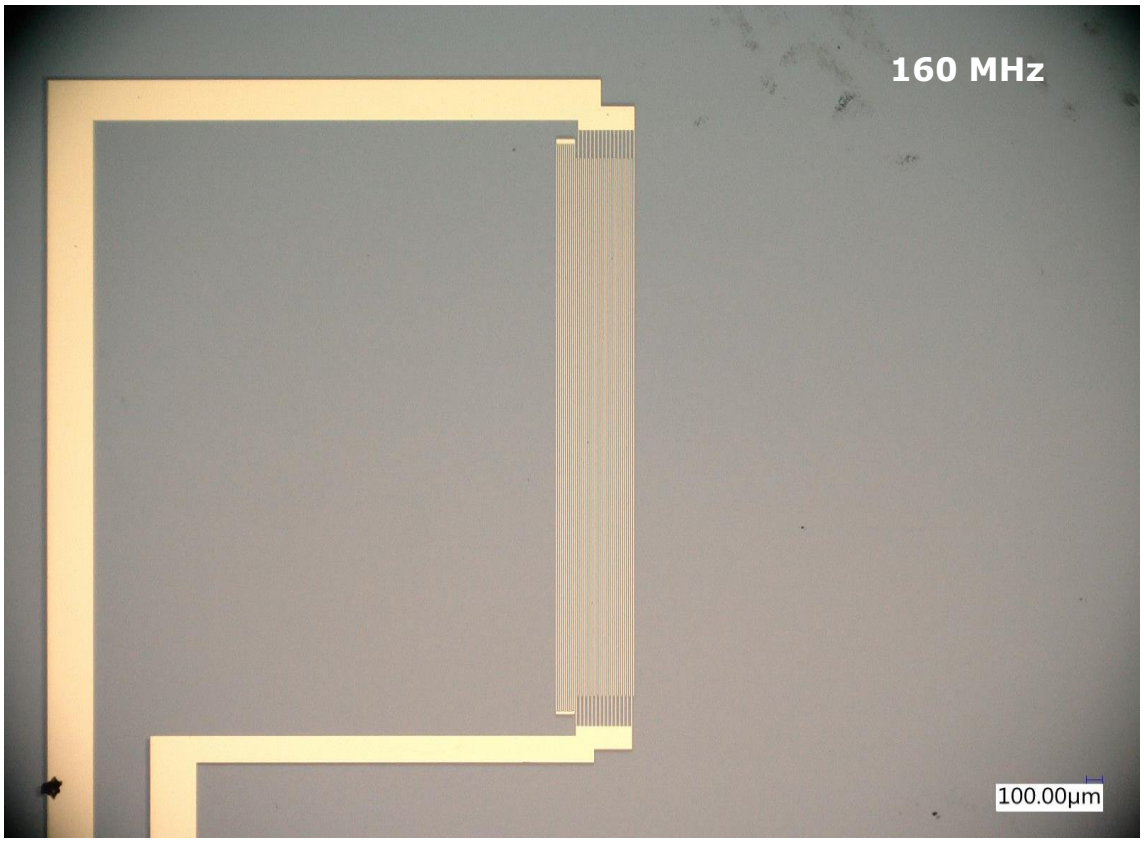

Figure 39 Detail of straight IDT 160 MHz

In this pictures are possible to observe with more detail the performance of the fabrication process.

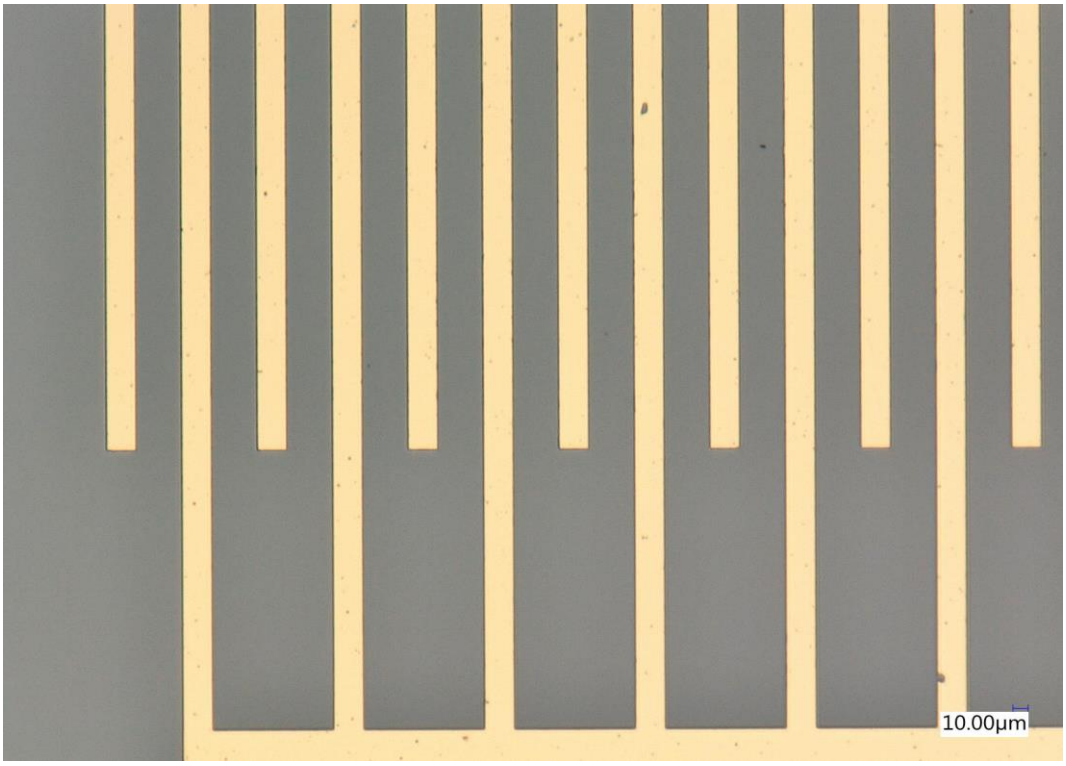

Figure 40. Zoom detail of the IDT fabrication

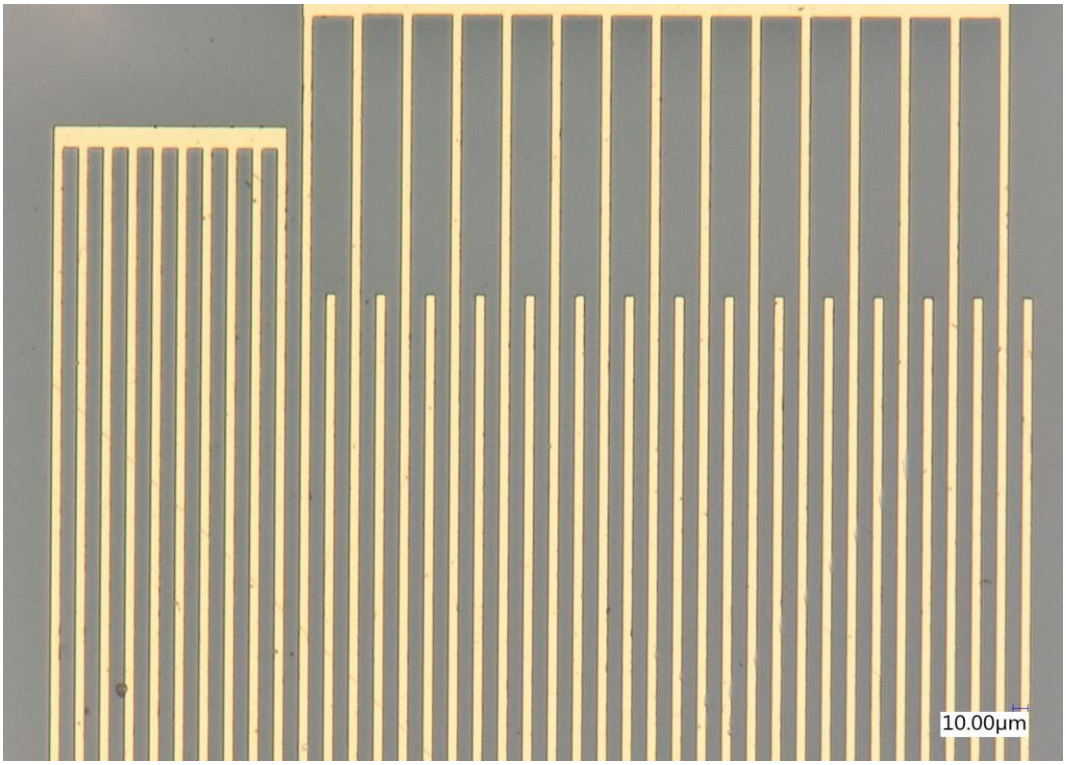

Figure 41. Zoom detail of the IDT fabrication

4.2.12 Stages of the process

To illustrate the entire process, in the following schema are represented all the stages presented before.

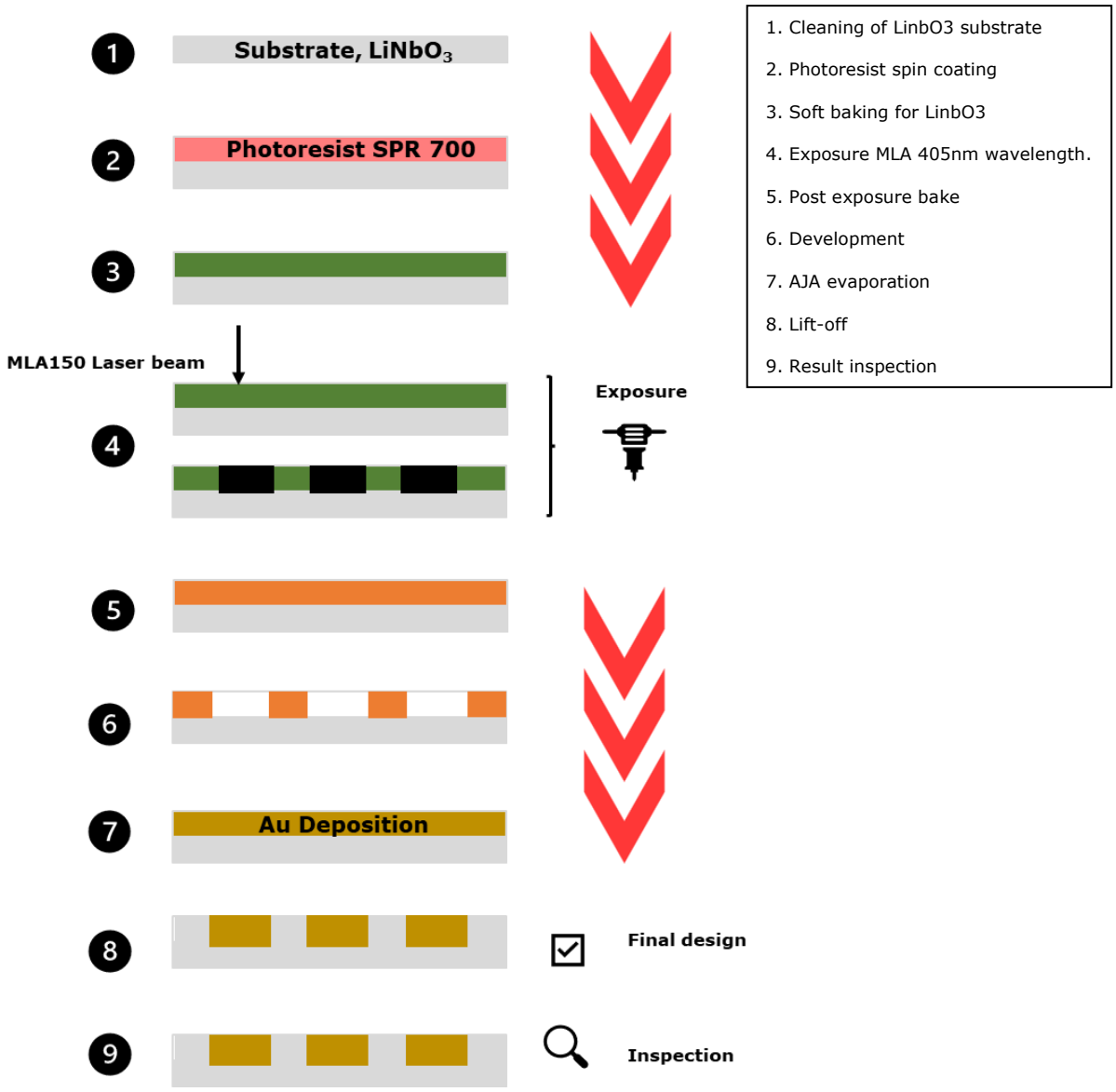

Figure 42. Schematic representation of the process stages

4.3 Stage description

To accomplish this project tools to analyse and processing data are needed. The following elements compose the stage: An inverted fluorescence microscope to observe the movement of the particles, a signal generator to transmit frequency and power to the

device and a printed plate attached to the microscope to place the substrate with the IDT. In the depicted picture, the elements which make up the stage are represented.

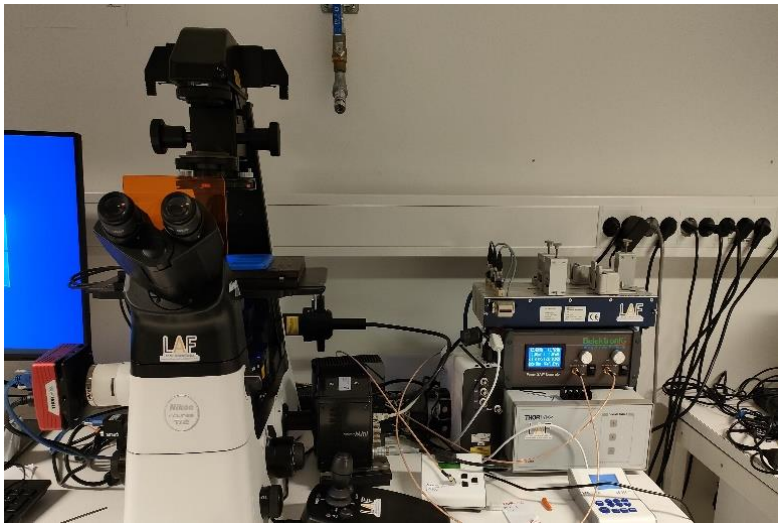

Figure 43. The stage with all the elements attached

To visualize the polystyrene particles movement inside of the water droplet, an inverted fluorescence microscope equipped with an ultra-slow-motion camera is used. This camera enables to capture the movement of particles and observe it in the pc computer screen thanks to an installed software called (PFV4). This feature is significant remarkable because allows to process the observed data with an external software, such as, MATLAB or COMSOL and obtain a valuable information to predict and analyzed the behaviour of the model. In the depicted figure, the utilized inverted fluorescence microscope is represented.

Figure 44. Inverted fluorescence microscope

Signal generator is used to transmit potence to the device, which are the most important parameters indeed to study the behaviour of the particle movement. Even though the

handling can be manually, it is also controlled through a software named (PSG Control). In this manner, the potence and the frequency which are given to the inscribed IDT in the $LiNbO_3$ substrate can be controlled. In the following picture the signal generator is shown.

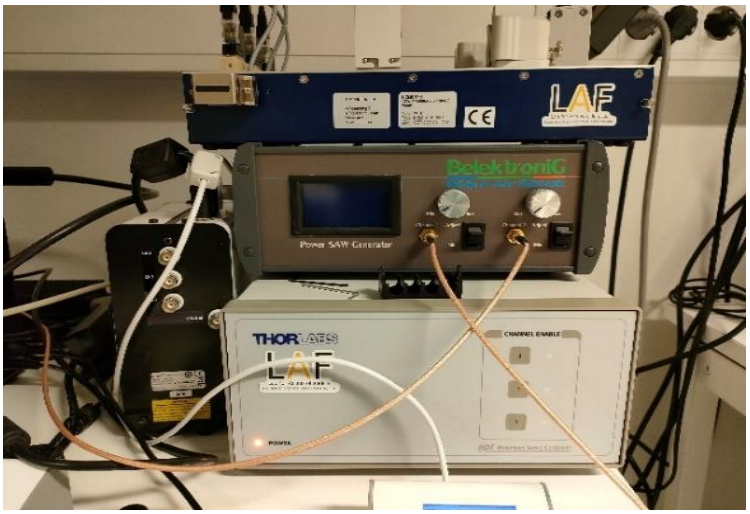

Figure 45. BelektroniG signal generator of the NTNU laboratory

Using a 3D printer, a plate was specially designed using AutoCAD to place the substrate with the IDT. The improvement introduced by this work is double. In one hand this is expected to improve the wire connectivity between IDT connectors and the signal generator as well as increase of the accuracy of the measured data. Additionally, the plate must adjust perfectly to the existent plate of the microscope. For this reason, the plate was designed considering the existent measures of the base of the microscope. The connection between the wire and the IDT connectors is as well as the entire plate depicted in the next picture.

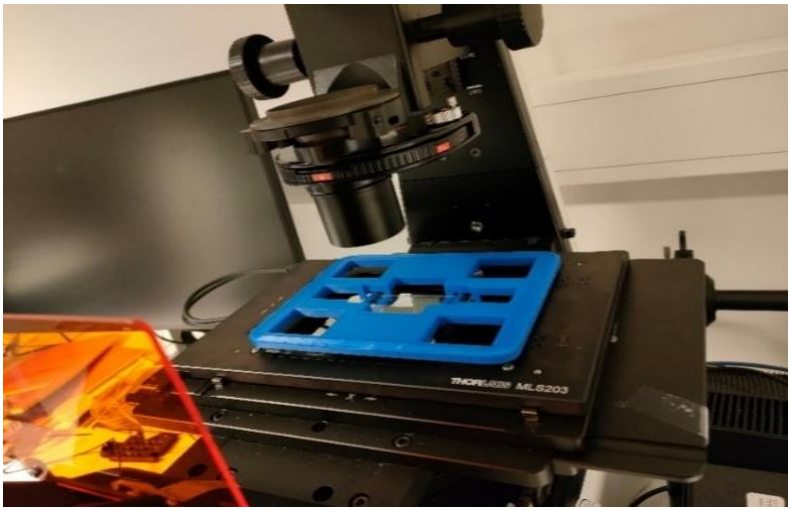

Figure 46. Printed plate

5 Method for data analysis

5.1 Sample preparation

The sample fluid is prepared by mixing polystyrene (PS) particles having required diameter with deionized (DI) water inside of a pipette, like shown in the upper left picture. The following different diameter fluorescent particles (1 µm and 7 µm) of PS particles are used. One kind of different diameter fluorescent particles are used. 1 µm (Fluorescent polystyrene dragon Green 7 µm, Particle Concentration (PC): 1% solids (10 mg/mL), Mean Diameter (MD) ~50nm - 15.00µm, catalogue number (CN) FCDG008, Bangs Laboratories, Inc) and 7 µm (Fluorescent polystyrene dragon Green 7 µm, Particle Concentration (PC): 1% solids (10 mg/mL), Mean Diameter (MD) ~50nm - 15.00µm, catalogue number (CN) FSDG007, Bangs Laboratories, Inc).

To continue with the preparation, the particles are mixing using a mixer like the shown in the upper right picture. The pipette is set in vertical position in the mixer housing, after 20 seconds approximately the particles inside of the pipette are mixed.

With the help of a dispenser like the ones shown in the figure below, we extract the specified drop size from the pipette (2 µl). For this, the dispensers are classified according to the range of volumes that they are capable of dispensing.

Figure 47. Tools for sample preparations

5.2 Experiment set up

In this section the part regard to the set-up of the stage to carry experiments is detailed. To begin with the experiment the IDT has to be placed in the housing of the printed plate. To connect the IDT with alternative electric current source, a 4-pin connection element is connected to the IDT. The objective of making this type of connection is avoid making a wire bonding and at the same time improve the quality of the connection between the IDT and the signal generator.

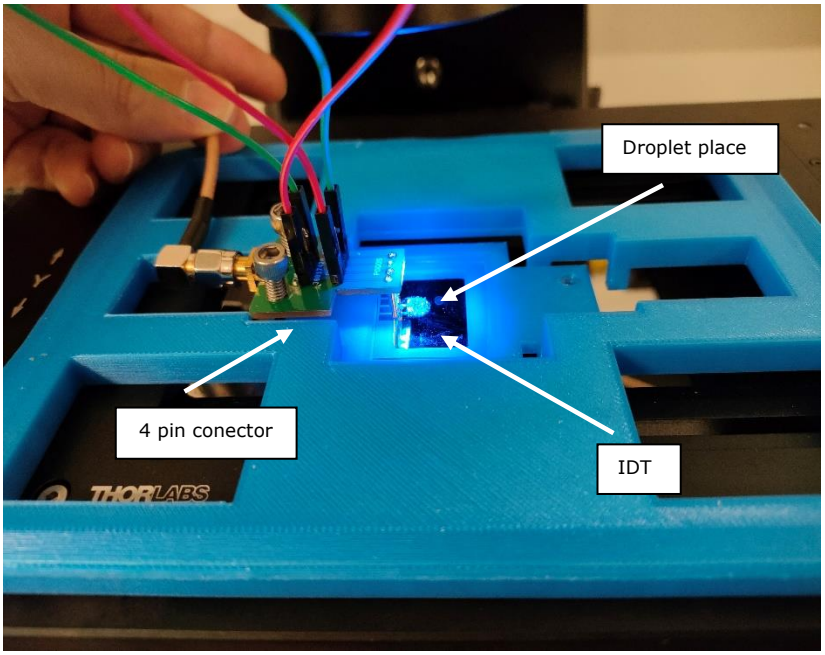

Figure 48. IDT connexion

Once the connection of the device has been made, the prepared sample in the previous step can be placed in the IDT substrate as can be observed in the picture. Hereinafter, the procedure to acquire data is explained in the following section.

5.3 Experiment protocol

To carry out the experiments, some parameters are controlled while others are calculated. For example, by managing the parameters which governates the generation of the SAW, thus are frequency and input power is possible to achieve a concentration of the particles in the centre or a ring in the periphery of the droplet. On the other hand, in order to characterize this movement i.e., the particle concentration or the ring formation, the attenuation of SAW X_s along the substrate and the *k factor* are calculated.

To proceed with the experiment, as it was mentioned before a sample is prepared and placed in the offset of the IDT. As it was explained, is difficult create one single vortex inside the sessile droplet when the incoming SAW is in front of the droplet, however, by

placing the droplet in the offset of the IDT it is possible to overcome this issue [22]. In the following picture is shown how the droplet is placed in front of one edge of the IDT. Due to the rigor of the experiments, this is the configuration that was followed for all the experiments. In the following picture a droplet with particles inside is placed at the offset of the IDT located on the left part in the picture as can be observed.

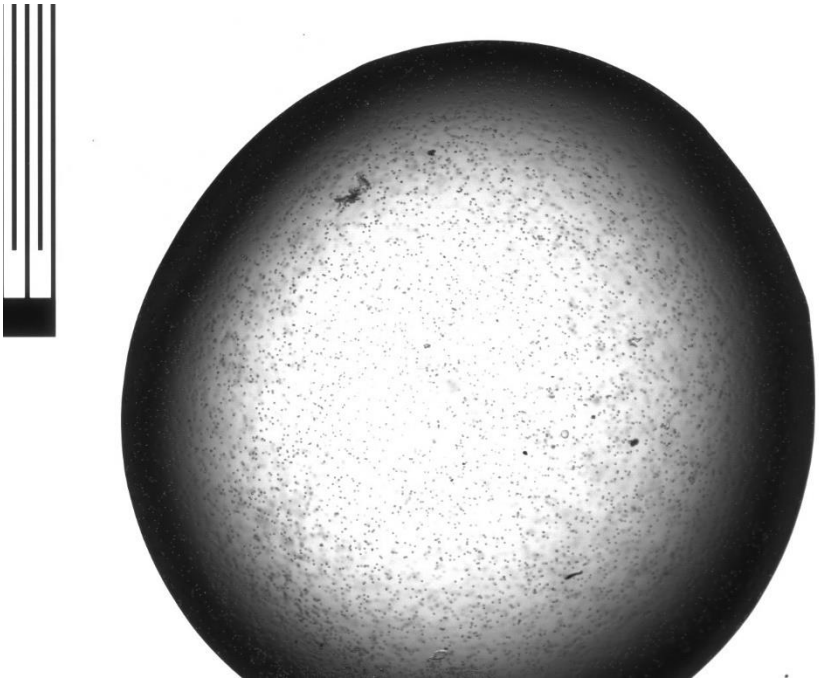

Figure 49. Experiment set up

To reach an appropriate field of view with the fluorescence microscope a 2 μL volume of the droplets is fixed in this study. The particles diameter has a size of 1 μm and 7μm. Four IDTs were designed to operates at the frequencies 20,40,80 and 160 MHz, respectively. The temperature of the room at the time of the experiments was 21 °C with a 46% of moisture in the air.

5.4 Method of data analyse

5.4.1 Fluorescence microscope

The followed procedure, consist basically, in use an inverted microscopy equipped with a slow-motion camera to visualize the movement of particles through the droplet when it is under the effects of SAW. This visualization is achieved because we can record under the $LiNbO_3$ substrate, which is transparent. The motion of the particles provoked by the SAW. is recoded and transmitted to the PC computer screen by the slow-motion camera. In this manner, the recorded video can be analysed and conclusions of it can be extracted. A picture sequence of the highlighted events during the experiment was extracted from the video recorded and is shown in the next section. A screenshot of one frame recorded by

the slow-motion camera is shown in the following image. It can be observed the quality of the recorded pictures can be obtained with the disposable equipment.

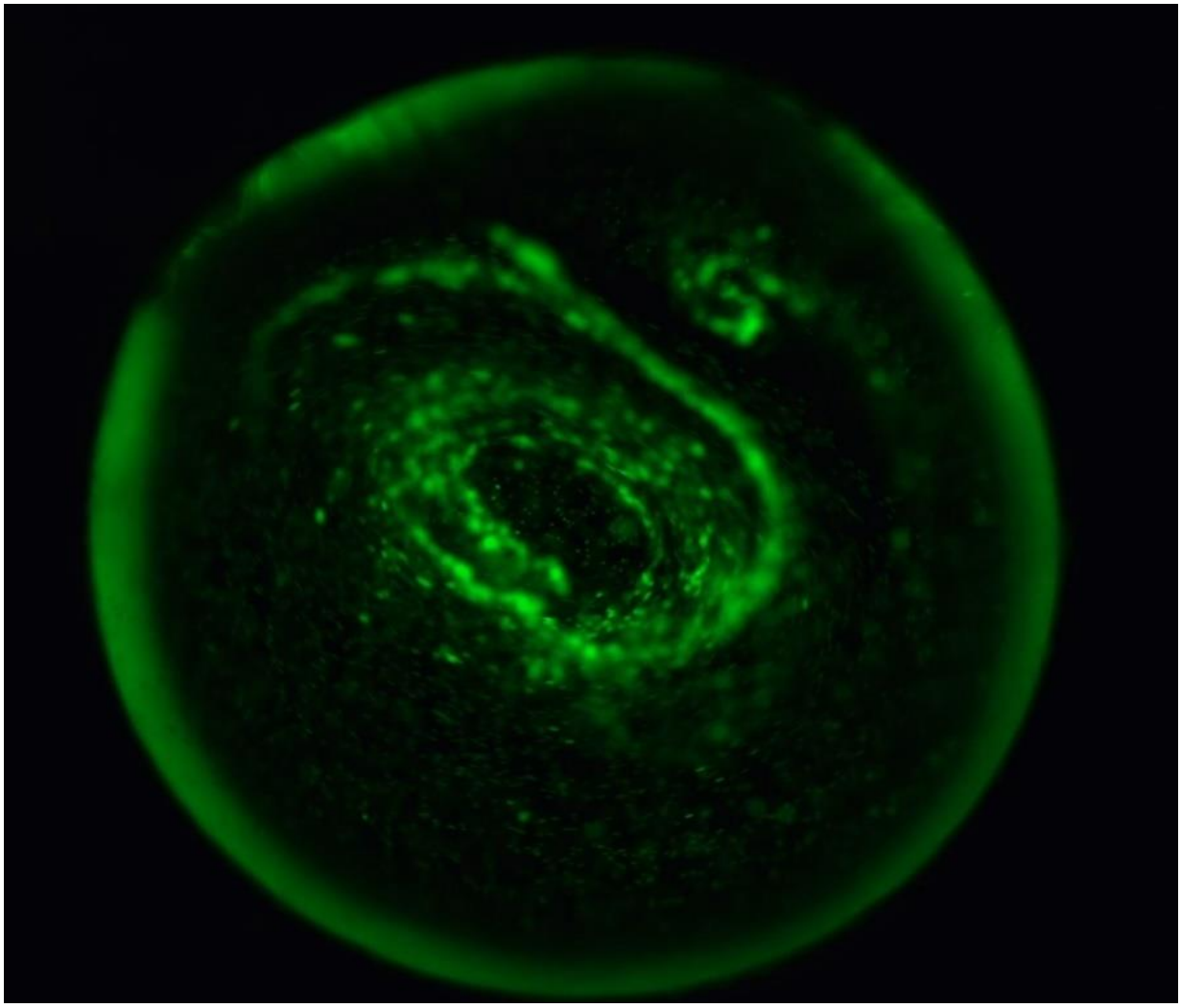

Figure 50. Frame of video recorded

5.4.2 PIVlab Software processing

To analyse the images observed the aid of an external software is needed. In this case an app of MATLAB served as great of help. PIVlab implemented as a toolbox and app for MATLAB is used to perform Particle Image Velocimetry (PIV) with image data, in the case of these study, these data consist in selected frames extracted from the recorded video in the previous stage. With the aid of these software is possible to obtain an estimation of the trajectories and velocity of the generated flows inside the droplet when it is subjected to a SAW. The procedure to obtain a good result by using this software depend greatly on the parameters selected. For example, the quality of the flow measurements is affected by computational details such as image pre-conditioning, sub-pixel peak estimators, data validation procedures, interpolation algorithms and smoothing methods. The accuracy of several algorithms was determined, and the best performing methods were implemented.

However, it is not always possible to achieve such precision that the analysis accurately reflects the exact movement of the flow inside the sessile droplet. In this regard by using the software options some graphics for a better understanding are depicted in the following section.

To contribute with the future students here there are some screenshots taken during the process in which some parameters to obtain good results with the software are presented. For example, the next picture shows how to draw the ROI for circumferential sections to shield the areas that the algorithm will not analyse. This is an important step to achieve a better precision of the calculated vectors.

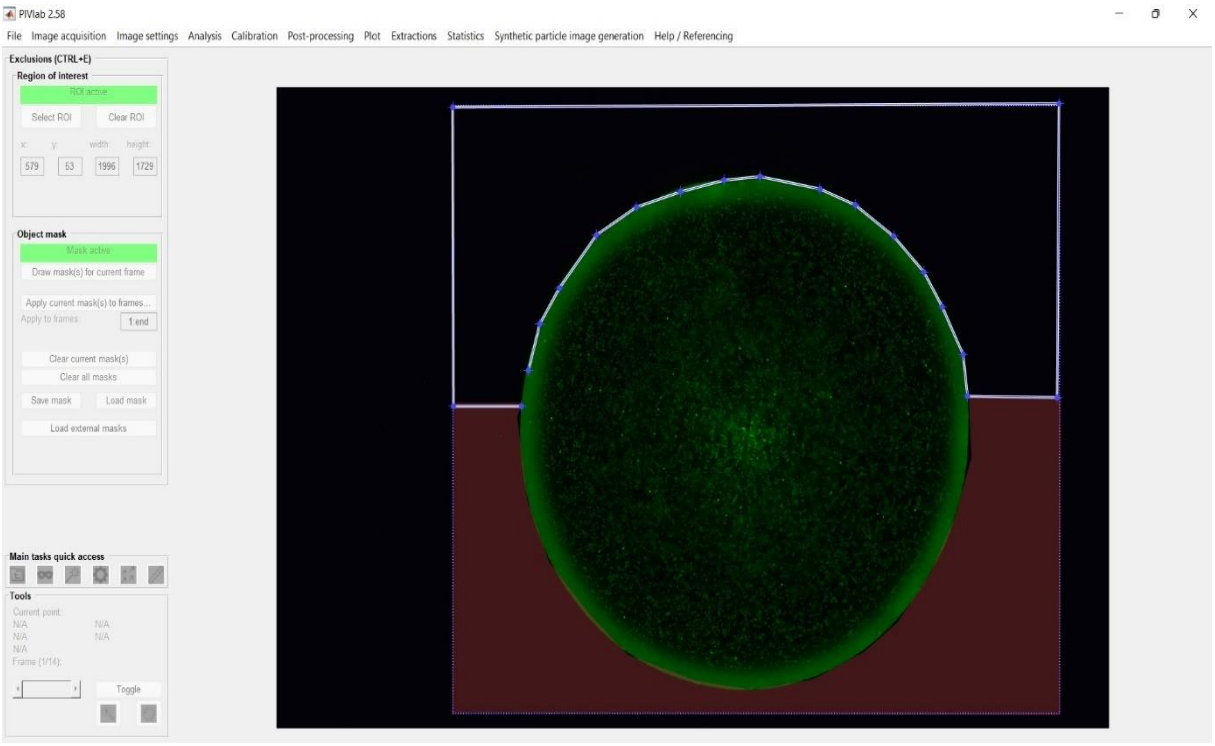

Figure 51. ROI selection

The next image shows the image pre-processing settings, depending on the studied object sometimes is better increase the parameters of the left menu. In the case of droplets with particles by increasing these values the light is filtered and the particles light reflected is minimized achieving a better accuracy of the particles displacement in every frame studied by the algorithm.

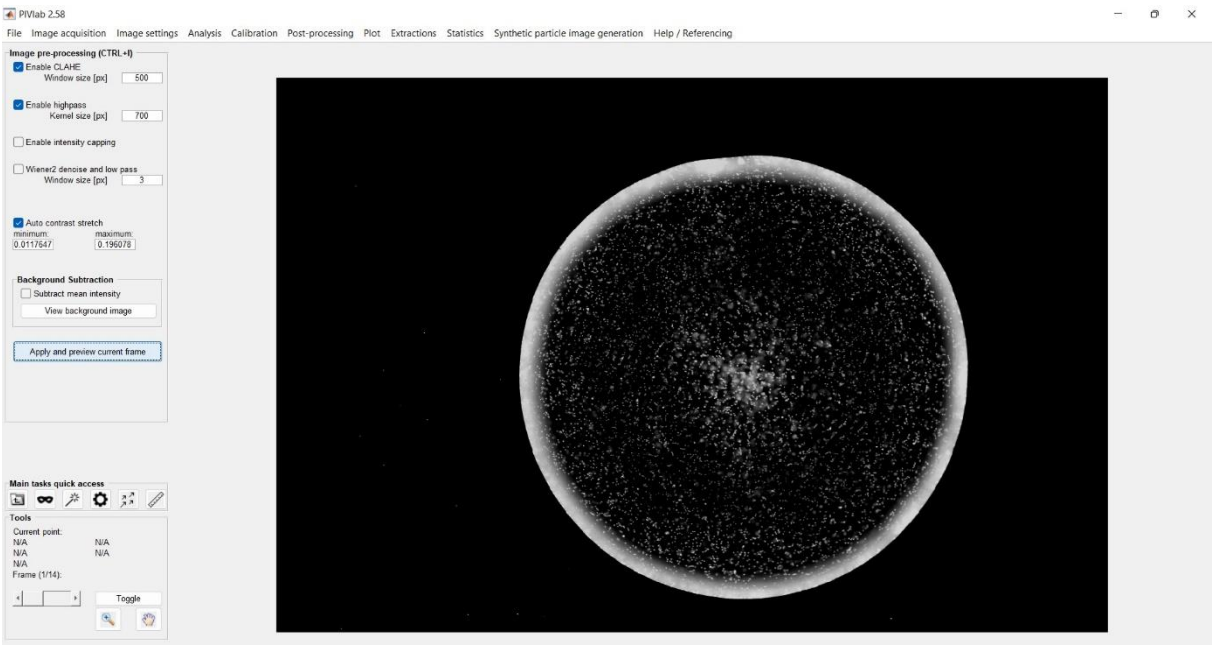

Figure 52. Image pre-processing

The next stage is to set up the size of the calculations step, here is recommended to use as more passes as possible, by doing this the accuracy of the obtained results would be higher since the number of passes increase the resolution of the algorithm to perform a better estimation about the trajectories traced by the particles frame by frame. In the next picture the selected values for that case are show in the depicted picture.

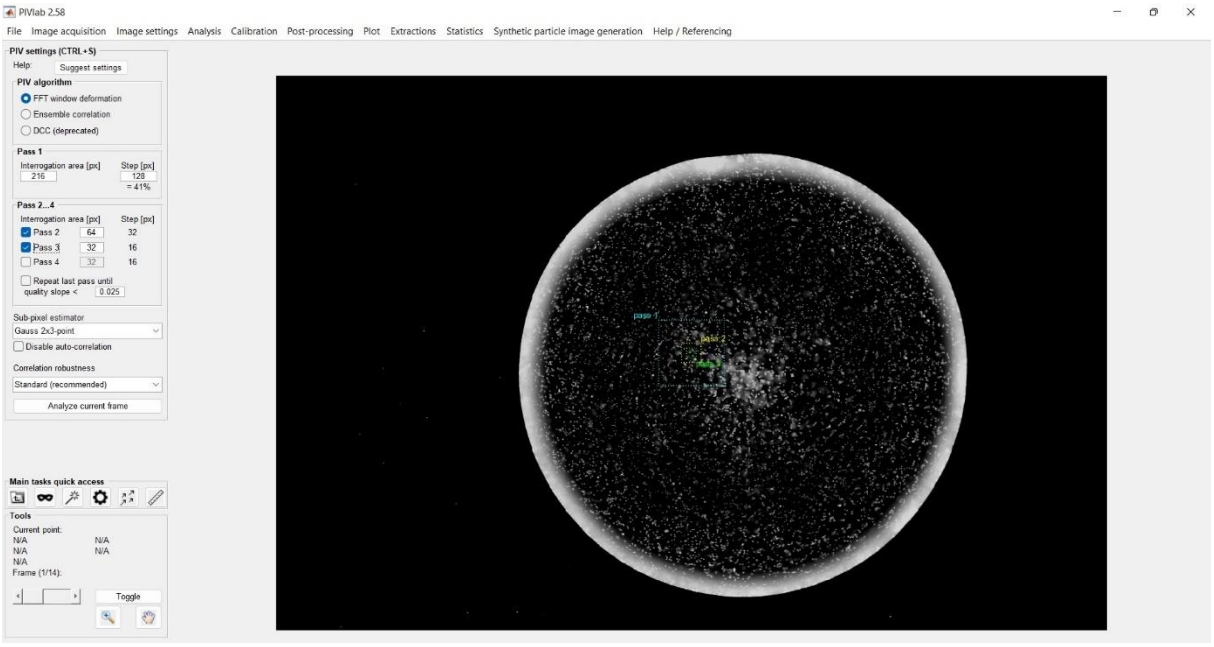

Figure 53. Frames analyse settings

After running the analyzed menu by analysing all the imported frames is important to do a calibration to give to the program the chance to have an approximately knowledge of the real areas and thus calculated with more precision the displacement generated inside the droplet as a consequence of the SAW applied. Here there are just two important parameters to fill, the first is the approximately diameter of the studied droplet and later the speed of the frames acquisition, in the case of this study the droplet had a diameter of 2,8 mm and the recorded video was set to 6 frames per second.

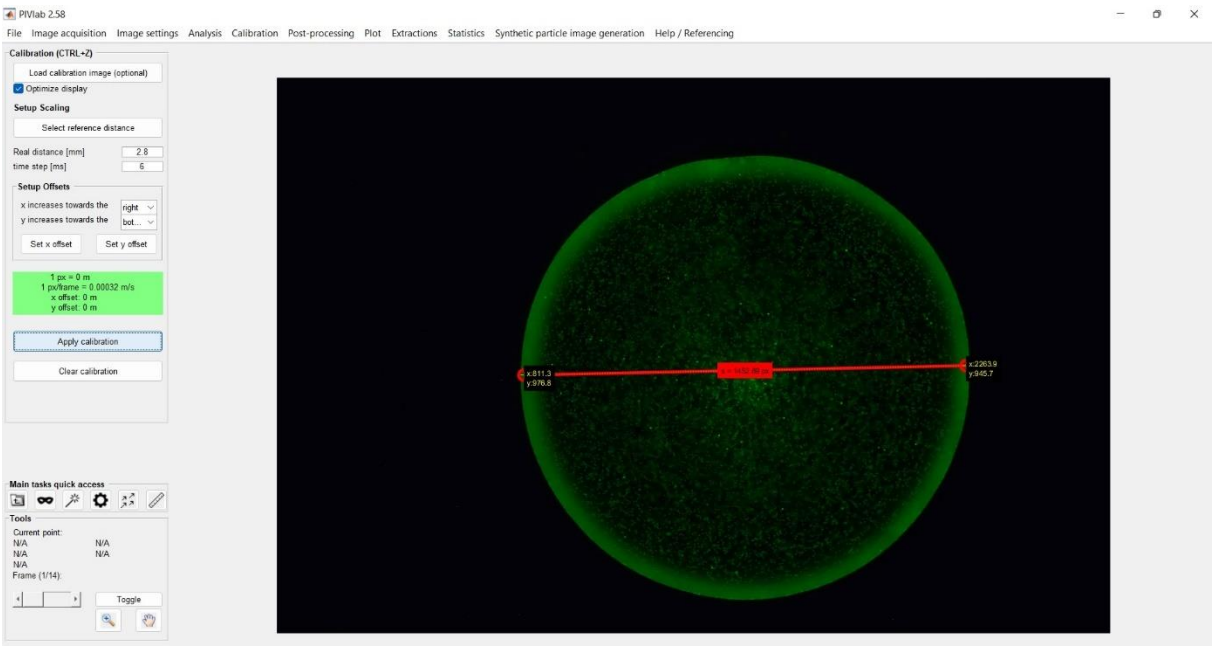

Figure 54. Droplet calibration

As previous step of the final processing a filtration of the speed areas is highly recommended by applying a post image processing in which the speed limits are selected. These parameters are difficult to fix and then many trials are necessary to obtain the desired result. Being not a general rule, in some cases of this study the suggested parameters were followed on many occasions as can be observed in the following picture. To select the most appropriated velocity limits exists another powerful tool but as best of my knowledge to analyse droplets the image-based validation worked better than the velocity-based validation This is the last step before applying the final algorithm which is dependant of the variables that are the subject of every study.

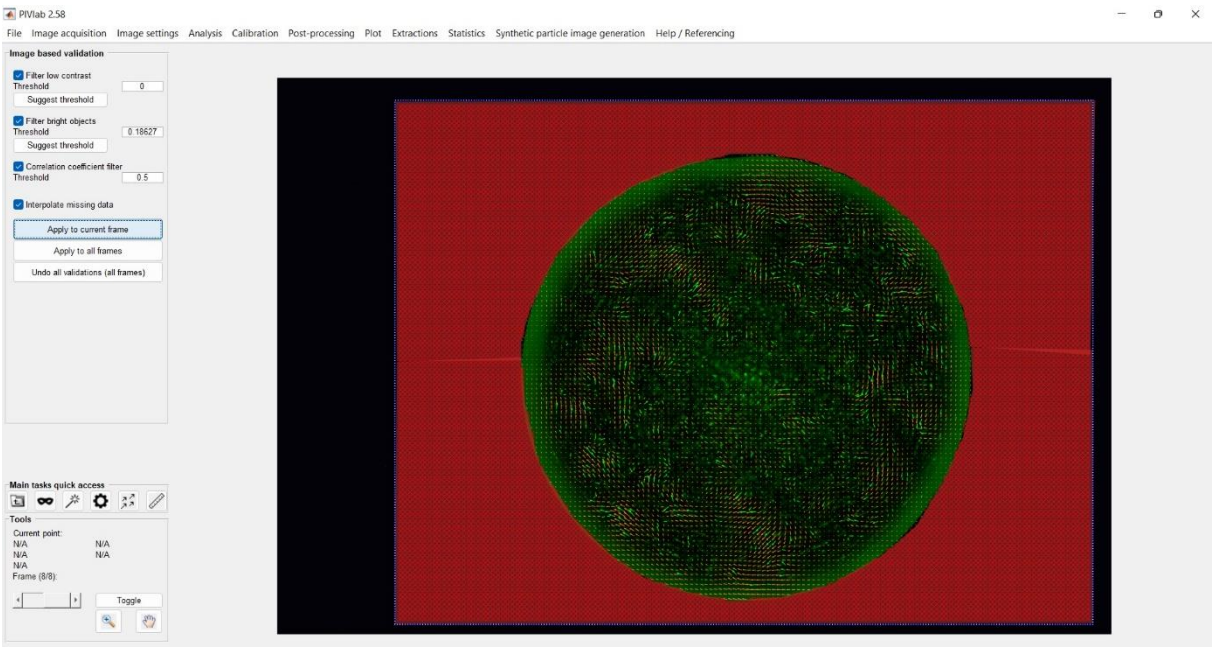

Figure 55. Image post-processing

By following the mentioned steps, the last stage is to plot the parameter at the convenience. The most interesting for this project of the variety options, is the magnitude of the speed inside the droplet. By doing this it will be possible to visualize the areas where the particles experience higher gradients of speed as a consequence of the SAW imposed. A one example of this is the next picture, it shows a droplet that have been already analysed. The legend in the left part in the picture indicates the speed of the particles in the occupied region. The higher the intensity of the colours the higher speed in that region. On the other hand, the groups of particles are represented as can be observed in the picture as aggregations of coloured areas like the shown in the picture. Can be seen four main groups of particles spread around the droplet which represents the areas where the algorithm calculated as the areas with the higher concentration of particles with the highest speed. The red colour around the droplet represents a mask, this area is set before the analyse and is used to mark areas that will not be studied by the algorithm as have been commented before. The following picture shows of what a look like of the analysed droplet in which measure the speed of the particles were the purpose.

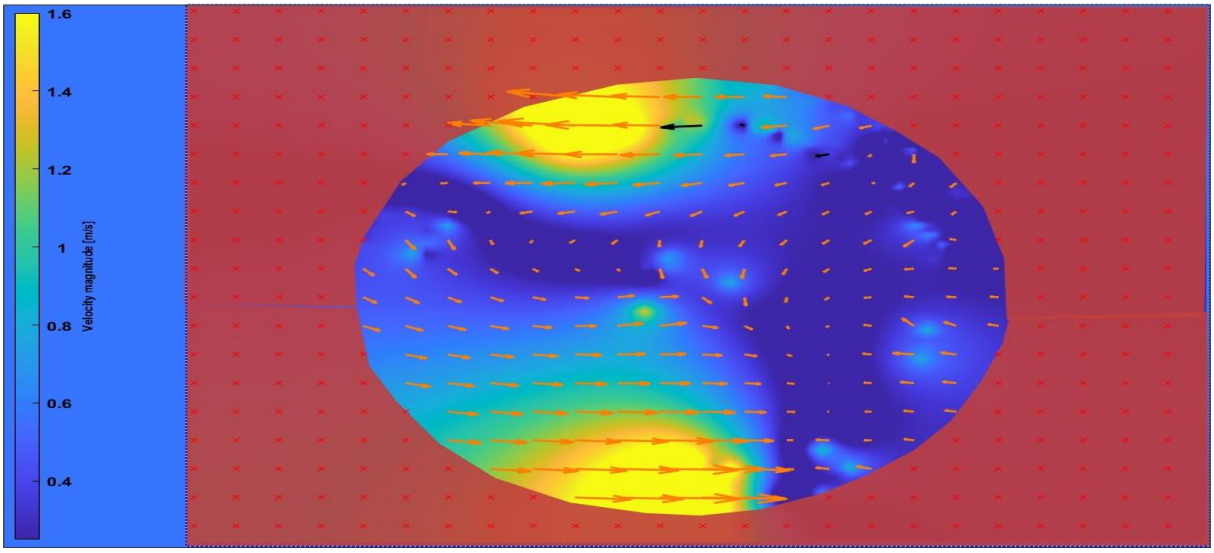

Figure 56. Example of analysed droplet

For the obtention of the graphics showed in the next section is necessary to draw a line. To achieve this, in the extraction menu there is the possibility to draw a polyline between other options like the shown in the picture below. In this way is possible to visualize for example the magnitude of the speed of all the points situated around the line. In other words, that line split the droplet and shows the velocity of the vectors that the plane contains. The first point of the line is the point of reference of the plotted graphic and represent the origin of coordinates for the plotted values. The accuracy of this graphics is limited and is highly dependent of the parameters chosen in the previous stages as well as the calibration of the image. For the purposes of this work the graphics help to shed light on the interpretation of the shown sequence video frames recorded.

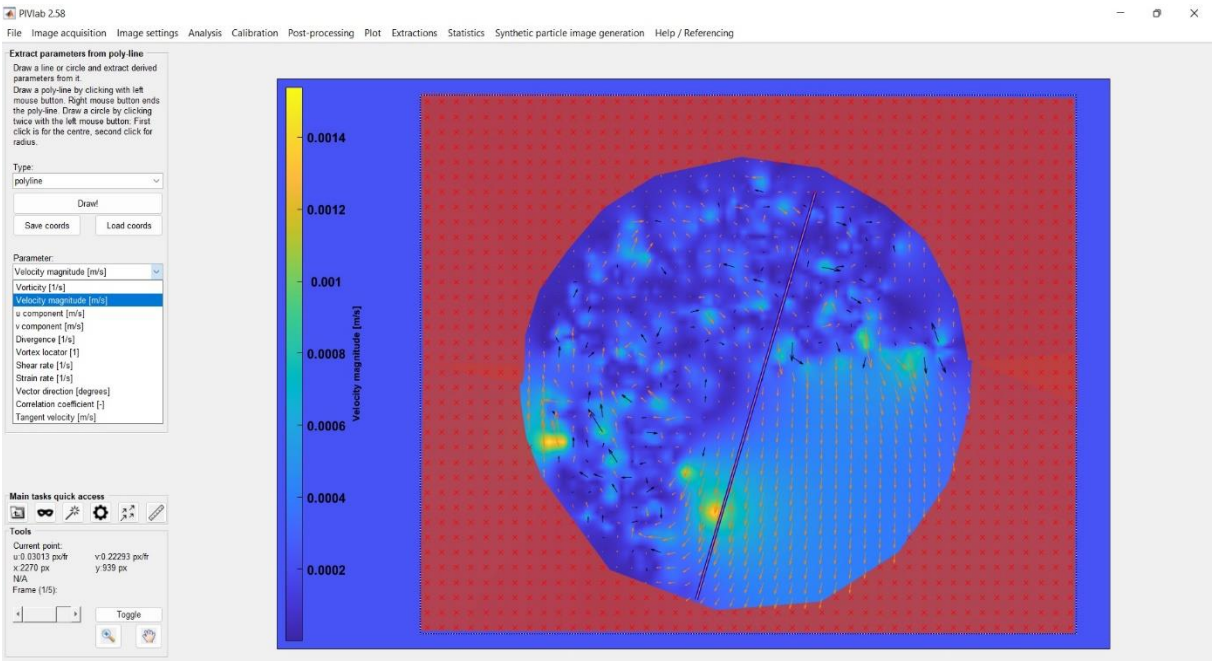

Figure 57. Plotting the magnitude of the velocity

6 Experiment results

In this section the results obtained are presented. These experiments seek to reproduce the concentration and the dispersion of the particles that were made in the previous studies and conduct a discussion of the results based on the theories behind the phenomena. Being the frequency and input power directly related to the *k factor* and the attenuation X_s and the different states of the particles are characterized. These results are compared with the observations made in these studies and a short discussion of the results is conducted for each case based on the gaps observed in the literature. To support this a post processing was run with PIVlab and the outcomes are also presented.

To support the compression of the results here presented, sequentially video captures are shown in which the most relevant states of the particles are observed.

6.1 Straight IDT 20 Mhz

In this first experiment a straight IDT with a nominal frequency of 20 MHz was used to achieve a 7 µm particle concentration in the centre of the droplet for achieving later a particle dispersion to form a ring shape in the periphery of the droplet.

6.1.1 Particle cluster 7 µm

In the following sequence of pictures can be observed the process in which the particles are concentrated in the centre of the droplet. a) The first picture shows the initial state when any force is applied. b) Few seconds later an input power of 15 dB is applied and the particles begin their movement. Trapped in concentrical circles as a consequence of the attenuation of the acoustic amplitude in the fluid this loss of energy is converted into mechanical motion into the fluid. This leads to faster motion of the vortex that can be seen in the picture. The *k factor* obtained for this situation in which the frequency is 8 MHz is equal to 0.11. Is in this situation when according to Yukai Liu et al. the ASF force is dominant over Fc and ARF and rule the movement of the particles in which is called acoustic streaming [31]. The effect of the ARF force at this power has a neglectable effect in the movement of particles, moreover, the vortex velocity is slow, and the Fc has a minimal impact in the particles trajectories as can be observed. On the other hand, the attenuation of the SAW *Xs* gives a value of 6 mm which is greater than the particles radius. This indicates that according with Destgeer et al. [11] the formation of the SAW when K<1 ARF due to S_{SAWs} dominate over that ARF due to $T_{SAW.}$ In this situation the smaller particles are not captured by S_{SAWs} and are dominated by ASF. c) By increasing the power to 20 dB and the frequency set at 18 MHz this assumption becomes more obvious the *k factor* is still below the unit and a cluster formation is achieve in the centre of the droplet as can be seen in the figure (58 c) in which the beginning of the cluster formation can be observed

for the first time. d) To achieve a clear concentration the power was increased to 35 dB with a significant increment of the frequency to 35 MHz which is explained by Yuka et al [29]. It is assumed that the aggregation behaviour of small particles can be achieved by high-frequency acoustic waves, because smaller wavelengths in the fluid can have a stronger backscattering effect on small particles. For these values, the vortex begins to rotate faster, observing large speed gradients with the *k factor* < 1 and *Xs* still greater than the particles radius. According with Destgeer et al. [11] the ARF due to S_{SAW} capture and concentrate the particles. Finally, a particle cluster is obtained as is shown in the last picture (58 d) taken by the fluorescence microscope.

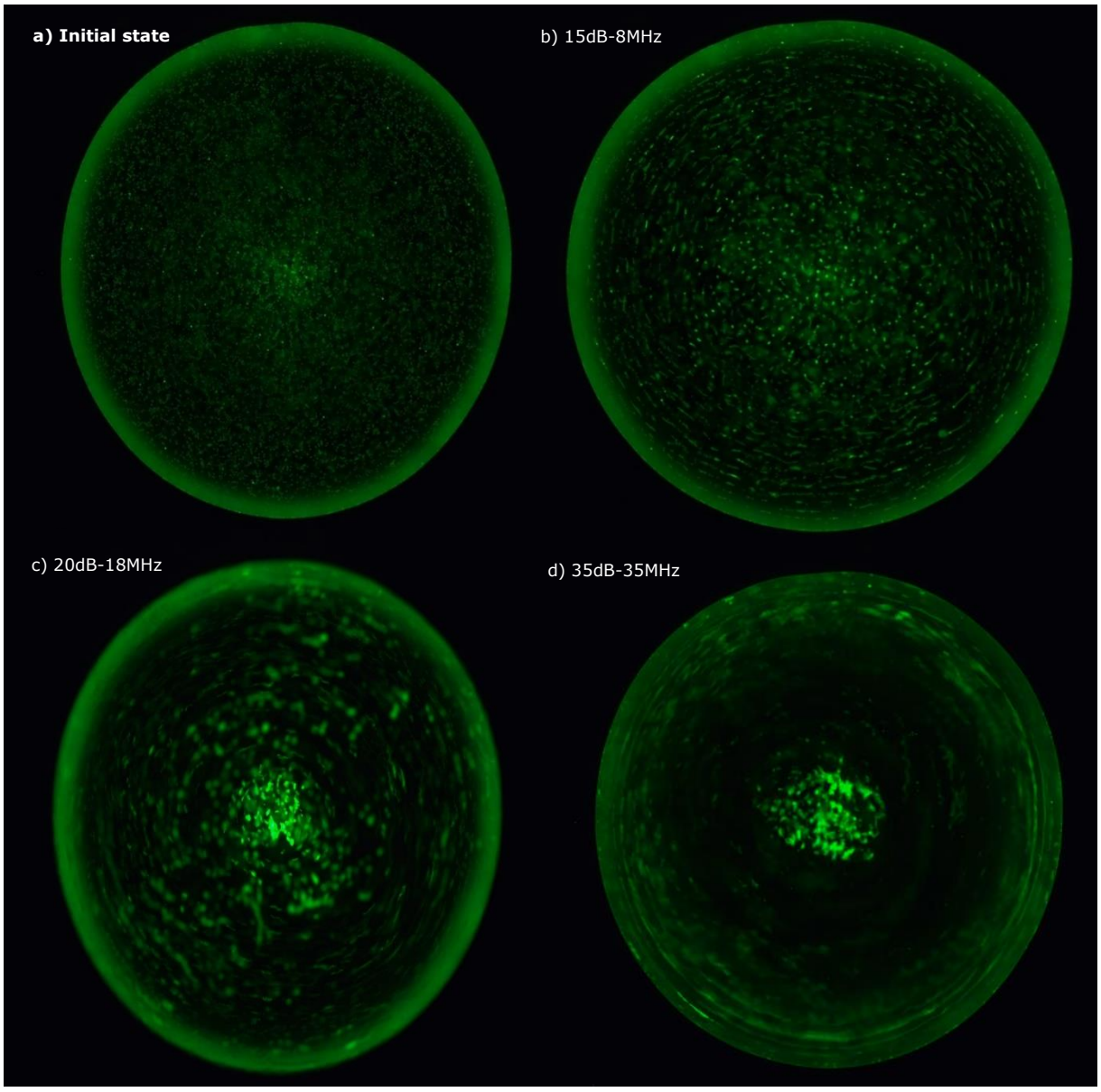

Figure 58. Sequence of particle cluster formation 20 MHz

In order to visualize this process more clearly, the following processing using PIVlab were made. In the following picture can be seen how the particles placed at the beginning of the experiment spread around all the volume of the droplet commence to rotate when an input

power is applied. As has been commented this input power is still low and the acoustic streaming governates the movement of particles. The vectors calculated by the program show the trajectories of the particles in this situation which is consistent with the observations made by Yuka et al [29]. in which the particle streaming was identified when the *K factor* is below the unit.

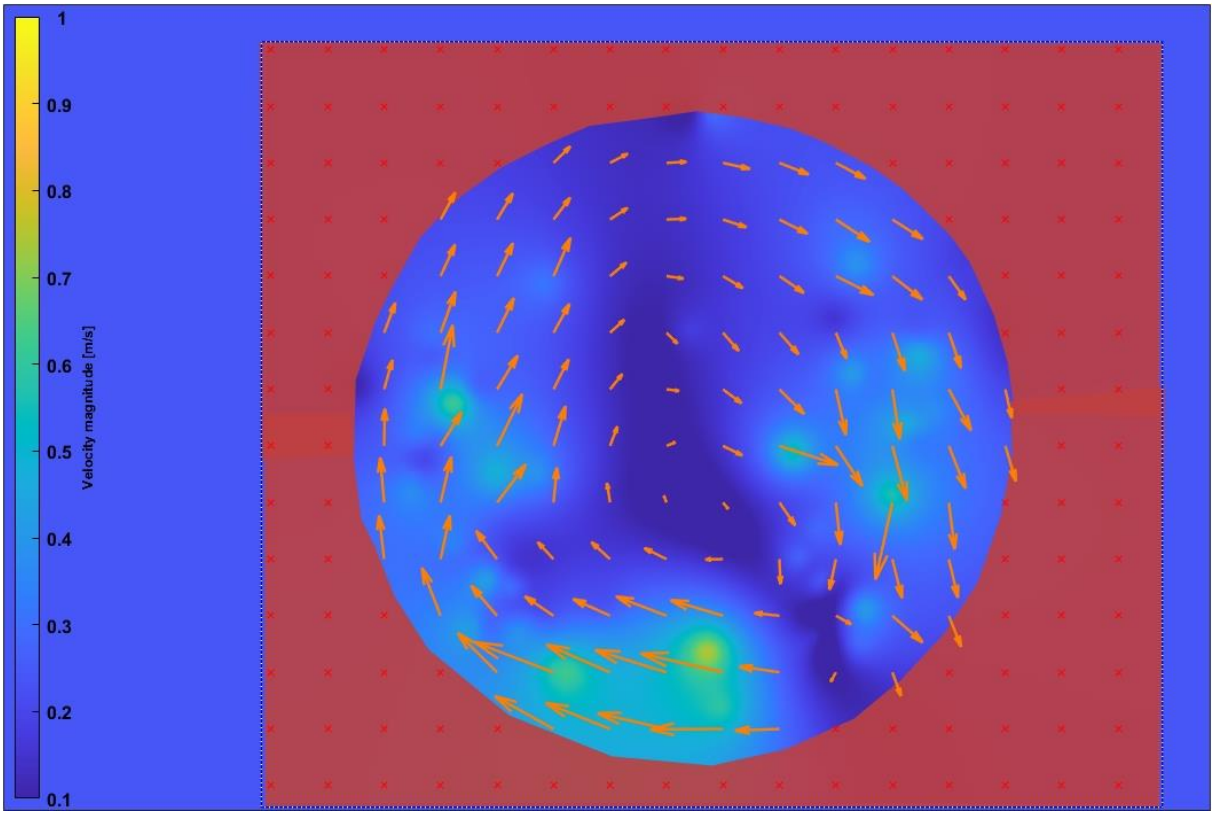

Figure 59. Vortex formation

The next graphic was obtained by drawing a line across the maximal circumferential section of the droplet. The velocity magnitude of the particles situated in this area was calculated and show how the velocity in the periphery of the droplet is higher than in the centre. This indicates the existence of the vortex inside the droplet as a consequence of the applied forces discussed before. This is consistent with the particle streaming observed in the experiment where the particles located in the periphery were rotating faster than those which were located in the centre of the droplet.

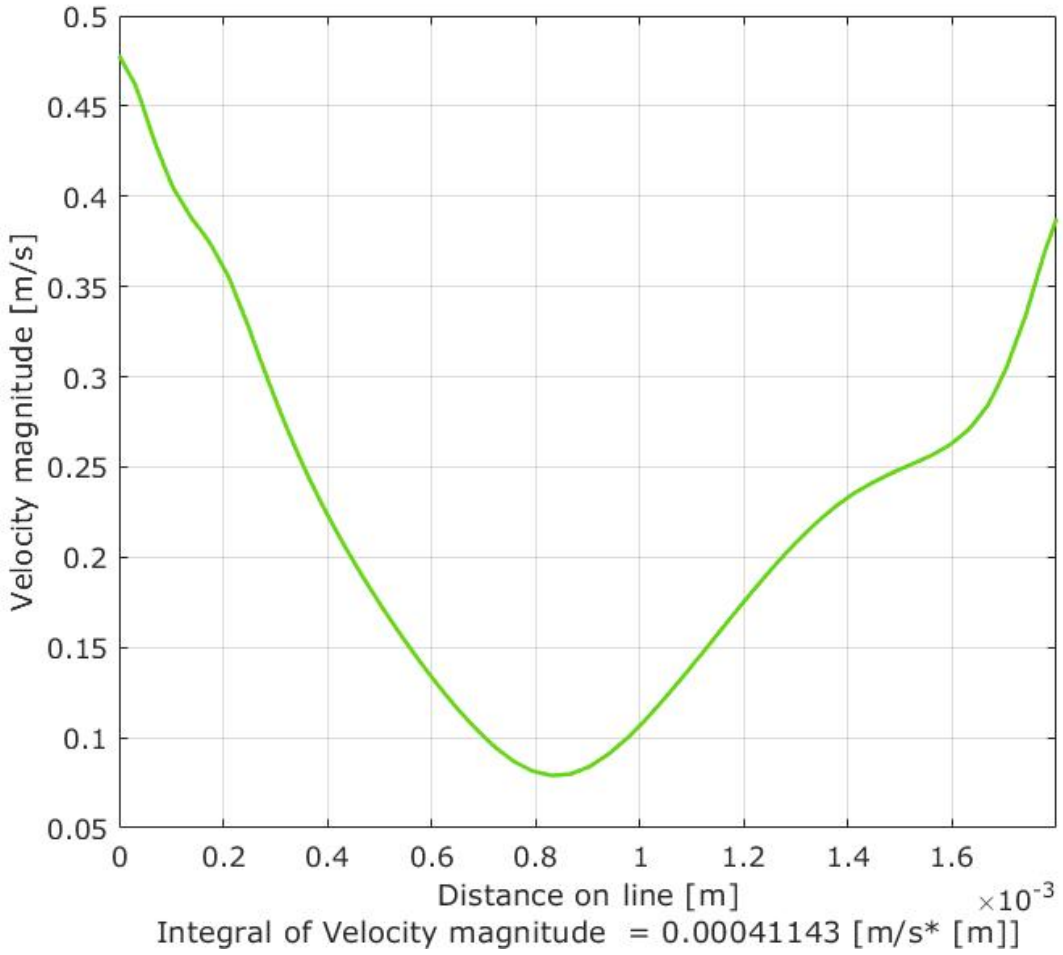

Graphic 1. Velocity magnitude in the particle streaming

The next picture proves how the change in the parameters of the SAW formation can change the trajectories of the particles. This case corresponds to the situation in which the input power was increased together an increment of the frequency. Can be observed how the vectors indicates the particles are moving to the centre trapped in the flow governate by the ARF when the k factor becomes higher than the unit. This can be consistent with observations made by Li et al. where the shear induced migration arising due to azimuthal velocity gradients result in the transportation of particles across azimuthal streamlines into the interior of the vortex, inward direction [5].

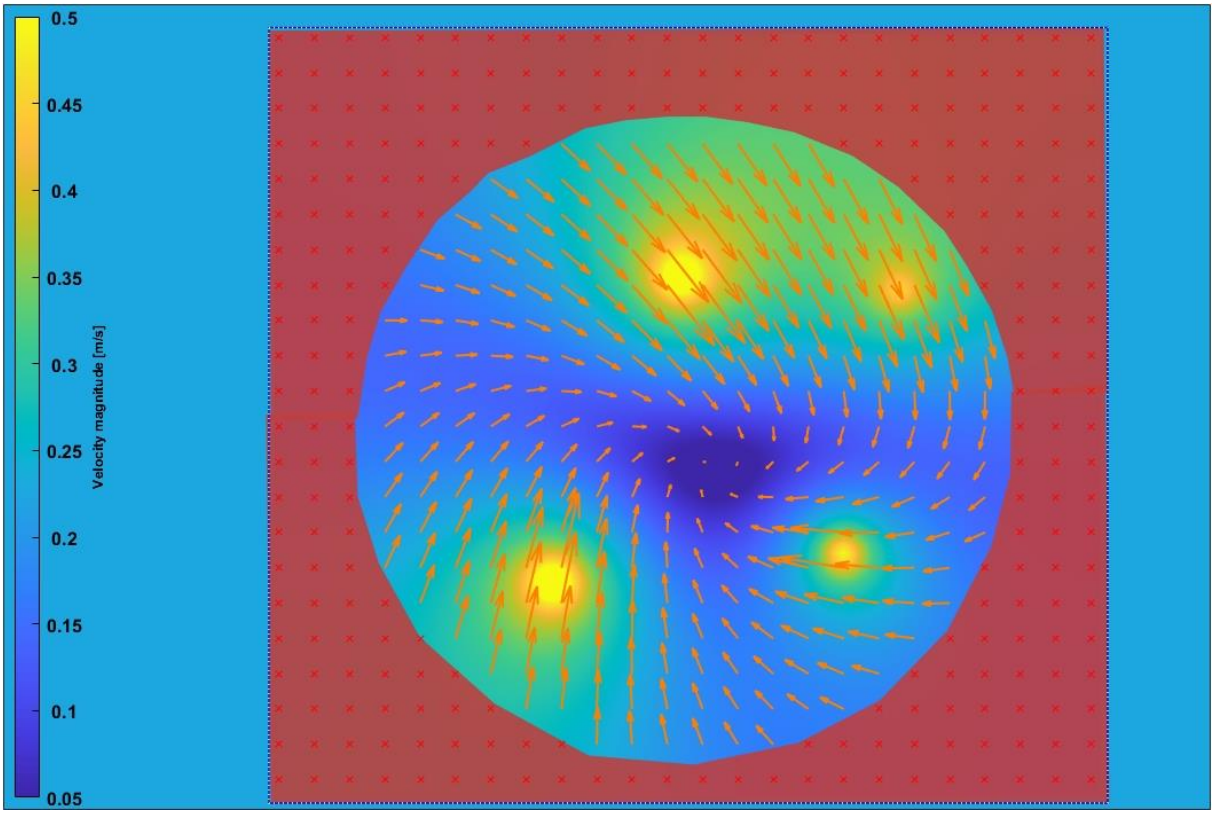

Figure 60. Particle concentration trajectories

By comparing the next graphic with the previous one plotted to show the particle streaming, this graphic shows the displacement of the maximum velocity of the particles from the periphery to the centre thus confirming the existence of a force which drag the particles to the centre and leading to a particle cluster.

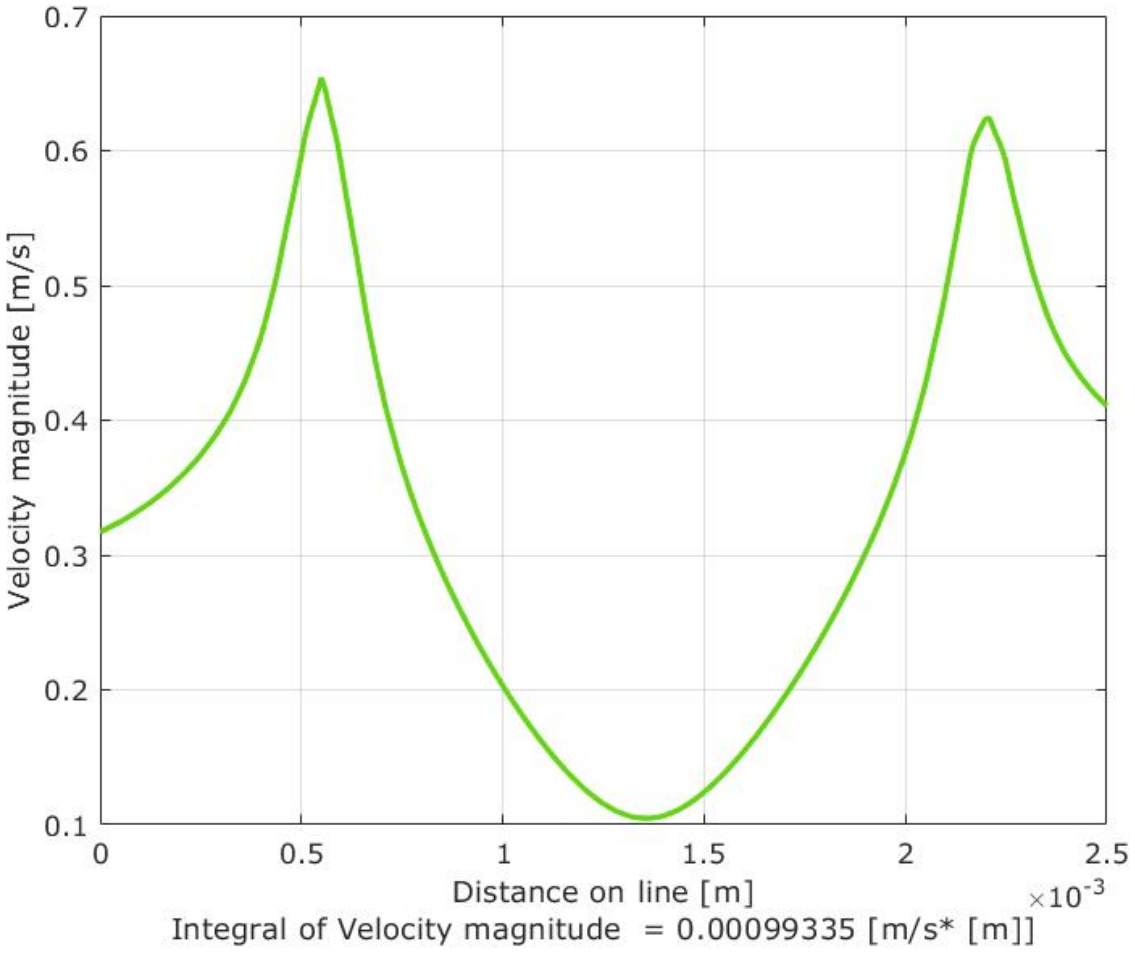

Graphic 2. Velocity magnitude in the particle vortex

The following last picture was included to show the streamlines followed by the particles and comes to confirm the dependence of the input power, the frequency, and the diameter of the particles with the forces arising of the SAWs.

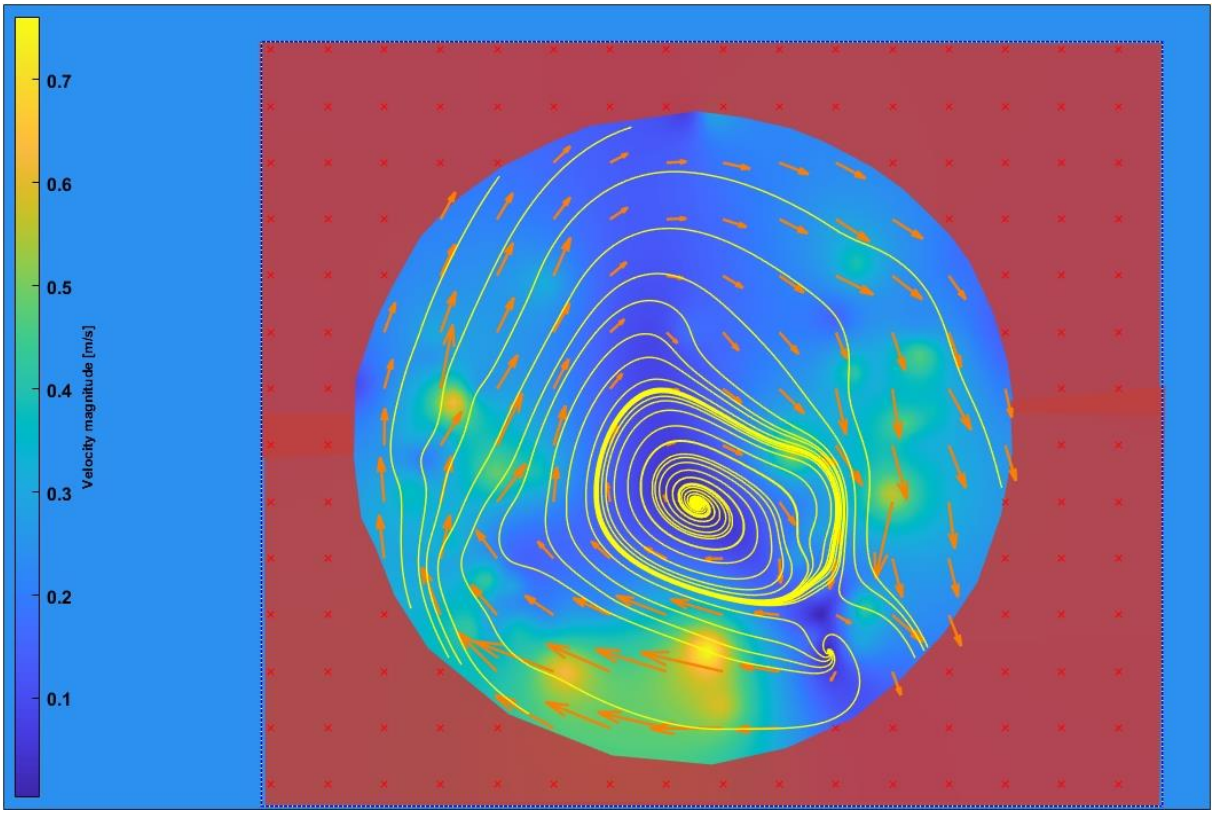

Figure 61. Particle concentration streamlines

6.1.2 Particle ring 7 μm

The next sequence of pictures represents the dispersion of the 7 μm particles inside the sessile droplet. a) Starting from the concentration achieved before the purpose now is to drive the particles to the periphery forming a ring shape like the show in the figure 62. b) By increasing the power to 45 dB the vortex starts to rotate faster by the losing of energy of the acoustic wave. This shorter attenuation as a consequence of the higher frequency provokes a faster vortex rotational speed improving the centrifugal force F_c which becomes dominant in the process and push the particles to the periphery. c) The ARF force that kept clustered the particles trapped before in the Eckman layer commence to leave this region cause of increment of the power applied. Thus, according to the observations made by Raghavan et al [4] by increasing the power is possible to drag out the particles from this region called Eckman Layer. d) With a power of 55 dB and a fixed frequency of 103 MHz most of the particles were conducted to the periphery as can be observed. In this situation the *k factor* become significatively higher than the unit and the particles are pushed towards the boundary of the droplet forming a ring shape confirming the dominance of the centrifugal force over the ARF.

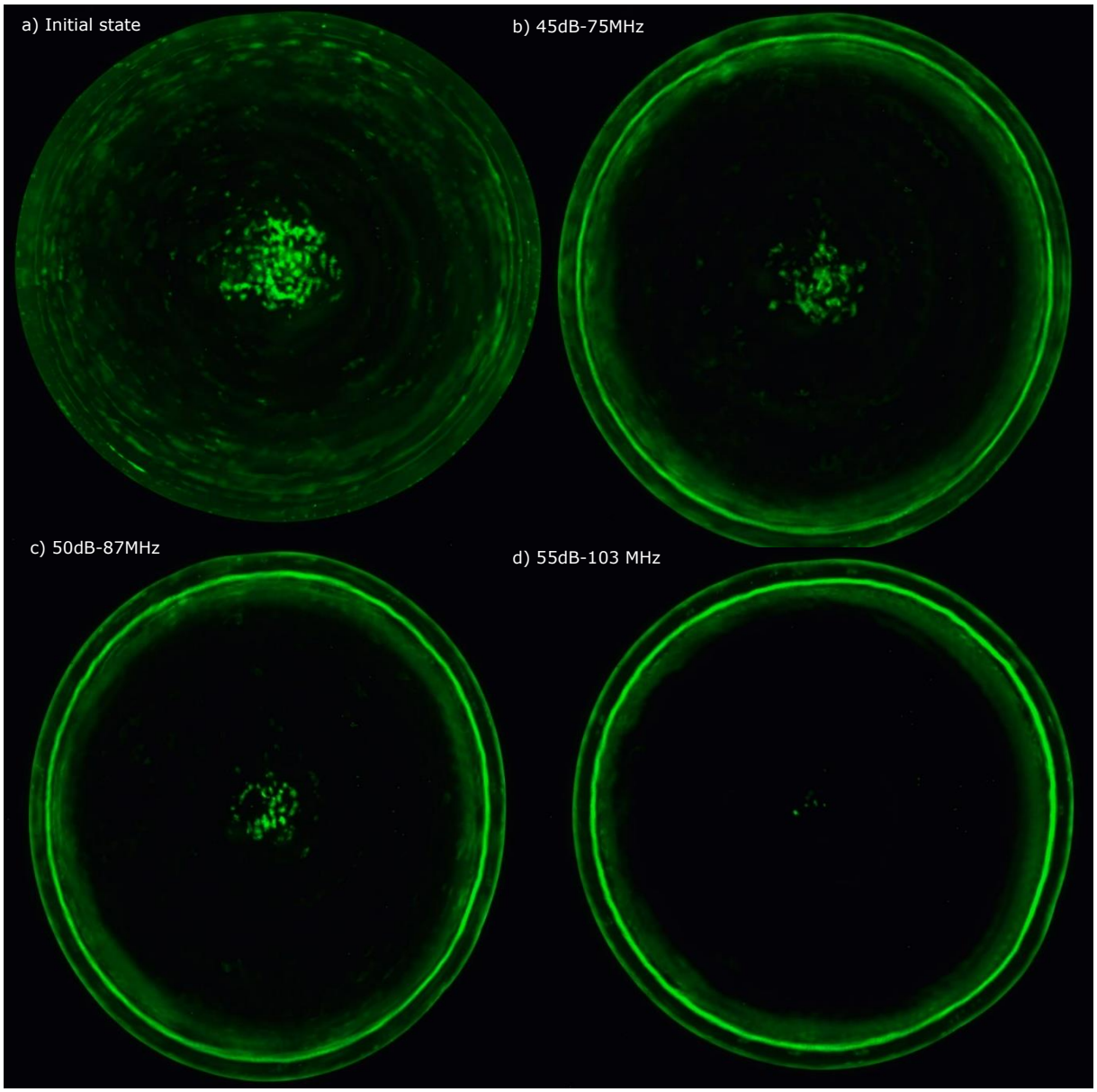

Figure 62. Sequence of particle ring formation 20 MHz

Next picture shows a set of vectors indicating a dispersion trajectory of the particles from the cantered positions outwards. This can be consistent with the relation proposed by Yuka et al. [31] in which the relation between the acoustic amplitude and the input power was described. According to the study a relation between Fc and acoustic amplitude was observed. The higher the input power leads to an increment of the rotation speed of the vortex improving the Fc and therefore and increment of the acoustic amplitude. This increment reflects the dispersion of the particles.

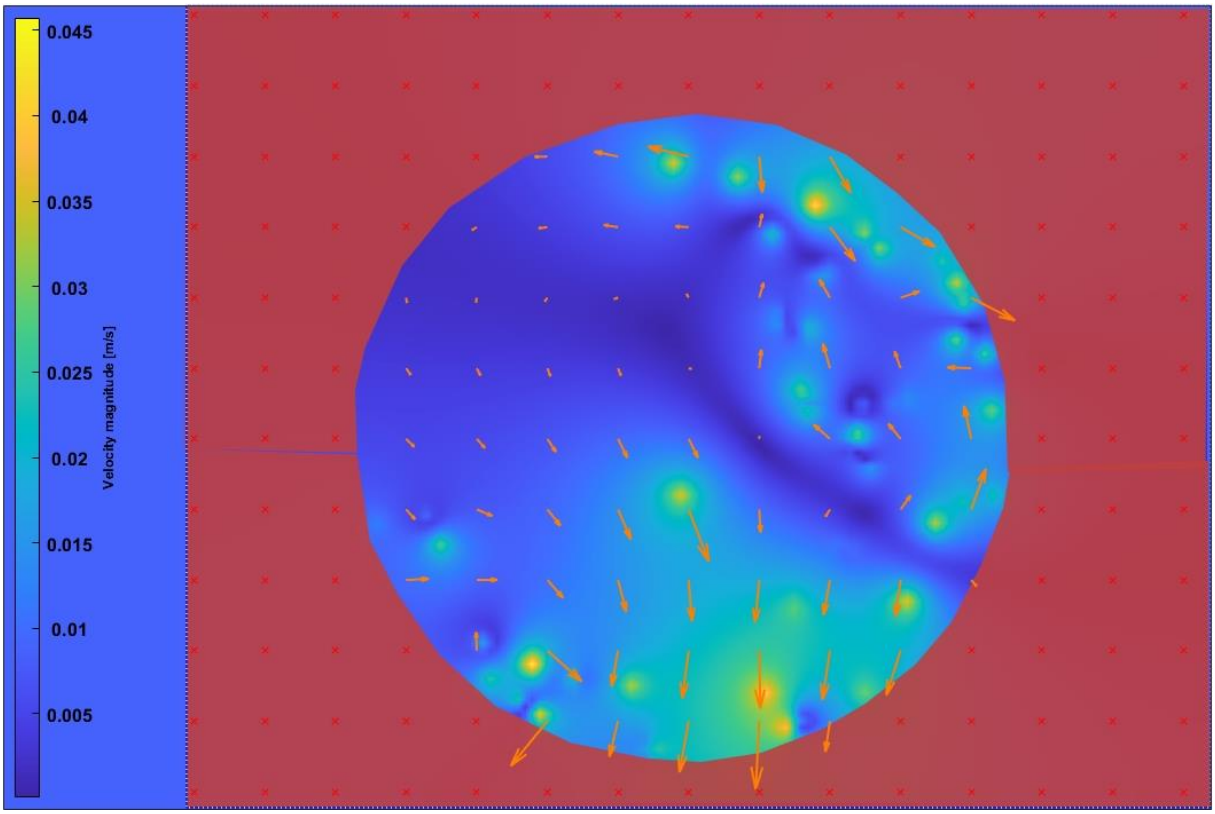

Figure 63. Particle dispersion processing

In the following graphic is described the change of the velocity of the particles from the centre of the droplet. Can be noted how the particles move faster in the outer regions than in the inner areas indicating a dispersion of the particles for this case.

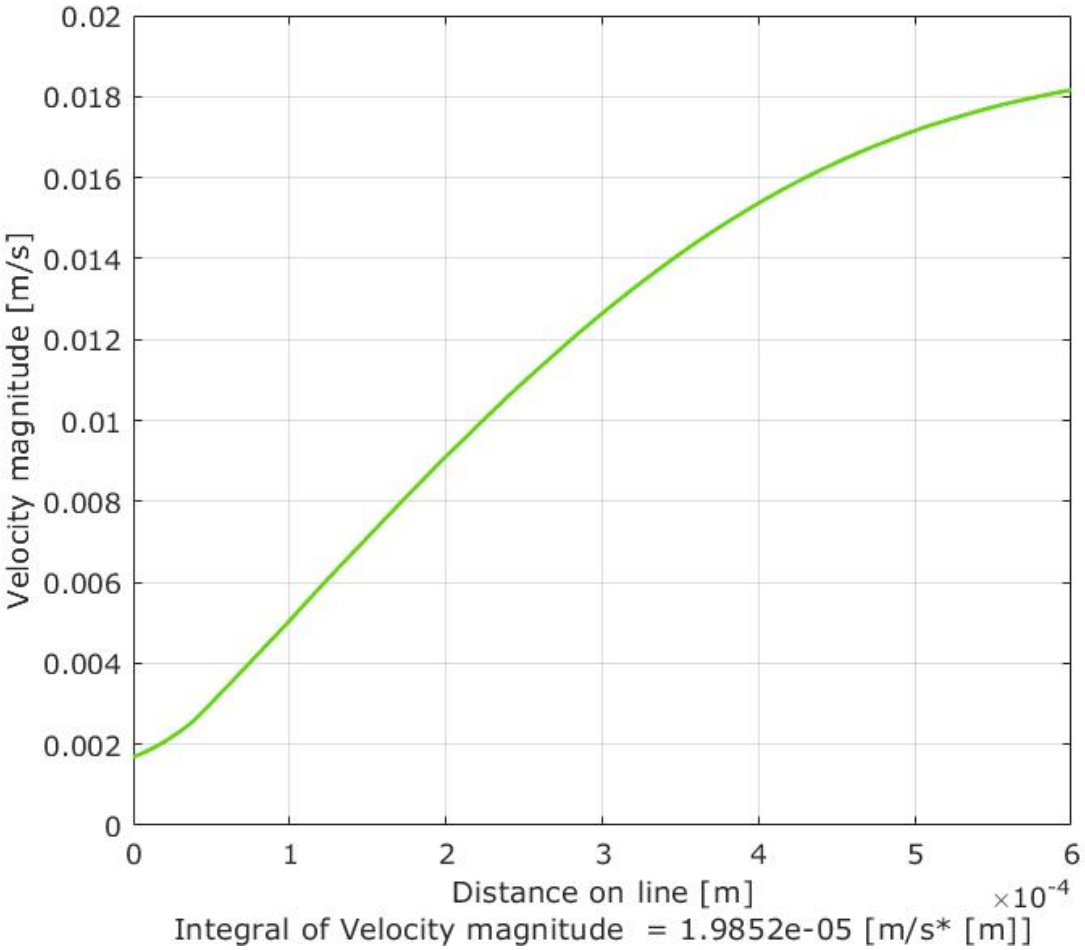

Graphic 3. Speeds calculated in the particle dispersion process

The streamline map shows how the groups of particles are moving to the periphery of the droplet from the previously occupied inner positions. This can be consistent with the observation made by Li et al [5] in which conversely of the previous case now is the Azimuthal acoustic streaming arises of the recirculation flow inside the droplet which push the particles in the outward direction.

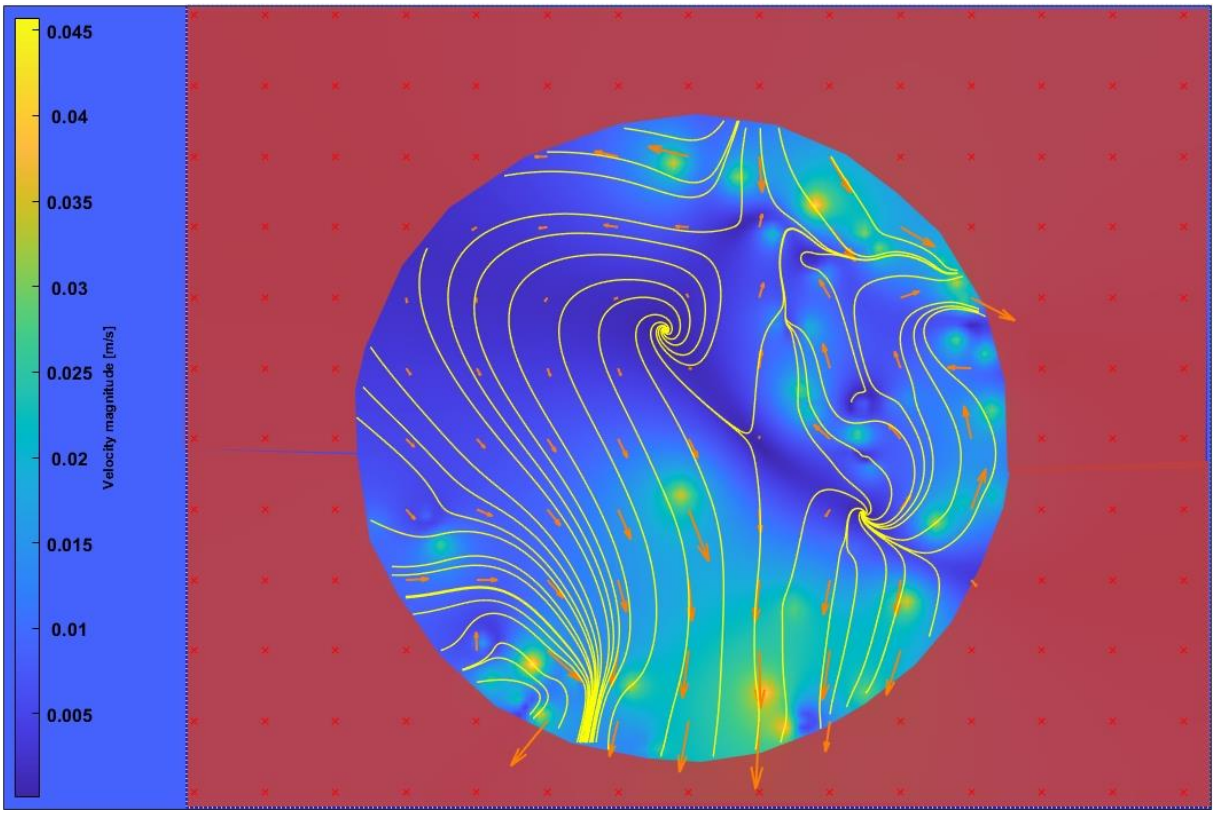

Figure 64. Particle dispersion streamlines

To conclude with this analysis, a static picture was taken at the end of the experiment in which the final situation is depicted. This image shows how the particles were gathered forming a clear ring around the periphery.

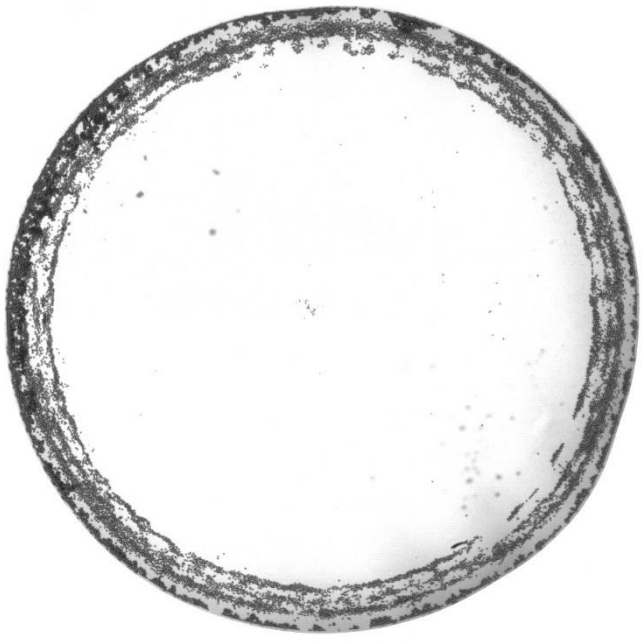

Figure 65. Final state of the droplet after the experiment

6.1.3 Discussion

In this point is important to note some assumptions that arise from the observations made during the experiment. As can be seen in the picture 62 d, not all the particles have managed to escape from the stagnation point. This may be due to several reasons. In one hand, if we consider the amount of heat exchanged with the environment to be negligible, we have that the greatest exchange of energy is produced by convection between the substrate and the droplet placed on it. By assuming this, then the droplet gets hotter as the experiment continues in time (measured 68 seconds from the beginning). We could assume that the surface tension of the droplet decreases with increasing temperature. This change in the surface tension could provokes an increment of the area in contact with substrate. This could lead to a rise in the friction between the droplet and the substrate affecting somehow to the Eckman layer where the remaining particles are located hindering the escape from that area. This could force to increase even more the input power and the time of the experiment making worst the situation because the spin of the created vortex could be higher enhancing then the friction. On the other hand, if this situation continues along the time a faster droplet evaporation and then a change in the contact angle of the droplet is expected. This effect somehow can compromise the movement of the particles and demands the use of different values of input power and frequencies than those predicted by the theory. In this regard, if the figure 58 d is observed, a clear concentration is not achieved because it would need more time to achieve it extending then longer the experiment duration than the optimal time to tackle after the dispersion of the particles.

6.2 Straight IDT 40 Mhz

A different IDT with a double nominal frequency is used to achieve the particle concentration and ring formation.

6.2.1 Particle cluster 7 μm

a) Starting from the steady state when no forces are applied a low power of 10 dB is transmitted to the IDT (see figure 66 b) that rapidly begin to concentrate the particles in the centre as can be observed. c) The higher nominal frequency of the IDT leads the ARF force can trap the particles into the vortex with less input power. Since the frequency increase significantly 47 MHz with little increases in the input power 25dB. As a consequence, the vortex which rotates fast becoming the ARF the dominant force in the process. In this case the frequency increase significantly for the power applied in comparison with the previous case and the *k factor* turns fast greater than the unit which suggest the ARF force is the force involved in the change of the direction of the particles. d) After few seconds, the power applied is increased to 30 dB and this force drag the particles into the Eckman layer whereas can be observed the particles shrinkages, demonstrating the role of the ARF in the particle concentration predicted by Destgeer et al [11]. The higher frequency of the IDT made possible to pass to the concentration as fast as it was exceedingly difficult to capture the moment in which the particle streaming took

place, this can have a positive effect since a rapidly concentration ease the thermal effects and the particles shrinkage before the evaporation of the droplet start to succeed.

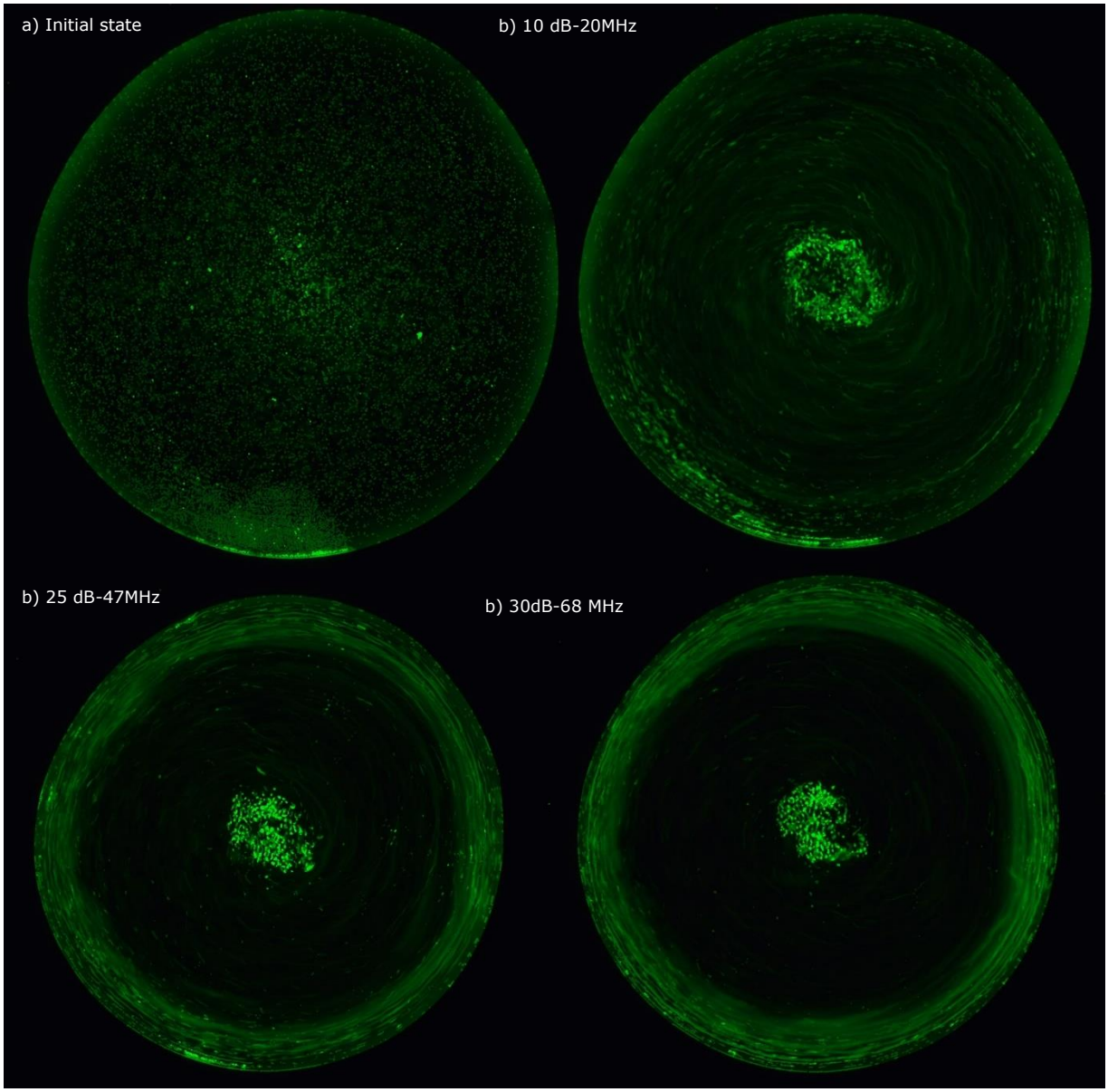

Figure 66. Sequence of particle cluster formation 40 MHz

In the post processing the calculated vectors show how the groups of aggregated particles moves towards the centre of the droplet. This is consistent with the experiment observed by Destgeer et al [16] where the regime R1 was observed also for higher nominal operation frequencies.

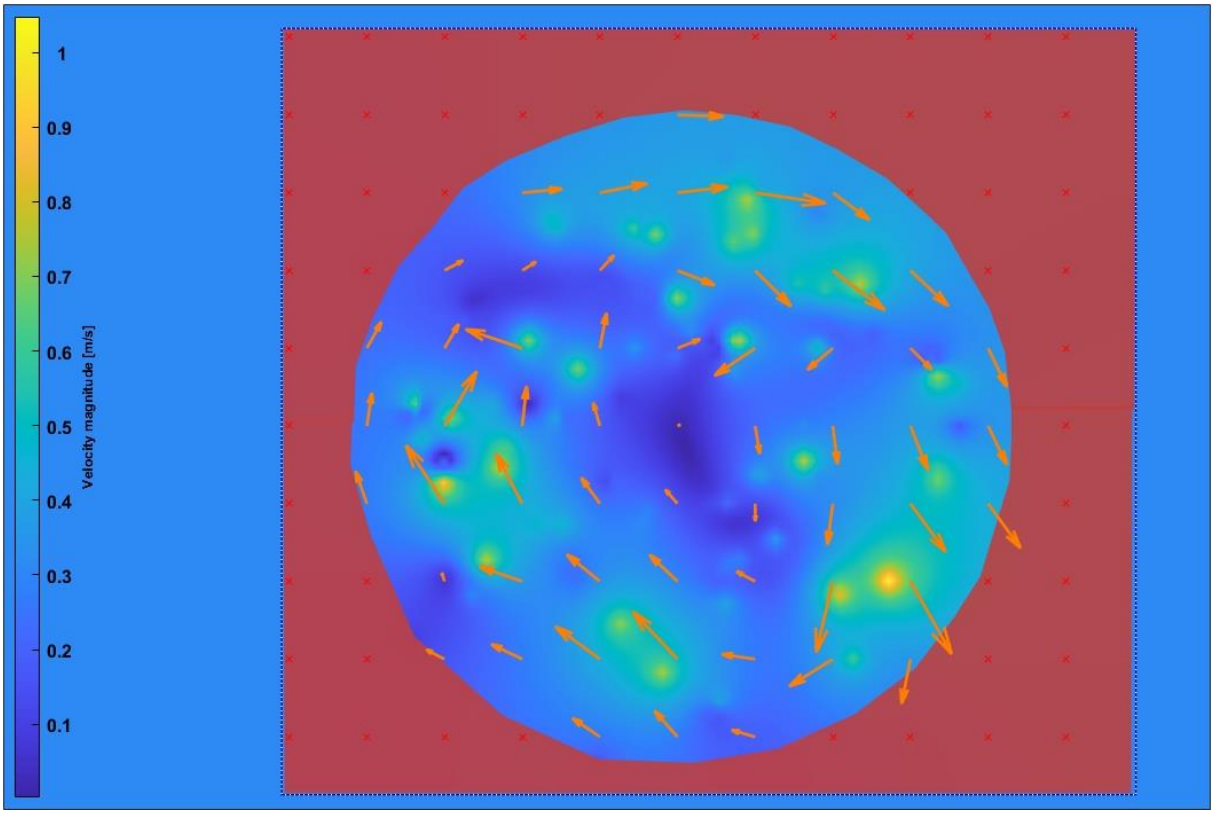

Figure 67. Processing of the particle shrinkage

The graphic presented below shows how the ARF force is acting when the power is increased. By drawing a line across the maximal circumference of the droplet is observed how the maximum peaks of the speed of the particles are displaced from the periphery to the centre demonstrating that there is force which push the particles to a shrinkage in the centre of the droplet.

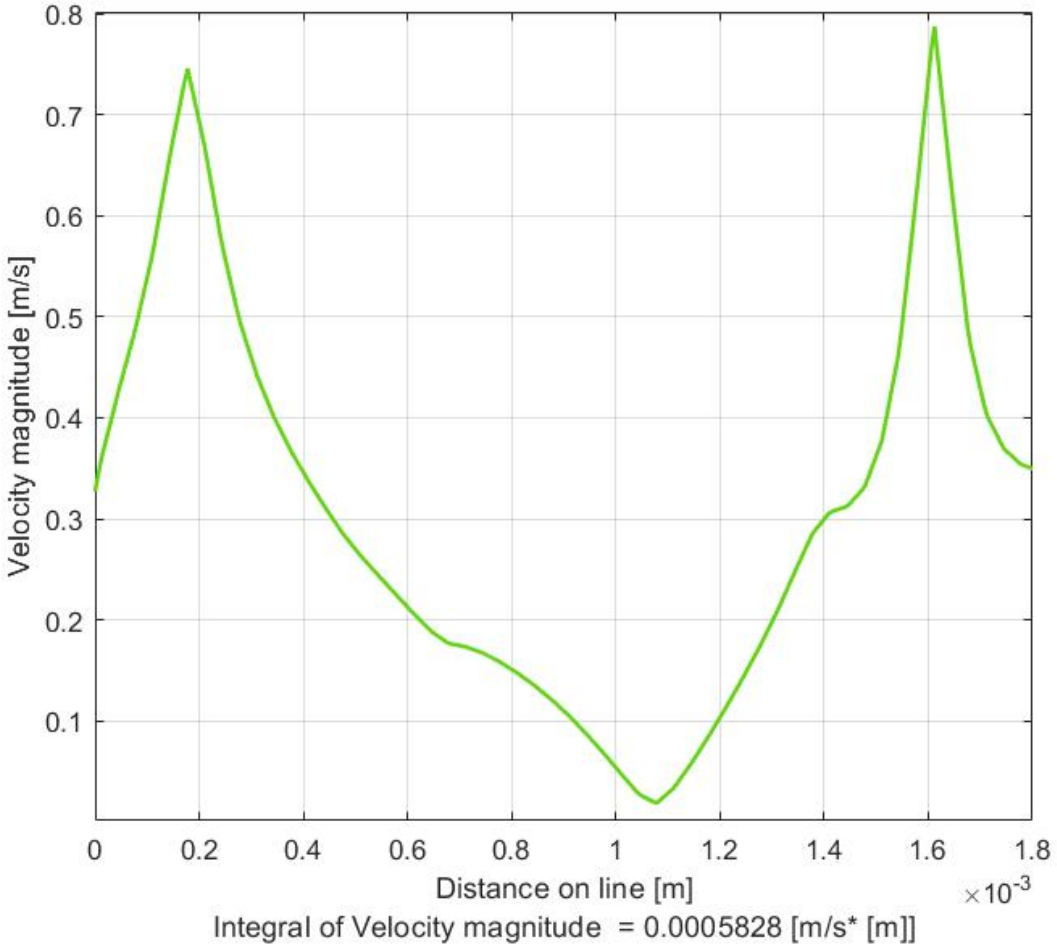

Graphic 4. Velocity magnitude in the particle cluster process

This last picture comes to confirm that the above mentioned, the drawn streamlines confirm the path followed by the particles in their movement when they are affected by the ARF force arising from the ASF.

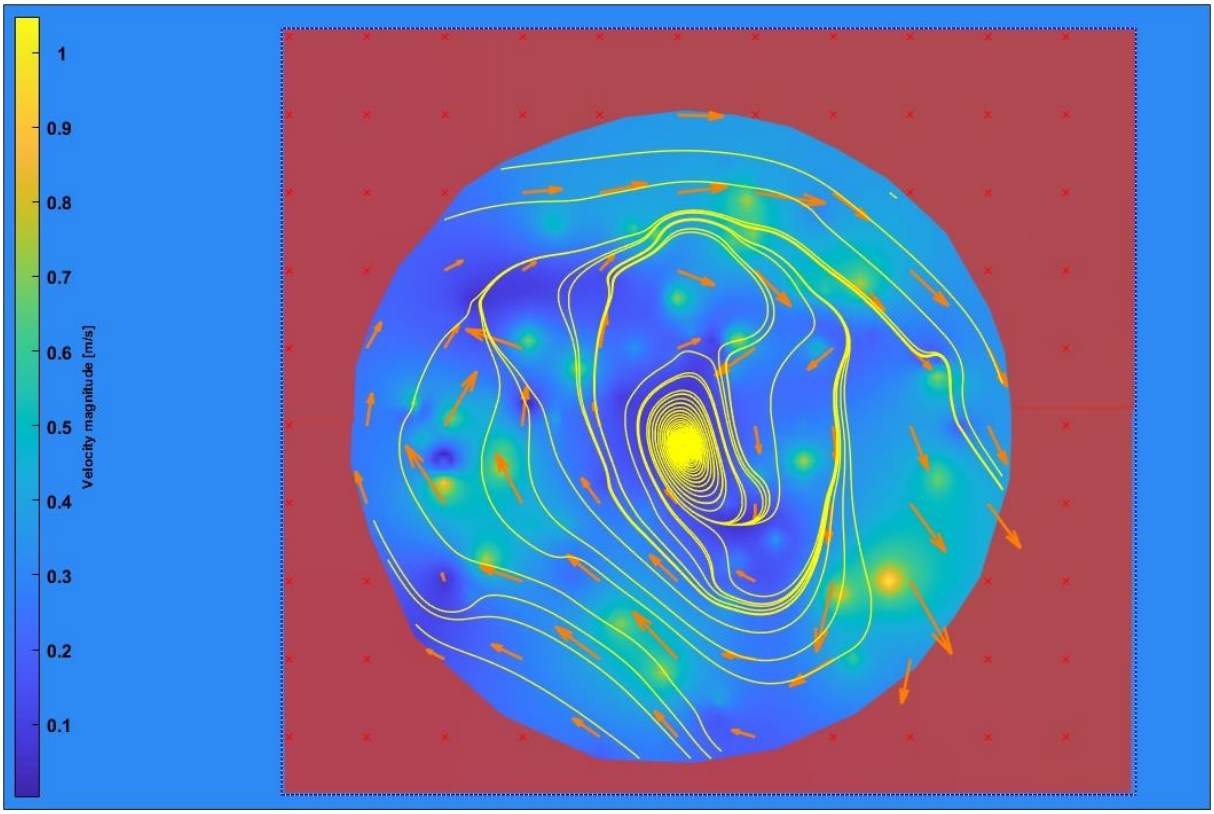

6.2.2 Particle ring 7 µm

As in the previous case, the fact of using an IDT with twice the nominal frequency makes the frequency more sensitive to changes in the applied power. Thus, and according to the theories explained for the first case, an increase in the applied power leads to a rapid dispersion of the particles. Starting from the previous concentration of the particles, the applied power is increased to 35 db with a frequency that for this case amounts to 87 MHz (see figure 68 b). It is observed how immediately the vortex begins to rotate faster and it is observed how more particles leave the vortex in which the ARF kept them aggregated to be dispersed to the periphery. By increasing the power to 40 dB this effect becomes more notorious (see figure 68 c). Finally, to prevent the IDT breaking, not more increments were applied and let the process continue until final state (see figure 68 d). As a consequence of this increment the speed rotation of the vortex was increased sharply which leads to assume that the Fc force is enhanced and becomes the main responsible for the movement of the particles. To conclude a ring shape formation was achieved in the periphery of the droplet.

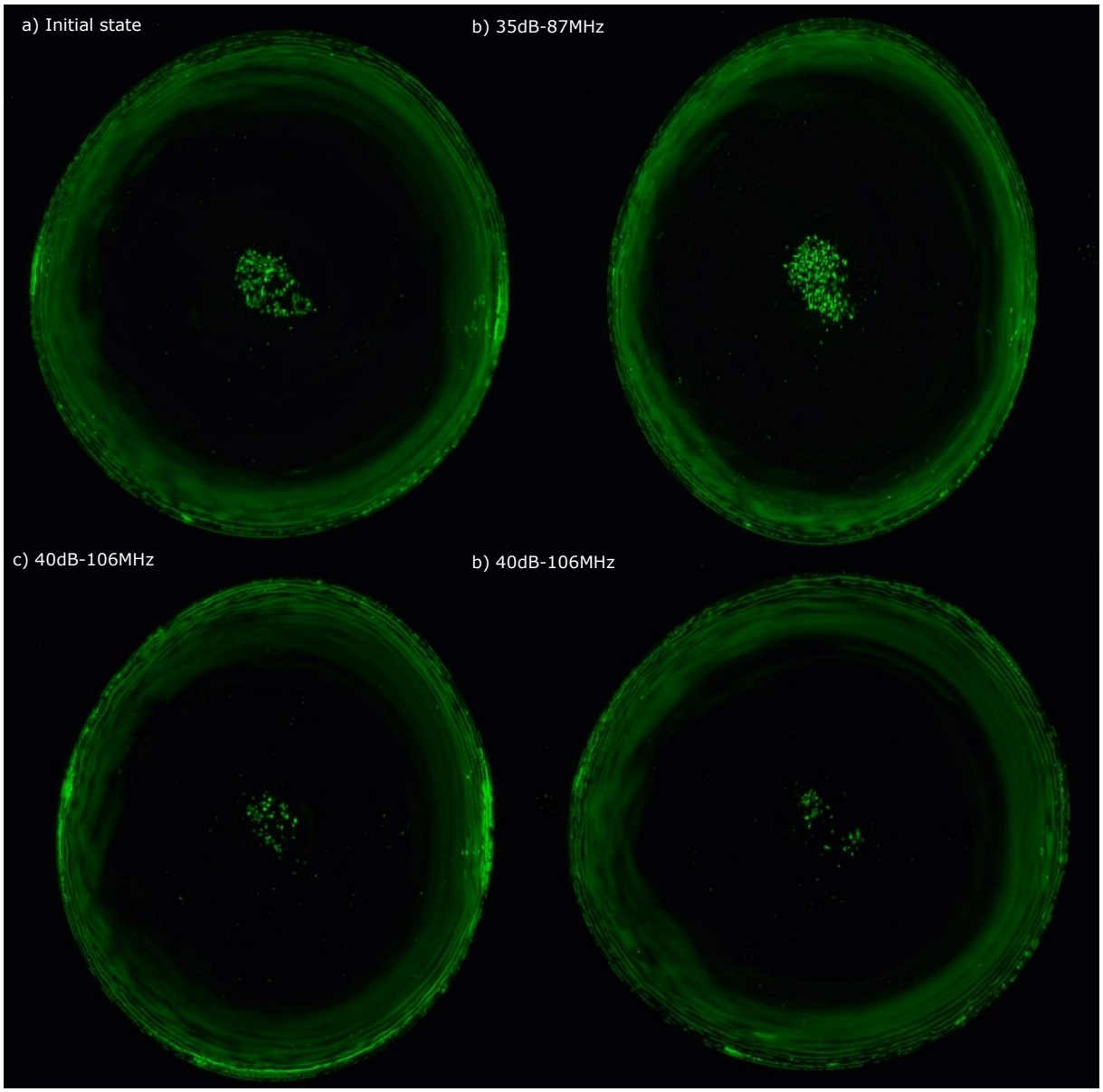

Figure 68. Sequence of particle ring formation 40 MHz

The post processing confirms all of the above mentioned. The vectors showing the trajectories followed by the particles in this situation and clearly shows the trend in the particle's movement. In the same way as commented in the previous case now the following picture predicts the consistence of the observation made Rogers et al. [31] Given a certain particle diameter, there is a value of frequency which can make the difference between the dominant force, the drag force and the ARF. As the particle size becomes smaller the higher frequency provokes that the ARF change the trajectories of particles aggregated and the particles move outwards, given the increment of the vortex speed rotation an enhanced centrifugal force push the particles outwards where jointly to the effect of ARF the ring formation is observed.

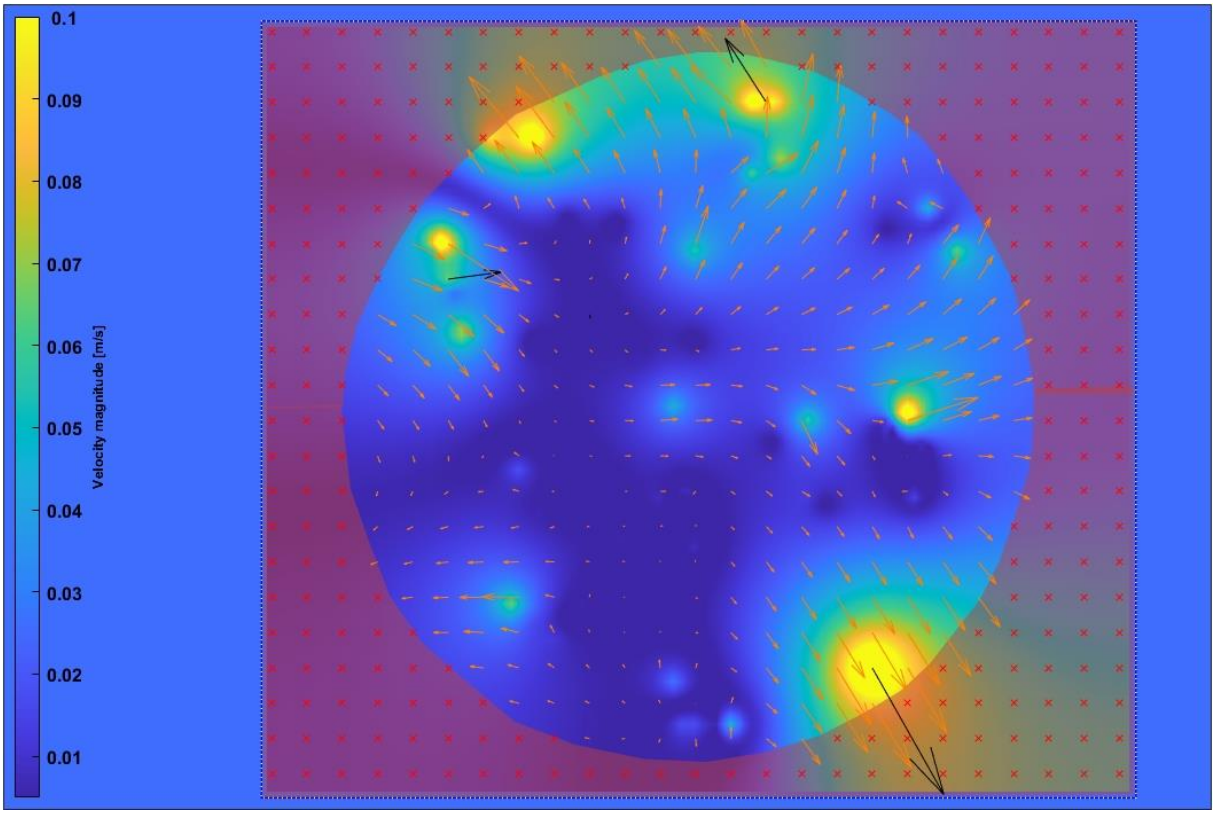

Figure 69. Post processing of particle dispersion

Once again, the graphic comes to demonstrate that the higher velocities measured in the droplet take place in the periphery as a consequence of the enhanced centrifugal force the particles are rotating when the droplet is subdued to an ultrasonic field under these conditions.

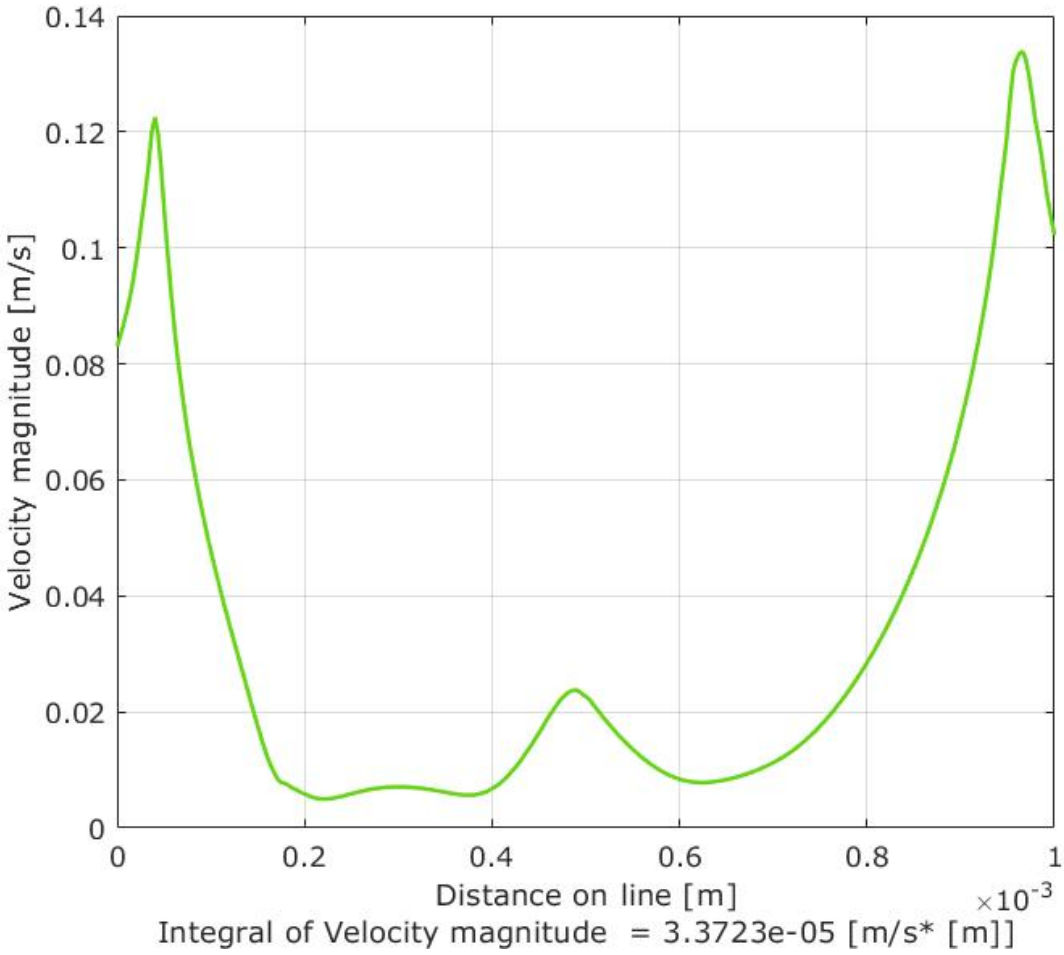

Graphic 5. Velocity magnitude of the particles in the ring formation

To conclude the streamlines map pretends to show which were the trajectories followed by the particles. In the next picture can be seen how the particles were pushed from the centre outwards demonstrating the existence of a force capable to achieve this.

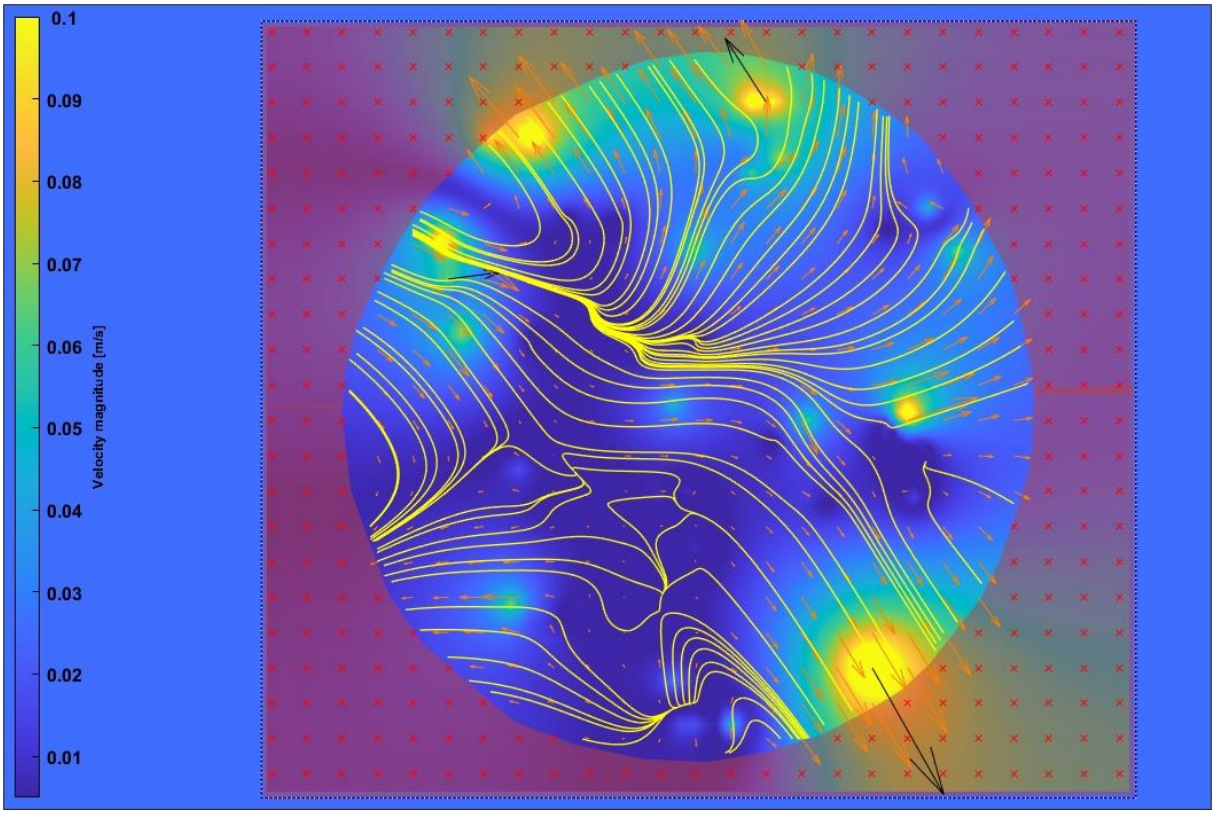

Figure 70. Streamlines in a particle ring

6.2.3 Discussion

In this second experiment, the IDT now has a nominal frequency of 40 MHz, which makes its frequency more sensitive to changes in power. As we can see in figure 68 d, for a lower input power than in the previous case, the frequency increases considerably. If we pay attention to what was commented in section 2.3.7, we observe that the higher the frequency, the lower the penetration and the less important the thermal effects. However, the number of particles that have been trapped is greater. This could be because the time must have been extended to get the particles to leave the stagnation point arising then the thermal effects related to the time that have been commented in the previous case. On the other hand, another phenomenon that can explain this is the agglomeration suffered by the particles when they are very close to each other. This could cause the particle to increase its volume due to the agglomeration, causing the forces to be perceived by them differently. It is also important to point out that this agglomeration of the particles together with a low hydrophobicity of the substrate could improve the frictional forces on the Eckman layer. This would force not only to increase the time but also to increase the input power and then the frequency.

6.3 Straight IDT 80 Mhz

Continuing with the analysis of the acting forces, an IDT with a nominal frequency of 80 MHz is now tested to generate a SAW on a drop loaded with particles, this time with a size of less than 1 um.

6.3.1 Particle ring 1 μm

What is intended with this experiment is to study the effect of the forces involved with the diameter of the particles. a) Starting from an initial state in which no force is applied, the applied power begins to increase. b) For the situation in which the power input is established at 45 dB a fast change in the trajectories of the particles is observed, with a frequency of 132 MHz the k factor is higher than the unit and the attenuation of the wave still greater than the radius starts to decrease sharply. The motion of the particles under these conditions seems to be dominated by the centrifugal force which push the particles to the periphery as is observed in the sequence. c) A slightly increment in the applied power to 48 dB together the increment of the frequency to 146 MHz becomes the Fc more dominant and the colour of the ring formed becomes stronger given the amount of fluorescence particles aggregated in the periphery. This is consistent with the observations of Destgeer et al who observed this phenomenon in their experiments. The shorter attenuation length Xs can result in the reflection of the acoustic waves within the fluid close to the wave-liquid interface and thus in the formation of standing wave field near the periphery of the droplet that acts along with the Fc to concentrate the particles in a ring shape.

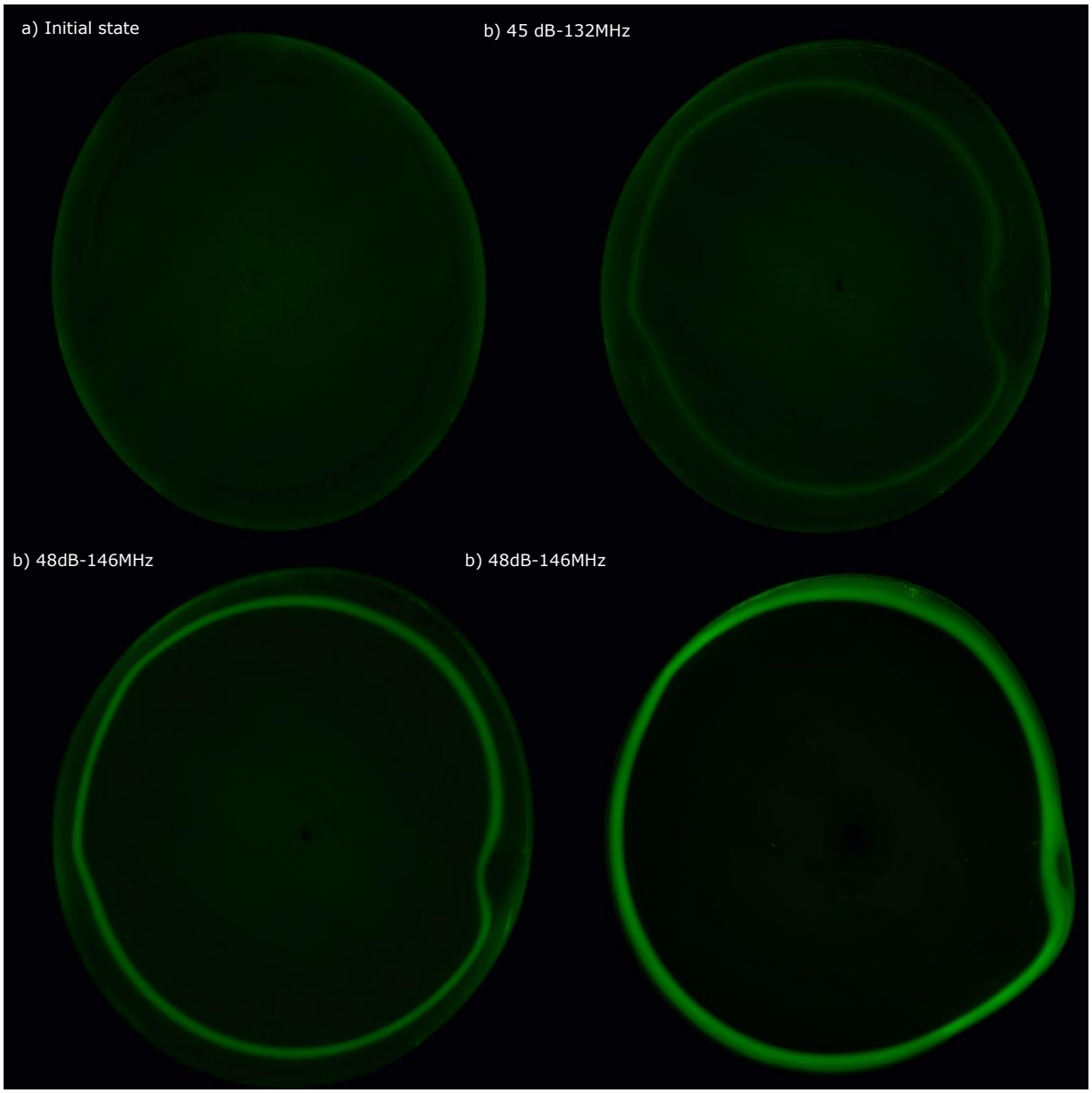

Figure 71. Particle ring formation 80 MHz

The image obtained after the post processing is presented below, on it can be observed how the map of the velocities show the higher speeds succeeding on the periphery as it should be. In the picture is clearly observed how big groups of aggregated particles are gathered in the periphery rotating thanks to the action of a strong centrifugal force arising as a consequence of the features of the SAW applied.

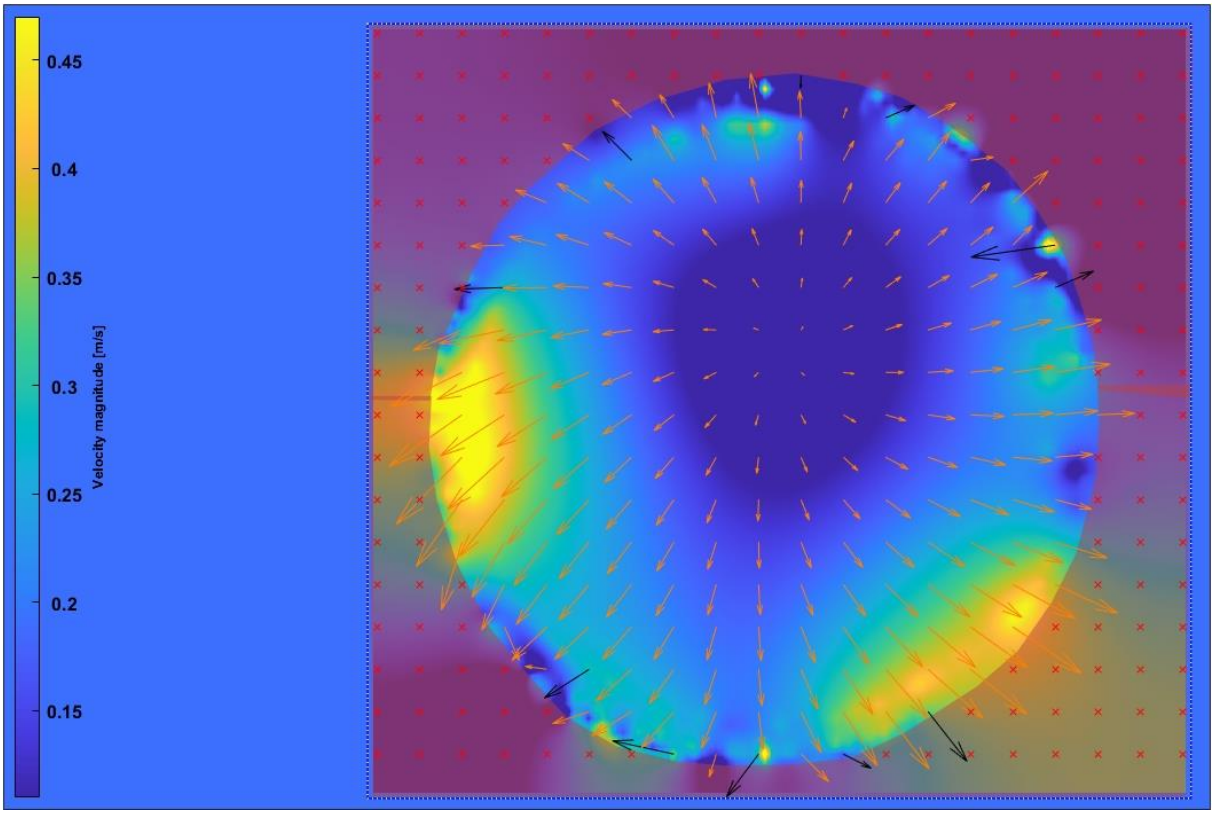

Figure 72. Particle dispersion

The following graphic demonstrates that in the centre of the droplet the velocity of displacement under these conditions is close to zero since the particles are gathered rotating in the boundary of the droplet according with the theories explained before.

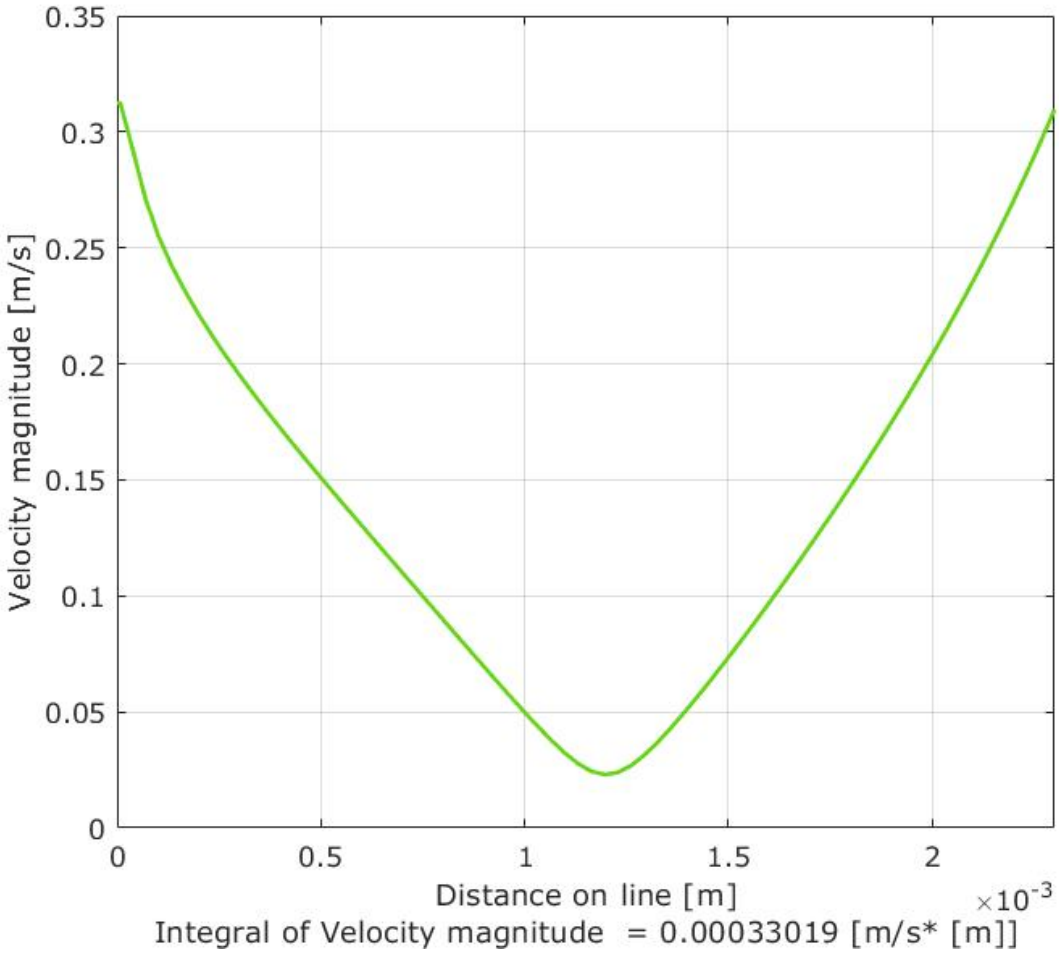

Graphic 6. Particles velocity magnitude inside droplet

The streamline map shows clearly the trend explained above. In this case the visualization of the trajectories shows a particle dispersion from the centre to the boundary's areas of the droplet as can be seen.

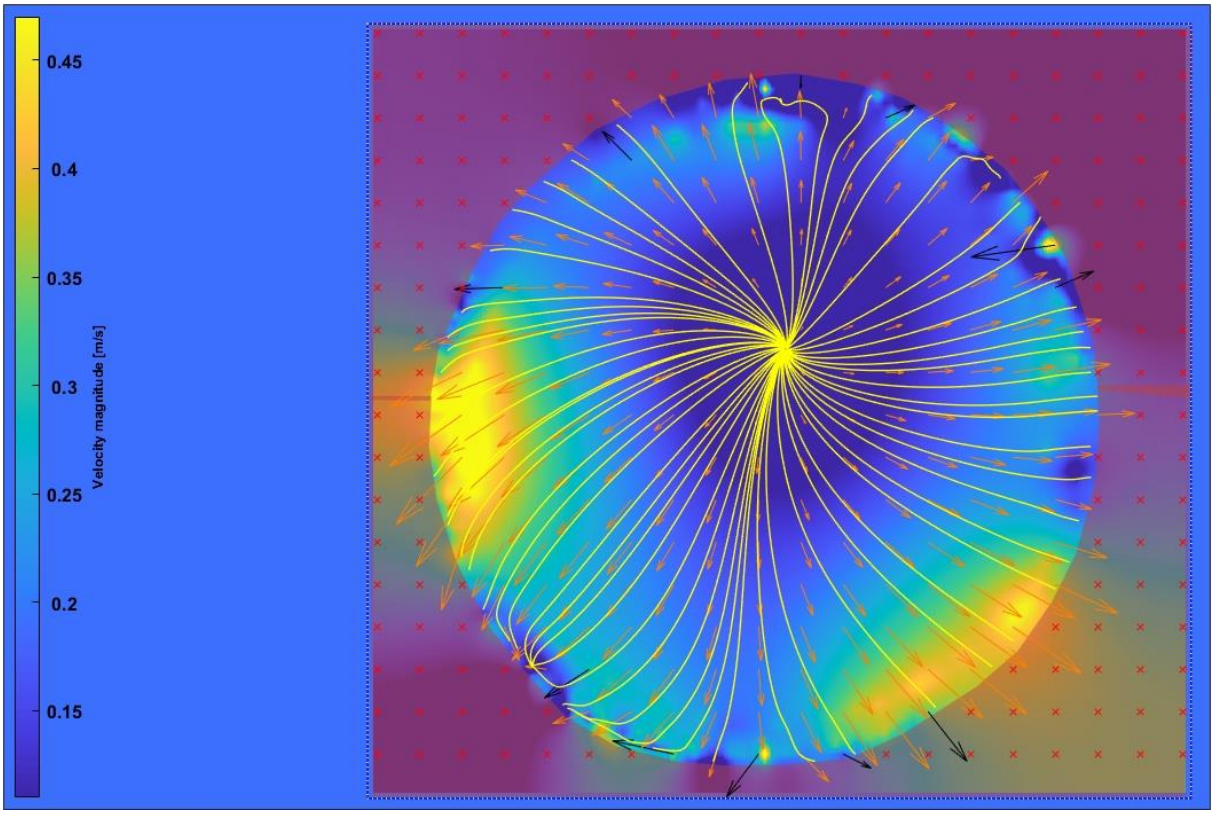

Figure 73. Streamlines of particles ring formation

6.3.2 Discussion

In this experiment, a just a particle dispersion is carried out. In this experiment, the power is increased progressively so that small stops are made between power increases to be able later to identify the exact moment in which that increase occurs. Because of that the starting point is not the initial one where all the particles are dispersed throughout the droplet. If we look only at the time it takes to disperse the particles clearly with a last increase in power, the time needed is only 14 seconds. This reduction in time is also linked to a reduction in the changes in the properties of the fluid as has been commented in the previous discussions. The dispersion when the particle diameter is smaller could be enhanced. Due to a reduction in the energy exchange that takes place in the drop-substrate contact as well as the heat transfer between the substrate and the droplet. Also is important to highlight for example, the distribution of the particles at the beginning of the experiment. If we consider that the experiment was carried out in different steps in which a small pause was done to increase the applied power. Then it implies that some previous favourable distribution of these particles was achieved. These factors possibly contribute positively to the dispersion of the particles.

6.4 Straight IDT 160 Mhz

Additionally applying the concepts observed before a trial for achieving the concentration of the particles in a middle position of the droplet was carried out. This time a powerful IDT was manufactured for this purpose. This case represents the most complex of all, since there is the connivance of two forces to keep the particles rotating in the mentioned region.

6.4.1 Middle particle ring formation 7μm

As always, a) starting from the state at rest, the applied power begins to increase. b) At this moment, the vortex is spinning fast but not fast enough to be Fc the dominant in the process, but the ARF which push the particles to the periphery. c) The powerful IDT rapidly increase the operation frequency when the input power is applied and then turns greater than the unit the *k factor*. As a consequence of this the attenuation *Xs* becomes significantly lower than the radius of the particles provoking that the SAW formation is governed by TSAW. Under these circumstances the *Fc* forces pushes the particles outwards, however, when the motion is dominated by TSAW the ARF force still have an important effect over the particles, in particular if the diameter of them is enough big to trap them. In this case as can be observed the two involved forces keep the particles rotating in the middle region of the droplet. This is consistent with Rogers et al. [17] observed, since for certain values of frequency and particle size it is possible to reach an equilibrium that leads the particles to the situation reached in the last image (see figure 74 d). However, the relationship given by Yuka et al. [31] is more obvious. If is compared the size of the particles between the previous experiment and this one, we observe that it was necessary to apply more power to form a complete outer ring when the size of the particles was 1 um. In this case, being the particles of 7 um, the applied power is lower, and it is observed how the diameter of the inner and outer ring are smaller compared to the previous case obtaining a ring shape formation in the middle region of the droplet. Since a certain increment of the power will leads to a complete ring formation in the periphery. This shows the consistency of the relationship proposed in the study by Yuka et al. [31] The diameter of the outer and inner ring is formed related to the power that is applied.

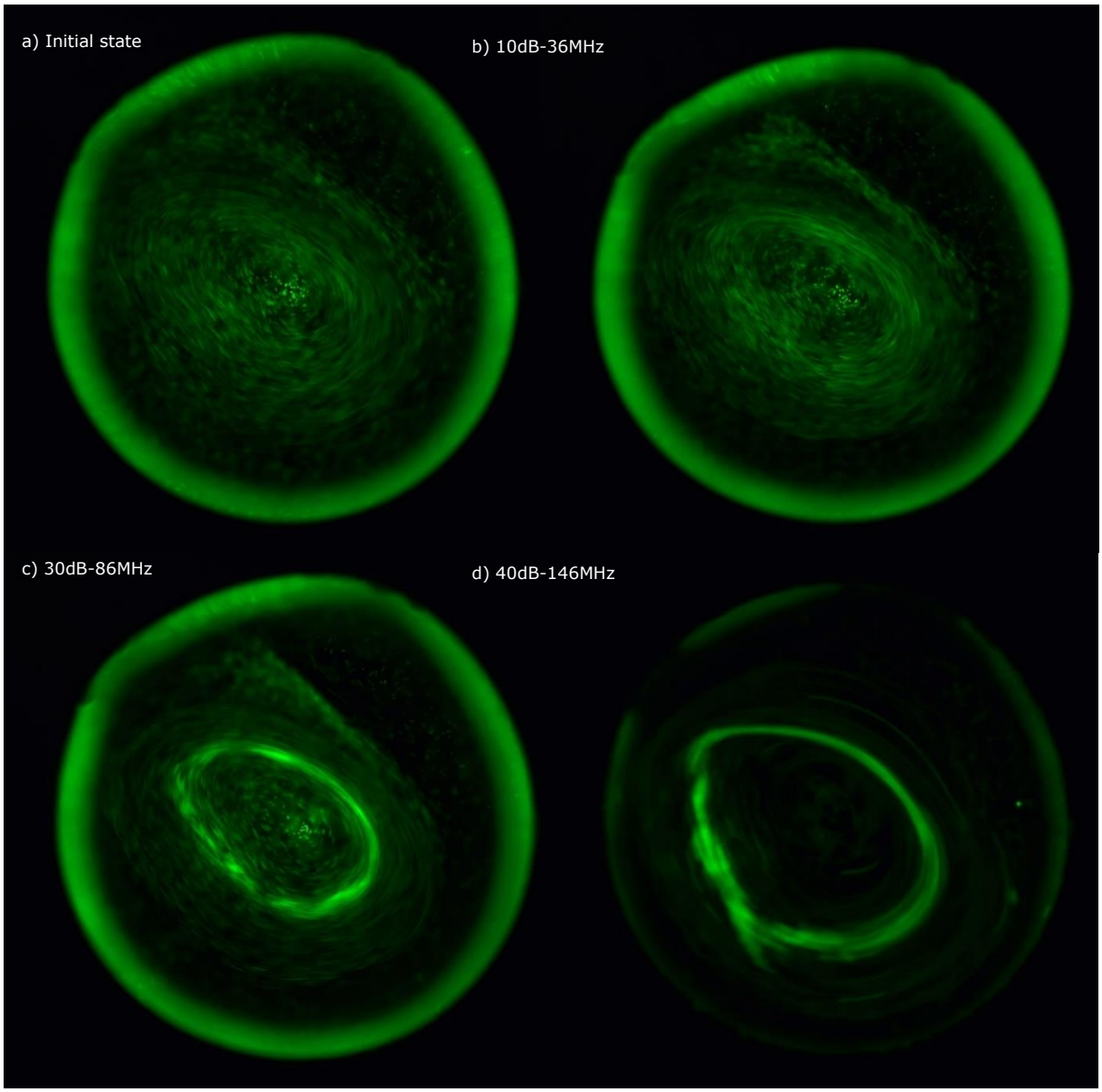

Figure 74. Middle ring formation 160 MHz

Although for this case it was more complicated to obtain good captions of what was happening in the experiment, the following image shows how the particles with the highest speed are close to the regions observed in the experiment, confirming the existence of forces able to balance themselves to keep the particles in a given region. In the same way, and given the limitations of the software, it was quite complicated to obtain a graph that would show that the maximum velocities effectively overlap with the regions occupied by the majority of the particles, due to that reason the graphical representation for this case has been omitted.

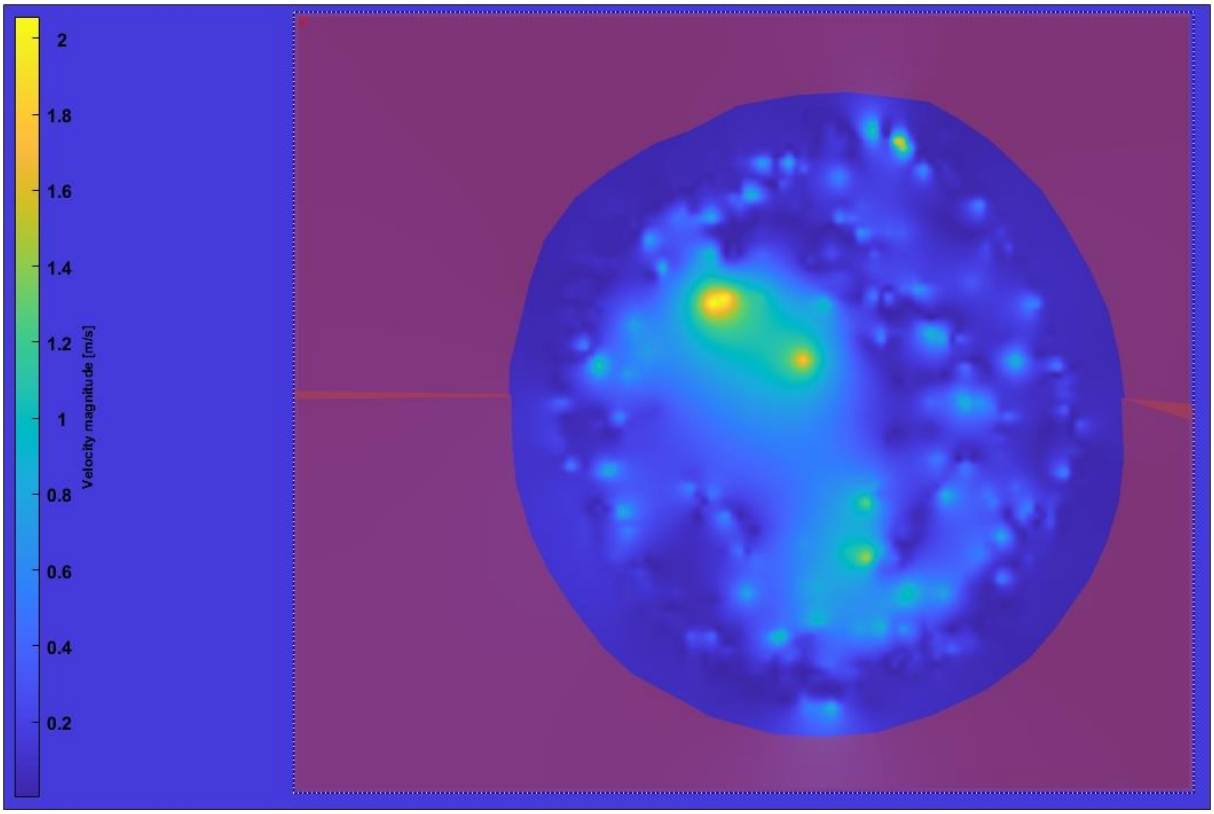

Figure 75. Middle particle ring speeds

6.4.2 Discussion

In this last experiment, an inner ring was formed. In this experiment, the coexistence between two forces is assumed, on the one hand the centrifugal force that pushes the particles out and on the other hand the ARF that keeps the particles in that position over time. Assuming an ideal case, the ring should have formed concentrically to the periphery of the drop. However, during the experiment, certain vibrations were observed in the droplet that possibly came from internal forces that were observed when the power was suddenly increased. Although it is known that the SAW can translate the droplet under certain conditions of power and frequency. What draws the attention of this is that it is possible that there is a force capable of damping these sudden changes in the SAW under certain threshold. This can be due to the density of the fluid, its viscosity and also the spin of the vortex itself which increase sharply when the power input is increased.

7 Conclusions

This project aims to give continuity to the work carried out during the specialization project. In this sense, observing how the acting forces interact with the droplet and its particles was the main motivation of this work. In this sense, the gaps appreciated in the literature are also discussed. Bearing this in mind, studying the relationship that the different parameters involved in this interaction over the particles was the main resource to verify the theories proposed. For this, four different IDTs were produced, and different types of particle movements were shown, which were recorded and analyzed. Finally, the analysis by comparison of the results obtained with those observed in the literature and the discussion of the gaps identified complete the content of this work.

The following conclusions emerge from this study.

1- The centrifugal force Fc is the main force in pushing the outward and forming a ring shape in the periphery of the droplet.
2- At a lower power, the particles are captured by the streaming force rotating in a concentric circles inside the droplet.
3- The ARF force is responsible for the motion of the particles inside of the droplet.
4- An offset location for the droplet study is needed whether a single vortex creating is the objective.
5- The diameter of the particles plays a crucial role in the amount of ARF force is perceived by the particles and this determinates their movement.
6- The k factor is the main indicator to predict how the particles will move.
7- The frequency is the main parameter to establish a regime of movement.
8- The centrifugal force Fc is affected by the input power applied.
9- The attenuation of the acoustic wave in the surface decrease when increase the frequency applied.
10- Is possible to create patterns of movements inside the droplet.
11- When the size of the particle decrease becomes more complicated to concentrate the particles, the input power required is higher and this leads to a enhance in the centrifugal force and the evaporation of the droplet takes place faster as well.
12- Is necessary to implement more effective methods to concentrate smaller particles.

The following assumptions were not measured but arise from the observations made during the experiments and could be the cause of a significant affections to the motion of the particles. These are some of the conclusions extracted after the experimentation.

1. The time seems to play a crucial role in the change of the mechanical properties of the fluid affecting the behaviour of the particles.
2. The greater the time of the experiment duration, the higher the energy exchange between the droplet and the substrate and more negative effects are observed.

3. The higher the input power, the higher is the temperature over the substrate, then the higher is the heating up by convection inside the droplet. This could lead to a decreasing in the surface tension, contact angle, viscosity, and density.
4. A change in the surface tension or the liquid volume could lead to a change in the contact angle of the droplet regarding the substrate line.
5. A change in the contact angle of the droplet could improve the dispersion of the particle and complicate the particle concentration.
6. By the study of the mathematical expressions, the higher the viscosity, the higher force is needed to trap the particles in the ASF.
7. Should be exist a threshold for the viscosity of the fluid to succeed the particle streaming.
8. The hydrophobicity properties of the substrate plays and important role to achieve the concentration and dispersion of the particles.
9. From the friction of the surface of the droplet in contact with the substrate arise a force that somehow play a role in the Eckman layer and could affects upstream.
10. Improve the properties of the substrate in terms of its hydrophobicity could improve the results acquired.

8 Further work

When the objective is to concentrate particles of the order of nanometres, it is necessary to significantly increase the input power. This results in a rapid evaporation of the droplet which prevents the particles from concentrating. To this end, in this section a method is proposed as a further work by which this could be achieved by overcoming these difficulties.

Firstly, it is proposed to use spiral IDTs, as is described in the literature these IDTs have shown to be able to concentrate particles faster than the straight IDTs that are used.

In this way, more time is gained for the particles to be captured by the ARF and to be conducted to the centre of the droplet. Even with this, it is sometimes difficult to achieve it, so it is also proposed to increase the hydrophobicity of the substrate in which the drop is found when it is subjected to an ultrasonic field.

Recently, some cases have been described in the literature, in some of them a small housing was built for the droplet in which it spins on itself, however, other applied a PDMS coating over the surface to achieve the droplet spin, some examples of this can be found in the following references [40] [41] [42]. This rotation of the droplet, together with the vortex created by the SAW inside, increased the drag force and pushed the particles towards the centre much faster, which gave the possibility of concentrating exceedingly small particles in less time.

With this same idea, what is proposed is to eliminate that housing and apply a superficial coating with superior properties able to create superhydrophobicity on the substrate, in such a way that the droplet can rotate supported on a single point free pinned over the substrate in the centre of the spiral IDT. Thus, eliminating the friction produced with the housing and achieving much higher rotational speeds.

One of the disadvantages of this idea would be the process to achieve the optimal set up. In one hand is required to find an appropriate coating with such properties. On the other hand, the $LiNbO_3$ needs to be pre-treated before any coating is applied. This treatment consists of plasma activation process. Being possible to make it the difficulties would be in to find the correct parameters to obtain a lower as possible contact angles on the surface to achieve a good adhesion of the coating applied.

The question that arises from this idea raises the following question. What would happen if the power applied to the IDT increased significantly, it would be possible to atomize the droplet in the same place without displacing it first. And if this were true and inside the droplet instead of particles there were cells, they could be cells split as a consequence of the atomization. The prove of this theory and its implications could be an interesting object of researching in a future work.

Appendix 1: Fabrication recipe

1. Cleaning of LinbO3 substrate

- Acetone, Isopropanol, N2
- Plasma cleaner 1 min O2/50/50

2. Photoresist spin coating

- SPR-700
- 4000 rpm – 46 sec - rampage 4000rpm (900 nm)

3. Soft baking for $LinbO_3$

- Type: Soft baking
- Temp: 95°C
- Time: 1 min

4. Exposure MLA 405nm wavelength laser

- Dose 100 mJ/cm2

5. Post exposure bake

- Temp: 115°C
- Time: 1 min

6. Development

- 2 TIMES MF-26A during 15 sec + DI + N2

7. AJA evaporation

- 10 nm Titanium
- 80 nm Gold

8. Lift-off

- 2-3 min electronic bath with acetone + IPA + N2

References

[1] G. Destgeer, J. H. Jung, J. Park, H. Ahmed, and H. J. Sung, "Particle Separation inside a Sessile Droplet with Variable Contact Angle Using Surface Acoustic Waves," *Anal Chem*, vol. 89, no. 1, pp. 736–744, Jan. 2017, doi: 10.1021/acs.analchem.6b03314.

[2] Y. Liu *et al.*, "Enhanced Detection in Droplet Microfluidics by Acoustic Vortex Modulation of Particle Rings and Particle Clusters via Asymmetric Propagation of Surface Acoustic Waves," *Biosensors (Basel)*, vol. 12, no. 6, p. 399, Jun. 2022, doi: 10.3390/bios12060399.

[3] P. R. Rogers, J. R. Friend, and L. Y. Yeo, "Exploitation of surface acoustic waves to drive size-dependent microparticle concentration within a droplet," *Lab Chip*, vol. 10, no. 21, pp. 2979–2985, Nov. 2010, doi: 10.1039/c004822d.

[4] R. v. Raghavan, J. R. Friend, and L. Y. Yeo, "Particle concentration via acoustically driven microcentrifugation: MicroPIV flow visualization and numerical modelling studies," *Microfluid Nanofluidics*, vol. 8, no. 1, pp. 73–84, Jan. 2010, doi: 10.1007/s10404-009-0452-3.

[5] H. Li, J. R. Friend, and L. Y. Yeo, "Surface acoustic wave concentration of particle and bioparticle suspensions," *Biomed Microdevices*, vol. 9, no. 5, pp. 647–656, Oct. 2007, doi: 10.1007/s10544-007-9058-2.

[6] H. Bruus, "Acoustofluidics 7: The acoustic radiation force on small particles," *Lab on a Chip*, vol. 12, no. 6. Royal Society of Chemistry, pp. 1014–1021, Mar. 21, 2012. doi: 10.1039/c2lc21068a.

[7] J. D. Whitehill, I. Gralinski, D. Joiner, and A. Neild, "Nanoparticle manipulation within a microscale acoustofluidic droplet," *Journal of Nanoparticle Research*, vol. 14, no. 11, Nov. 2012, doi: 10.1007/s11051-012-1223-8.

[8] Z. Mao *et al.*, "Enriching Nanoparticles via Acoustofluidics," *ACS Nano*, vol. 11, no. 1, pp. 603–612, Jan. 2017, doi: 10.1021/acsnano.6b06784.

[9] P. H. Huang *et al.*, "An acoustofluidic micromixer based on oscillating sidewall sharp-edges," *Lab Chip*, vol. 13, no. 19, pp. 3847–3852, Oct. 2013, doi: 10.1039/c3lc50568e.

[10] P. H. Huang *et al.*, "An acoustofluidic sputum liquefier," *Lab Chip*, vol. 15, no. 15, pp. 3125–3131, Jun. 2015, doi: 10.1039/c5lc00539f.

[11] P. H. Huang *et al.*, "A reliable and programmable acoustofluidic pump powered by oscillating sharp-edge structures," *Lab Chip*, vol. 14, no. 22, pp. 4319–4323, Nov. 2014, doi: 10.1039/c4lc00806e.

[12] F. Petersson, L. Åberg, A. M. Swärd-Nilsson, and T. Laurell, "Free flow acoustophoresis: Microfluidic-based mode of particle and cell separation," *Anal Chem*, vol. 79, no. 14, pp. 5117–5123, Jul. 2007, doi: 10.1021/ac070444e.

[13] G. Destgeer, J. H. Jung, J. Park, H. Ahmed, and H. J. Sung, "Particle Separation inside a Sessile Droplet with Variable Contact Angle Using Surface Acoustic Waves," *Anal Chem*, vol. 89, no. 1, pp. 736–744, Jan. 2017, doi: 10.1021/acs.analchem.6b03314.

[14] Y. Ai, C. K. Sanders, and B. L. Marrone, "Separation of escherichia coli bacteria from peripheral blood mononuclear cells using standing surface acoustic waves," *Anal Chem*, vol. 85, no. 19, pp. 9126–9134, Oct. 2013, doi: 10.1021/ac4017715.

[15] N. Zhang *et al.*, "Microliter ultrafast centrifuge platform for size-based particle and cell separation and extraction using novel omnidirectional spiral surface acoustic waves," *Lab Chip*, vol. 21, no. 5, pp. 904–915, Mar. 2021, doi: 10.1039/d0lc01012j.

[16] G. Destgeer, H. Cho, B. H. Ha, J. H. Jung, J. Park, and H. J. Sung, "Acoustofluidic particle manipulation inside a sessile droplet: Four distinct regimes of particle concentration," *Lab Chip*, vol. 16, no. 4, pp. 660–667, 2016, doi: 10.1039/c5lc01104c.

[17] P. R. Rogers, J. R. Friend, and L. Y. Yeo, "Exploitation of surface acoustic waves to drive size-dependent microparticle concentration within a droplet," *Lab Chip*, vol. 10, no. 21, pp. 2979–2985, Nov. 2010, doi: 10.1039/c004822d.

[18] S. Li *et al.*, "Standing surface acoustic wave (SSAW)-based cell washing," *Lab Chip*, vol. 15, no. 1, pp. 331–338, Jan. 2015, doi: 10.1039/c4lc00903g.

[19] M. Wu *et al.*, "Acoustic Separation of Nanoparticles in Continuous Flow," *Adv Funct Mater*, vol. 27, no. 14, Apr. 2017, doi: 10.1002/adfm.201606039.

[20] M. C. Jo and R. Guldiken, "Active density-based separation using standing surface acoustic waves," *Sens Actuators A Phys*, vol. 187, pp. 22–28, Nov. 2012, doi: 10.1016/j.sna.2012.08.020.

[21] J. Nam, Y. Lee, and S. Shin, "Size-dependent microparticles separation through standing surface acoustic waves," *Microfluid Nanofluidics*, vol. 11, no. 3, pp. 317–326, Sep. 2011, doi: 10.1007/s10404-011-0798-1.

[22] L. Ren *et al.*, "Standing Surface Acoustic Wave (SSAW)-Based Fluorescence-Activated Cell Sorter," *Small*, vol. 14, no. 40, Oct. 2018, doi: 10.1002/smll.201801996.

[23] S. Li *et al.*, "An On-chip, multichannel droplet sorter using standing surface acoustic waves," *Anal Chem*, vol. 85, no. 11, pp. 5468–5474, Jun. 2013, doi: 10.1021/ac400548d.

[24] M. Dao *et al.*, "Acoustic separation of circulating tumor cells," *Proc Natl Acad Sci U S A*, vol. 112, no. 16, pp. 4970–4975, Apr. 2015, doi: 10.1073/pnas.1504484112.

[25] J. L. Han, H. Hu, Q. Y. Huang, and Y. L. Lei, "Particle separation by standing surface acoustic waves inside a sessile droplet," *Sens Actuators A Phys*, vol. 326, Aug. 2021, doi: 10.1016/j.sna.2021.112731.

[26] H. C. Hao and D. J. Yao, "Highly sensitive and rapid detection of shigella flexneri in liquid sample by an immunomagnetic assay with shear horizontal surface acoustic wave sensors," in *2013 Transducers and Eurosensors XXVII: The 17th*

International Conference on Solid-State Sensors, Actuators and Microsystems, TRANSDUCERS and EUROSENSORS 2013, 2013, pp. 2114–2117. doi: 10.1109/Transducers.2013.6627218.

[27] W. Connacher *et al.*, "Micro/nano acoustofluidics: Materials, phenomena, design, devices, and applications," *Lab on a Chip*, vol. 18, no. 14. Royal Society of Chemistry, pp. 1952–1996, Jul. 21, 2018. doi: 10.1039/c8lc00112j.

[28] Colin Campbell, "Surface acoustic wave devices for mobile and wireless communications," *Academic press*, 1998.

[29] Ole Andreas Kvivik Kavli, "Surface Acoustic Wave Acoustophoresis for Microfluidic Based Micron and Submicron Particle Separation," 2016.

[30] B. H. Ha *et al.*, "Acoustothermal heating of polydimethylsiloxane microfluidic system," *Sci Rep*, vol. 5, Jul. 2015, doi: 10.1038/srep11851.

[31] Y. Liu *et al.*, "Enhanced Detection in Droplet Microfluidics by Acoustic Vortex Modulation of Particle Rings and Particle Clusters via Asymmetric Propagation of Surface Acoustic Waves," *Biosensors (Basel)*, vol. 12, no. 6, p. 399, Jun. 2022, doi: 10.3390/bios12060399.

[32] H. Bruus, "Acoustofluidics 7: The acoustic radiation force on small particles," *Lab Chip*, vol. 12, no. 6, p. 1014, 2012, doi: 10.1039/c2lc21068a.

[33] K. Yasuda and T. Kamakura, "Acoustic radiation force on micrometer-size particles," *Appl Phys Lett*, vol. 71, no. 13, pp. 1771–1773, Sep. 1997, doi: 10.1063/1.119395.

[34] F. Villa, M. Marengo, and J. de Coninck, "A new model to predict the influence of surface temperature on contact angle," *Sci Rep*, vol. 8, no. 1, Dec. 2018, doi: 10.1038/s41598-018-24828-8.

[35] L. Korson, W. Drost-Hansen, F. J. Millero, L. Korson, W. Drost-Hansen, and F. J. Millero, "Viscosity of Water at Various Temperatures." [Online]. Available: https://pubs.acs.org/sharingguidelines

[36] M. Tanaka, G. Girard, R. Davis, A. Peuto, and N. Bignell, "metrologia."

[37] S. Ebnesajjad, "Surface Tension and Its Measurement," in *Handbook of Adhesives and Surface Preparation: Technology, Applications and Manufacturing*, Elsevier, 2010, pp. 21–30. doi: 10.1016/B978-1-4377-4461-3.10003-3.

[38] "Engineering ToolBox, (2004). Surface Tension of Water in contact with Air. [online] Available at: https://www.engineeringtoolbox.com/water-surface-tension-d_597.html [Accessed Day Mo. Year]."

[39] P. Delsing *et al.*, "The 2019 surface acoustic waves roadmap," *Journal of Physics D: Applied Physics*, vol. 52, no. 35. Institute of Physics Publishing, Jul. 03, 2019. doi: 10.1088/1361-6463/ab1b04.

[40] T. Peng, C. Fan, M. Zhou, F. Jiang, D. Drummer, and B. Jiang, "Rapid Enrichment of Submicron Particles within a Spinning Droplet Driven by a Unidirectional Acoustic Transducer," *Anal Chem*, vol. 93, no. 39, pp. 13293–13301, Oct. 2021, doi: 10.1021/acs.analchem.1c02914.

[41] Y. Gu *et al.*, "Acoustofluidic centrifuge for nanoparticle enrichment and separation," 2021. [Online]. Available: https://www.science.org

[42] S. Song, J. Zhou, and A. Riaud, "Effect of viscosity on surface acoustic wave driven collective particle dynamics in sessile droplets: Cloud, cavities, and aggregates," *Physics of Fluids*, vol. 34, no. 8, p. 083604, Aug. 2022, doi: 10.1063/5.0097354.

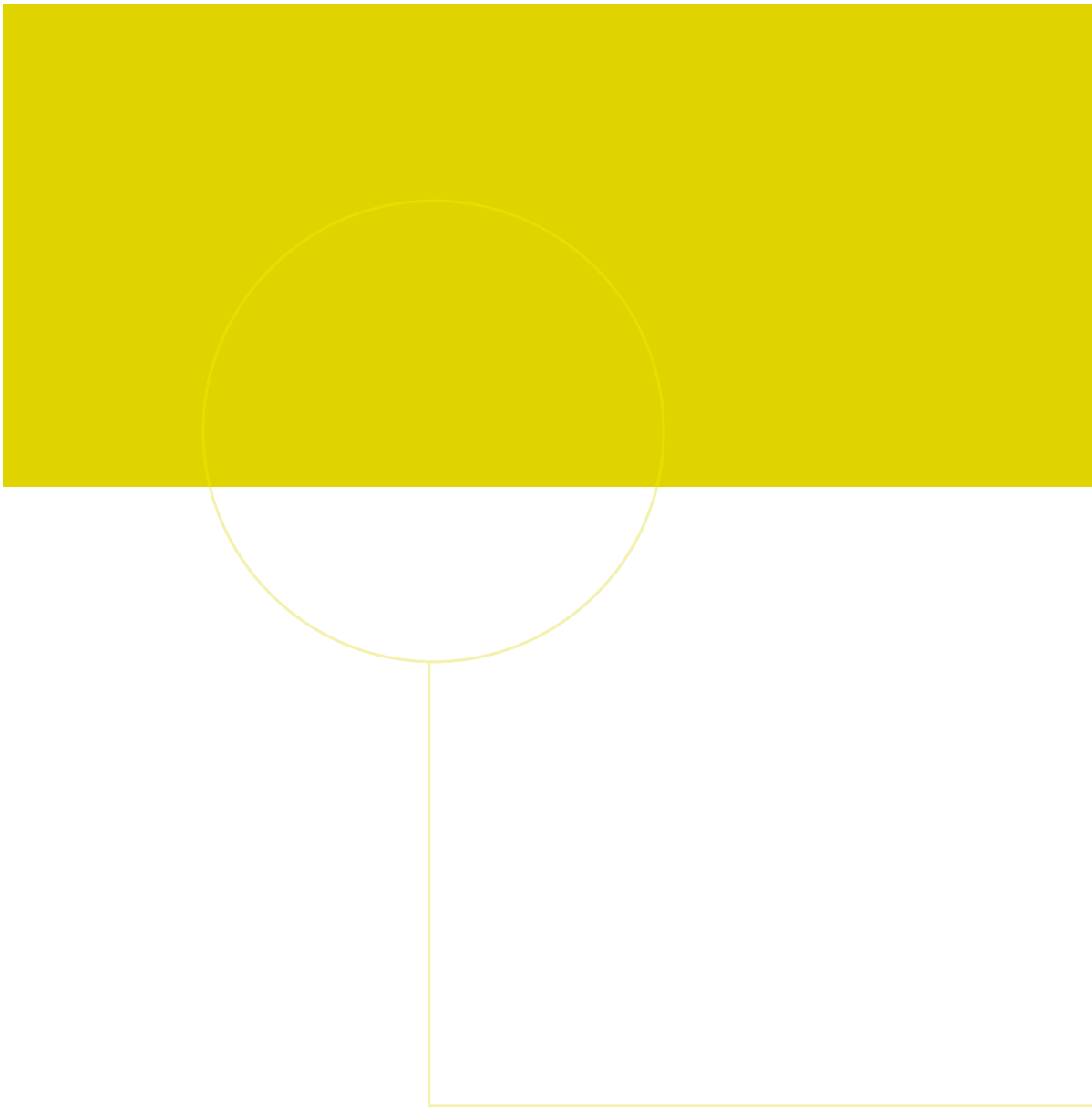

NTNU

Norwegian University of
Science and Technology